UNIVERSITÀ DELLA CALABRIA

**Dipartimento di Fisica**

---

**Doctorate School of Science and Technique**
**"Bernardino Telesio"**

*A thesis submitted for the degree of Doctor of Philosophy in Mesophases and Molecular Materials*

XXVI Cycle
02/B3 - FIS/07

# "Advanced numerical models for highly frustrated liquid crystalline phases"

**School Director**
Prof. Roberto Bartolino

**Supervisors**
Prof. Riccardo Barberi

Dr. Eng. Giuseppe Lombardo

**Curriculum Coordinator**
Prof. Carlo C. Versace

**Candidate**
Caldera Teresita de Jesus

# Table of Contents

## 1. Thesis Dissertation

An external sinusoidal electric field induces inside a nematic π-cell a nematic distortion that oscillates with two maxima for each period of the applied electric field. The sinusoidal behaviour of the electric field allows an elastic relaxation of the nematic texture between two maxima of the electric intensity and hence the excitation of the nematic matrix follows an alternation of increasing induced distortions, when the electric field grows, and spontaneous visco-elastic relaxations, when the field intensity decreases, with a period which is two times the period of the electric sinusoid. As the visco-elastic relaxation time is about 1 ms, for frequencies $f > 1$ kHz, the induced biaxial distortion accumulates in the middle plane of the cell and the order reconstruction takes place after a suitable number of undulations. Despite the accumulation rate, the electric threshold tends to increase with the frequency, as expected from previous studies on electric rectangular pulses, i.e. the field intensity grows when the pulse duration decreases. Shorter signal periods always require higher electric fields to induce the order reconstruction.

The electric current flowing across a nematic liquid crystal cell submitted to an electric field, depends on the variation of the external electric field itself but also by the variation of the liquid crystal dielectric properties, and thus it is intrinsically related to the director reorientation. We aim to study the induced biaxial distortion inside the cell by means of the experimentally measured electric current, comparing it with theoretical previsions from a numerical model. Therefore, the main purpose of this thesis involves the development of a computer numerical model for exploring the order reconstruction phenomenon within symmetric and asymmetric π-cells when submitted to an external sinusoidal electric field.

To study the dynamical behaviour of calamitic nematic liquid crystal, a finite element method (FEM), based on Galerkin's formulation, was implemented in numerical algorithms to solve adequately the equations of a full Landau-de Gennes **Q**-tensor model.

For a better and complete understanding of the order reconstruction dynamics, we performed also experimental measurements. In order to measure the variation of the electric current density inside the cell, we connected the liquid crystal cell in series with an electrical resistor and we measured the voltage drop across the resistor. Furthermore, to optically observe the splay-bend transition, a polarized optical microscope has been used.

For a full characterization of the phenomenon, different voltage amplitudes and frequencies have been tested.

For model validation, we performed simulation of the physical problem using a one-dimensional π-cell of thickness $d$=1μm, with a strong anchoring energy on both boundary surfaces. We imposed different electric field amplitudes on the boundary plates, then we analysed the temporal evolution of the biaxiality and current density inside the cell.

This thesis is organized as follow: an introduction to liquid crystals in general and to the nematic phase in particular, which will be of interest in this work, will be discussed for first. We detail the physics properties of the nematic liquid crystal mesophase.

The third chapter concerns the description of a novel numerical model using the **Q**-tensor representation method. This model will be used in the following for a better understanding of the experimental results. The experimental techniques used for our investigations, the detailed procedure of cells preparation and the experimental setup used to investigate the nematic order reconstructions behaviour throughout the measurement of the electric current has been described in this chapter.

The fourth chapter is devoted to results and discussion. We start by our numerical studies of the nematic order reconstruction inside a π-cell when submitted to a sinusoidal electric field. We present the theoretical time evolution of the biaxiality and electric current for different frequencies and amplitudes of the applied external sinusoidal electric field. We then present our experimental observations and compare them to the theoretical results.

The fifth chapter contains the conclusions of this work.

# 2. Nematic Liquid Crystals

## 2.1. Introduction

Liquid Crystals (LC) are anisotropic fluids in which a certain order in the arrangement of the molecules occurs. They are a mesophase of matter that exhibit intermediate order between that of a crystalline solid, where both positional and orientational order exists, and that of a isotropic liquid, where both the positional and orientational order vanish [1,40].

Liquid crystal materials posses a level of fluidity consistent with the liquid state of matter, but unlike in a fluid, the molecules form a partially ordered system where they tend to align with each other on a macroscopic scale. They are free to move and flow like a liquid, while retaining a degree of orientational and sometimes positional order.

## 2.2. Liquid Crystal Phases

According to the distribution of molecular order, the liquid crystal phases can be classified as:

- Lyotropic liquid crystals form when the phase depends on the concentration of a solvent. The phase transitions occurs when dissolved in a given solvent over a particular concentration range.
- Thermotropic liquid crystals form when the phase depends on the temperature. The phase transition occurs over a particular temperature range.

Currently, most electro optic liquid crystal devices are based on calamitic thermotropic materials in the nematic phase. For this reason, this Thesis will be focus mainly in this kind of liquid crystals.

Calamitic liquid crystals are generally composed of rod-like molecules with one axis longer than the other two and tend to align with their long axes parallel. Calamitic molecules can form a number of mesophases distinguishable from each other, from the liquid and crystal phases by their structure.

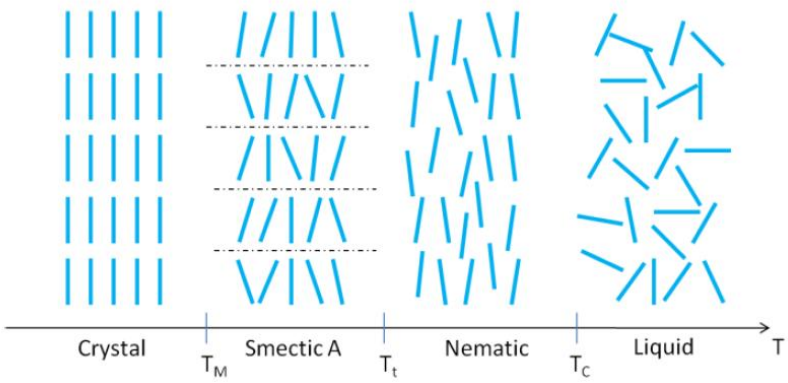


**Fig 2.2.1 Typical liquid crystalline phases between solid and isotropic phases**

Fig 2.2.1, shows a schematic illustration of the crystal, liquid crystal and liquid phases of possible material as the temperature $T$ increases through a melting point ($T_M$), and a clearing point ($T_C$). The crystal phase is characterized by a long-range positional order. For temperatures between $T_M$ and $T_C$, there may be one or more liquid crystal phases. In Fig. 2.2.1, smectic A and nematic phases are separated by a transition temperature ($T_t$). The isotropic liquid present neither positional nor orientational long-range order.

It is possible to divide Calamitic liquid crystals into three classes, depending on their degree of order as, see Fig. 2.2.1:

- Nematics: characterized by the orientational order of the elongated molecules, but the centers of mass of the molecules are randomly distributed throughout the sample. They present the least order phase.
- Smectics: they tend to have an increased degree of order in the direction parallel to the long axis of the molecule causing layers to form in the sample.
- Cholesterics: they are nematic structures characterized by a spontaneous twits. The molecules arrange themselves in a helical structure with its axis normal to the alignment direction.

## 2.3. Nematic Liquid Crystal Order

The nematic liquid crystal phase is the simplest liquid crystalline phase and it is also the most widely used in display industries. In the nematic phase, the molecules have no positional order, but long range orientational order: they tent to orient with their long molecular axis in a preferred direction. There is no long-range correlation between the center of mass of the molecules; that is, they can translate freely while being aligned, on

average, parallel to one another. There is rotational symmetry around the anisotropic axis, which means that the nematic is uniaxial. Under certain condition, it is possible to have a second direction along which the short axes of molecules align and the nematic becomes biaxial.

The molecules in the nematic phase, on average, align parallel to a particular direction defined by the unit vector ***n*** called the director. The order parameter is the quantifying parameter of this orientational order. The direction of the ***n*** vector is arbitrary in space and represents the direction of the optical axis of the system. Since, the axis has no macroscopic polarity, **+*n*** and **–*n*** are equivalent; This equivalence means that no change occurs on turning the molecules upside-down (no ferroelectricity) in an ordinary nematic. Thus if the molecules have an electric dipole there will be as many "up" molecules as "down" ones.

### 2.3.1. Scalar Order Parameter

The orientational order in nematics is usually described by a scalar order parameter, *S*:

$$S = \frac{1}{2}\langle 3cos^2\theta - 1\rangle \qquad \text{[e.q. 2.3.1]}$$

Where $\theta$ is the angle between the long axis of a nematic molecule and the direction ***n***, and the symbol "< >" denotes the average over the orientational distribution function of the nematic molecules. *S* is a numerical parameter which measures how much the molecular long axes deviates from the director. For an isotropic fluid $\langle cos^2\theta\rangle = \frac{1}{3}$ and $S = 0$. For a perfectly ordered sample (all molecules are oriented in the ***n*** direction) $\langle cos^2\theta\rangle = 1$ and $S = 1$. Liquid crystals typically have $0.2 < S < 0.6$ and *S* decreases as the temperature increases [1,40].

### 2.3.2. Tensor Order Parameter

The scalar order parameter is able to correctly describe elastic problems, i.e. the application of an external field (electric, magnetic or mechanic) inducing elastic stress to the fundamental state of the nematic molecules. However, there exist situations in which experimental results cannot be fully described by this classical approach. For systems, where spatial and temporal changes of the nematic order are relevant and biaxial transient nematic configurations arise, require a full Landau-de Gennes **Q**-tensor description [5].

A nematic liquid crystal texture is globally described by the symmetric, second-rank, traceless tensor in the orthonormal basis of its eigenvectors $\{\boldsymbol{e}_1, \boldsymbol{e}_2, \boldsymbol{e}_3\}$

$$\boldsymbol{Q} = \sum_{i=1}^{3} \boldsymbol{\lambda_i e_i} \oplus \boldsymbol{e_i} \qquad \text{[e.q. 2.3.2]}$$

Where $\lambda_i$ are the eigenvalues of **Q** corresponding to the eigenvectors $\boldsymbol{e}_i$, thus obeying the condition $\lambda_1 + \lambda_2 + \lambda_3 = 0$. The eigenvectors $\boldsymbol{e}_1$, $\boldsymbol{e}_2$, and $\boldsymbol{e}_3$ of **Q** are the directions of the preferred molecular orientations and the associated eigenvalues represent the degree of order along each corresponding direction.

## 2.4. Nematic Liquid Crystal properties

The rod-like shape of nematic liquid crystals means that their physical properties are anisotropic; that is, they exhibit different values when measured parallel or perpendicular to the director. This anisotropy is manifested in the dielectric, magnetic, optical and mechanical properties.

### 2.4.1. Elastic properties

Under mechanical stress, liquid crystals deform and try to restore the equilibrium configuration. The lowest energy state for a bulk nematic corresponds to a uniform orientation of the director throughout the material. Boundaries, mechanical stress and external fields can deform the liquid crystal molecular orientation and as consequence molecules tend to restore elastically their equilibrium state: a local restoring torque (elastic torque) arises which opposes to the induced director variations. The deformation of a nematic can be decomposed in three elementary cases [1], illustrated in Fig. 2.4.1.1.

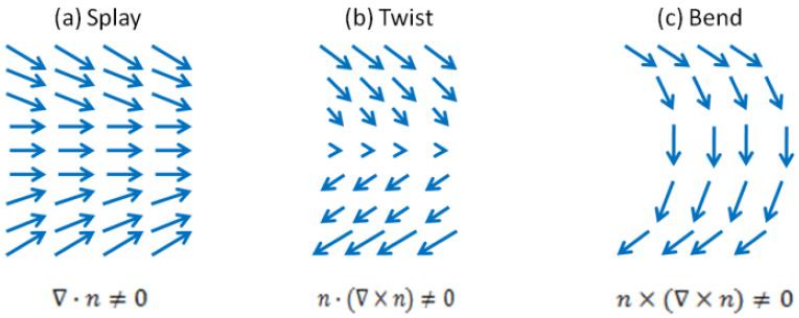


**Fig. 2.4.1.1 Relative orientation of the director in (a) splay, (b) twist and (c) bend distortions and the spatial derivatives associated with each distortion**

The nematic deformation depends on the splay, twist and bend elastic modulus (known as Frank elastic constants), $K_{11}$, $K_{22}$, $K_{33}$, whose dimension is energy/length and hence

Newton (N) in SI units. All three elastic constants assume values of about $10^{-12}$ N in magnitude and generally $K_{33} > K_{11} > K_{22}$.

### 2.4.2. Surface properties

When the nematic molecules are in contact with a boundary surface they tend to align along some direction. This phenomenon can be controlled by using special surface treatments. It has been shown that, when a glass surface coated with a polymer substance is carefully rubbed in one direction, then the molecules tend to line up along the same direction [35]. The rubbing creates an easy direction, direction in which the molecule would most like to lie, in the plane of the surface. When a surface is not rubbed and is very smooth, it may induce molecules to lie parallel to the surface without any preferred direction. Evaporating certain thin films on the surface at an oblique incidence, the same effect can be achieved. Moreover, using suitable materials that attach their polar head on the surface, it is possible to obtain a surface in which the easy direction is normal to the surface.

Another method of preparing a surface alignment is to use photo aligning techniques: they consist in control the nematic orientation on the surface layer by illuminating particular photosensitive polymer films by means of UV polarized light [36].

Three different types of anchoring can be achieved:

- Homogenous (planar) anchoring: the molecules prefer to lie parallel to the preferred direction within the plane of the surface.
- Oblique anchoring: gives a pretilt angle to liquid crystal molecules that is, the end of the molecules is slightly lifted of some degrees to the surface.
- Homeotropic anchoring: the molecules prefer to lie perpendicular to the surface.

### 2.4.3. Viscosity

Viscosity has remarkable effects on the dynamical behavior of nematic liquid crystals: increasing of viscosity at low temperature reduces the possibility of molecules to move. Cinematic and dynamical viscosity can be defined and they are referred to as $\nu$ and $\eta$ respectively. The relationship that relates these two parameter is:

$$\nu = \frac{\eta}{\delta} \qquad \text{[e.q. 2.4.1]}$$

Where $\delta$ is the material density. However, since the major part of liquid crystal material is characterized by a value of $\delta$ around 1 $N_X s^2/mm^3$, a distinction between $\nu$ and $\eta$ is often avoided.

Four viscosity coefficients are required to characterize completely a nematic liquid crystal. Three of these are of translational type $\eta_1$, $\eta_2$, and $\eta_3$ and one is rotational, $\gamma$, where the molecules rotate around an axis that is orthogonal to the director ***n***. The rotational viscosity $\gamma$, is of great importance for optical switching properties of nematics, when nematic molecules reorientate under the effect of an electric field. Typical values of dynamic rotational viscosities of nematics are in the range of 0.02-0.5 Pas.

### 2.4.4. Nematic Coherence length

The nematic coherence length $\xi_N$, is the length over which the nematic order vanishes [1]. When the system is near a phase transition, $\xi_N$ is the order of a few molecular lengths, and it defines the thickness of the transition zone between the nematic phase and the disturbed area. When the nematic phase is close to the nematic-isotropic phase transition, $\xi_N$ increases and can reach mesoscopic values.

$$\xi_N = \sqrt{\frac{L_2}{(a(T_c - T^*))}} \qquad \text{[e.q. 2.4.2]}$$

Where $a$ is defined as $a = \alpha(T - T^*) = \alpha\Delta T$, where $\alpha>0$ ,T* is the supercooling temperature at which the isotropic phase becomes unstable and $T_c$ is the clearing temperature.

### 2.4.5. Electric Coherence length

The electric coherence length is the length which reflects the competition between the elasticity of the liquid crystal and the electric field realignment [1]. The electric coherence length $\xi_E$ is defined as:

$$\xi_E = \frac{1}{E}\sqrt{\frac{K}{\epsilon_0 \Delta\varepsilon}} \qquad \text{[e.q. 2.4.3]}$$

$\xi_E$ is interpreted as the distance over which a local perturbation of the director will relax in space.

### 2.4.6. Biaxial Coherence length

The biaxial coherence length $\xi_b$ is the length over which the biaxial order decays in space inside a calamitic phase. This length depends on temperature and its maximum value ($\xi_b \approx 10^{-2}\mu m$) occurs close to the nematic-isotropic transition temperature [37]. $\xi_b$ depends on the third order term in the Landau-de Gennes potential, $F_t$, [1], which can be written as a Taylor series expansion [e.q.3.3.4].

The biaxial nematic coherence length can be written as follow:

$$\xi_b = \sqrt{\frac{L}{bS_{eq}}} \qquad \text{[e.q. 2.4.4]}$$

Where $S_{eq}$ is the equilibrium scalar order parameter and $L$ is a nematic elastic constant.

### 2.4.7. Nematic Response times

Nematic response time depends on the square of the liquid crystal cell gap and on liquid crystal parameters such as viscosity, dielectric anisotropy, and elastic constants. The response time of a nematic is proportional to $K^{-1}$, as define in equations 2.4.5 and 2.4.6 . A small elastic constant leads to a slow response time. In most nematics $K_{33} > K_{11} > K_{22}$.

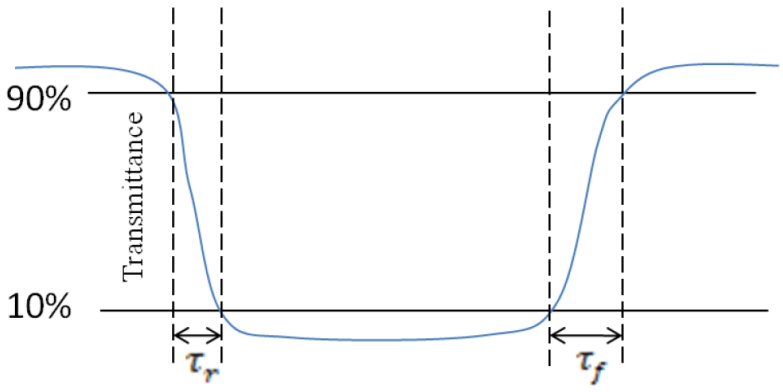


**Fig. 2.4.7.1 Definition of nematic liquid crystal response times**

The rise and fall response times $\tau_r$ and $\tau_f$ for a nematic cell are defined as the time that allows a transition from 10% to 90% transmittance and vice versa. See Fig. 2.4.7.1. They are given by:

$$\tau_r = \frac{\gamma d^2}{\epsilon_0 \Delta\varepsilon V^2 - \pi^2 K} \qquad \text{[e.q. 2.4.5]}$$

$$\tau_f = \frac{\gamma d^2}{\pi^2 K} \qquad \text{[e.q. 2.4.6]}$$

Where γ is the liquid crystal rotational viscosity, $d$ is the liquid crystal cell thickness, $V$ is the applied voltage, $K$ is the liquid crystal elastic constant and $\Delta\varepsilon$ is the liquid crystal dielectric anisotropy. From equation 2.4.5 and 2.4.6, both "field on time" and "field off time" are proportional to γ/K. In addition, the "field on time" depends on the applied electric field. Due to the electric field effect, $\tau_r$ is usually faster than $\tau_f$.

# 3. Numerical and experimental techniques

## 3.1. Introduction

In this chapter, a numerical model is derived from the continuum theory of nematic liquid crystal applicable to one dimensional liquid crystal π-cells submitted to an external sinusoidal electric field. The dynamical behavior of liquid crystal are governed by the Landau-de Genes theory: the evolution of nematic texture is described by a **Q**-tensor model rather than the usual vector field director. The model developed consists of the determination of the unknown coefficients of **Q**-tensor which minimize the free energy of the system, at each time step, for a specific boundary conditions. A finite element method (FEM) based on Galerkin's formulation, that consists on a weak formulation of the weighted energy of the residual of the non linear equations, was implemented in numerical algorithms by using Matlab and Comsol Multiphysics language programs.

In section 3.2 we will describe the **Q**-tensor order definition and its visual representation. In section 3.3 we will discuss about the free energy components of a nematic liquid crystal cell. A set of a system of non linear partial differential equations and boundary conditions which govern the director and electric field will be introduce in section 3.4. and its FEM implementation on section 3.5. In section 3.6 we will describe the equivalent capacitor of a Liquid crystal cell.

The experimental setup and the cell construction procedure will be present on sections 3.7 and 3.8.

## 3.2. Landau-de Gennes: Q-tensor model

A nematic liquid crystal inside a cell is described by the director field $\boldsymbol{n}(z,t)$, along which the degree of orientation is described by the scalar order parameter $S$. Most experimental phenomena are completely described by the classical elastic model described by the Frank-Ossen Theory, where usually $\boldsymbol{n}$ can vary and $S$ is considered practically constant everywhere. This theory is able to correctly describe elastics problems, i.e. the application of an external electric field inducing elastic stress to the fundamental state of the nematic molecules. Within this theory, the director varies continuously over the space, and the

nematic distortion always relaxes back to its initial equilibrium configuration when the external perturbation is removed.

However, when the distortion is very strong and it occurs over a length scale comparable with the nematic coherence length [5], that is the minimum distance over which the nematic molecules are on average aligned along $\boldsymbol{n}$, the molecular order may be significantly altered, as in the case for the electric field induced order reconstruction, and a more complete phenomenological description is required.

We address the problem using a full Landau-de Gennes **Q**-tensor description, in order to fully described the nematic phase where spatial and temporal changes of the nematic order are relevant and biaxial transient nematic configurations arise [1, 8].

The **Q**-tensor is a symmetric traceless rank 2 tensor (3x3 matrix), which can be expressed as:

$$\boldsymbol{Q} = S_1\left(n \otimes n - \frac{1}{3}\boldsymbol{I}\right) + S_2\left(m \otimes m - \frac{1}{3}\boldsymbol{I}\right) \qquad \text{[e.q. 3.2.1]}$$

Where $\boldsymbol{n}, \boldsymbol{m}$ and $\boldsymbol{n} \times \boldsymbol{m}$ are the eigenvector of the **Q**-tensor and the corresponding eigenvalues are $\lambda_1 = (2S_1 - S_2)/3$ , $\lambda_2 = (2S_2 - S_1)/3$ and $\lambda_3 = -(S_1 + S_2)/3$, respectively.

When $S_2 = 0$, the nematic is uniaxial, so the scalar $S_2$ can be interpreted as the biaxial amplitude known as $\beta$ and $S_1$ can be interpreted as the scalar order parameter $S \in \left(-\frac{1}{2}, 1\right)$. When *S=1*, all the molecules are aligned along $\boldsymbol{n}$. When *S=0* the distribution is isotropic and when $S = -1/2$, it is proportional to the projection operator on the plane orthogonal to $\boldsymbol{n}$ so that the distribution is planar isotropic.

In general, the expression of the degree of biaxiality $\beta$ as a function of **Q** is given by:

$$\beta = \sqrt{1 - \frac{6[tr(\boldsymbol{Q}^3)]^2}{[tr(\boldsymbol{Q}^2)]^3}} \qquad \text{[e.q. 3.2.2]}$$

Nematic configurations are fully defined by five degrees of freedom: namely three Euler angles, $\theta$, $\phi$, $\psi$, that define the orientation of the two orthogonal vectors, $\boldsymbol{n}$ and $\boldsymbol{m}$, and the two scalar order parameters $S_1$ and $S_2$. However, when the zenithal angle is $\theta = \pi/2$, the azimuthal angle $\phi$ is undefined and the solution is not unique [22].

To avoid difficulties, the problem can be restate in terms of five independent parameters $q_i$, $i \in [1,5]$, corresponding to the degrees of freedom of a rod-like nematic molecule:

$$\mathbf{Q} = \begin{pmatrix} q_1 & q_2 & q_3 \\ q_2 & q_4 & q_5 \\ q_3 & q_5 & -q_1 - q_4 \end{pmatrix} \qquad \text{[e.q. 3.2.3]}$$

The nematic phase is completely described by its three eigenvalues $\lambda_1$, $\lambda_2$ and $\lambda_3$, and by the corresponding eigenvectors, ***n***, ***k*** and ***l***. Each eigenvalues measure the nematic order along the three orthogonal directions defined by the corresponding eigenvectors.

Fig. 3.2.1 shows the graphic representation of the **Q**-tensor order ellipsoid for a uniaxial splay and bend configuration; each eigenvector represent an axis, and the corresponding eigenvalue represent the amplitude.

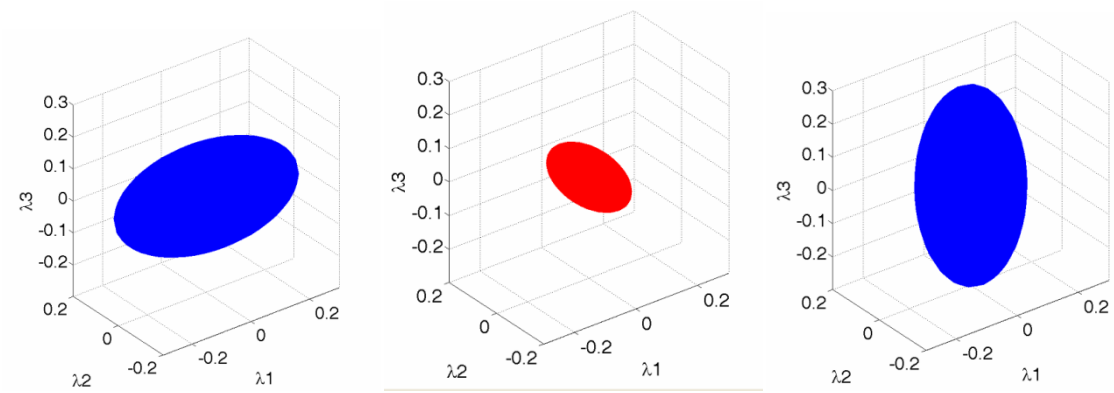


**Fig 3.2.1 Q-tensor order ellipsoid representation for the uniaxial splay configuration (left) , uniaxial bend configuration (right) and the biaxial phase (middle)**

The different nematic phases can be described by means of the **Q**-tensor ellipsoid considering the eigenvalues:

- In the isotropic phase: the **Q**-tensor order vanishes and optically behaves as an ordinary fluid, in this case the three eigenvalues are equal and zero: $\lambda_1 = \lambda_2 = \lambda_3 = 0$.
- In the uniaxial nematic phase: $\lambda_1 \neq \lambda_2 = \lambda_3$; two eigenvalues are equals and **Q** can be written as: $\boldsymbol{Q} = S(\boldsymbol{n} \times \boldsymbol{n} - \frac{1}{3}I)$. If the higher eigenvalue is positive, while the other two are equal an negative: $\lambda_2 = \lambda_3 = -\frac{1}{2}\lambda_1$; resulting in the uniaxial configuration $S_1 = \lambda_1 > 0$ and $S_2 = \lambda_2 - \lambda_3 = 0$; See Fig 3.2.1 (left and right

panel). On the other hand, if the higher eigenvalue is negative while the other two are positive and equal, the resulting uniaxial configuration is $S_1 = \lambda_1 < 0$ and $S_2 = \frac{1}{2}(\lambda_3 - \lambda_2) = 0$.

- In the biaxial nematic phase: all the eigenvalues of the **Q**-tensor are different and two optical axes are present: $\lambda_1 \neq \lambda_2 \neq \lambda_3$; in this case $S_1 = \lambda_1$ and $S_2 = \lambda_3 - \lambda_2 > 0$. See Fig 3.2.1 (middle panel).

## 3.3.Free Energy

The liquid crystal texture stays in a configuration which minimizes its total energy. The free energy of the configuration system consists of terms, each accounting for some physical property of the liquid crystal and its interaction with external effects [1, 38]. The free energy, $\mathcal{F}$, for a sample of liquid crystal can be written as a function of the **Q**-tensor:

$$\begin{aligned}\mathcal{F} &= \mathcal{F}_d(Q,\nabla Q) + \mathcal{F}_t(Q) + \mathcal{F}_e(Q,\nabla Q) + \mathcal{F}_s(Q) \\ &= \int_{\mathrm{V}} f_d(Q,\nabla Q) + f_t(Q) + f_e(Q,\nabla Q)d\mathrm{V} + \int_{\mathrm{A}} f_s d\mathrm{A}\end{aligned} \qquad [\text{ e.q. 3.3.1}]$$

Where $f_d(Q,\nabla Q)$ is the elastic distortion energy density, $f_t(Q)$ is the thermotropic energy density, $f_e(Q,\nabla Q)$ is the electric field induced energy density, $f_s$ is a surface energy density appearing at the cell surface plates and *A* is the boundary surface of the volume *V*. Each of these terms will be described in more detail in the following sections.

### 3.3.1. Elastic distortion energy

The elastic distortion energy density, $f_d(Q,\nabla Q)$, is written as a function of the **Q**-tensor and its spatial derivatives, since any gradients in **Q** would lead to an increase in distortional energy. For nematics, this term is minimized when the director field is in an undistorted configuration. The symmetry of our material does not allow all combination of **Q** derivatives and the most general expression for $f_d$ is [14]:

$$f_d(Q,\nabla Q) = \frac{L_1}{2}\left(\frac{\partial Q_{ij}}{\partial x_k}\right)^2 + \frac{L_2}{2}\frac{\partial Q_{ij}}{\partial x_j}\frac{\partial Q_{ik}}{\partial x_k} + \frac{L_6}{2}Q_{lk}\frac{\partial Q_{ij}}{\partial x_l}\frac{\partial Q_{ij}}{\partial x_k} \qquad [\text{e.q. 3.3.2}]$$

Where $Q_{ij}$ is the $(i,j)$ element of the **Q**-tensor and the elastic parameters $L_1$, $L_2$ and $L_6$ are related to the Frank elastic constants $k_{11}$, $k_{22}$ and $k_{33}$ as:

$$L_1 = \frac{1}{6S_{eq}^2}(k_{33} - k_{11} + 3k_{22}) \qquad \text{[e.q. 3.3.3]}$$

$$L_2 = \frac{1}{S_{eq}^2}(k_{11} - k_{22})$$

$$L_6 = \frac{1}{2S_{expt}^3}(k_{33} - k_{11})$$

It can be demonstrated that there are seven elastic terms of cubic order [15] but only one, $L_6$, include in the Eq.3.3.2, ensures the correct mapping from the **Q**-tensor to the Frank energy and it allows us to remove the $k_{11} = k_{33}$ degeneracy [16].

### 3.3.2. Thermotropic Energy

The thermotropic energy density $f_t$, is used to describe which state the liquid crystal would prefer to be in, i.e. a uniaxial state, a biaxial state or the isotropic state. The thermotropic energy density is expressed as a Taylor expansion truncated at the fourth order around Q = 0 [1]. A fourth-order expansion is sufficient to have the isotropic and the nematic states as local minima of the free energy. It is worth to mention that a sixth-order expansion would be required in order to allow us a stable nematic biaxial state [17].

$$f_t = atr(\boldsymbol{Q}^2) - \frac{2b}{3}tr(\boldsymbol{Q}^3) + \frac{c}{2}[tr(\boldsymbol{Q}^2]^2 \qquad \text{[e.q. 3.3.4]}$$

The coefficients $a$, $b$, and $c$ are in general temperature dependent, although usually, $b$ and $c$ are assumed independent of temperature and only the lowest order material parameter $a$ is taken as $a = \alpha(T - T^*) = \alpha\Delta T$, where $\alpha>0$ and $T^*$ is the supercooling temperature (the temperature at which the isotropic phase becomes unstable) [1]. The values of $a$, $b$ and $c$ can be determined e.g. by fitting expression with experimentally obtained data of order parameter variation with respect to temperature.

For any non positive value $\Delta T$, the equilibrium order parameter $S_{eq}$ of a uniaxial nematic system is given by

$$S_{eq}(\Delta T) = \frac{b}{4c}\left(1 + \sqrt{1 - \frac{24ac}{b^2}}\right) \qquad \text{[e.q. 3.3.5]}$$

### 3.3.3. Electric field energy

The presence of an irrotational electric field, $\boldsymbol{E} = -\nabla U$, gives rise to the electric energy density, which self-induces an internal electric field due to the dielectric and spontaneous polarization effects:

$$F_e = -\int \boldsymbol{D} d\boldsymbol{E} \qquad \text{[e.q. 3.3.6]}$$

Where $\boldsymbol{D}$ is the displacement field and $\boldsymbol{E}$ is the electric field. The constitutive equation which relates $\boldsymbol{D}$, $\boldsymbol{E}$, and the internal polarization $\boldsymbol{P}$ is

$$\begin{aligned} \boldsymbol{D} &= \epsilon_0 \boldsymbol{E} + \boldsymbol{P} \\ \boldsymbol{D} &= \epsilon_0 \boldsymbol{E} + \boldsymbol{P_i} + \boldsymbol{P_s} \\ \boldsymbol{D} &= \epsilon_0 \boldsymbol{E} + \epsilon_0 \boldsymbol{\chi} \boldsymbol{E} + \boldsymbol{P_s} \\ \boldsymbol{D} &= \epsilon_0 \boldsymbol{\epsilon} \boldsymbol{E} + \boldsymbol{P_s} \end{aligned} \qquad \text{[e.q. 3.3.7]}$$

Where $P_i$ and $P_s$ are, respectively, the induced and the spontaneous polarizations. $P_i$ depends on the dielectric susceptibility $\boldsymbol{\chi}$ and on $\boldsymbol{E}$. The quantity $\epsilon_o$ is the vacuum electric permeability constant and $\boldsymbol{\epsilon}$ is the dielectric tensor, which describes the local anisotropy response of the nematic ordering to $\boldsymbol{E}$.

One common expression of $\boldsymbol{\epsilon}$ is [18]:

$$\boldsymbol{\epsilon} = \boldsymbol{\epsilon}_a \boldsymbol{Q} + \boldsymbol{\epsilon}_i \boldsymbol{I} \qquad \text{[e.q. 3.3.8]}$$

Where $\boldsymbol{\epsilon}_a$ and $\boldsymbol{\epsilon}_i$ are, respectively, the anisotropic and isotropic dielectric susceptibilities. $\boldsymbol{\epsilon}_a = \frac{\epsilon_\parallel - \epsilon_\perp}{S_{eq}}$, $\boldsymbol{\epsilon}_i = \frac{\epsilon_\parallel + 2\epsilon_\perp}{3}$ , and $\epsilon_\parallel$ , $\epsilon_\perp$ are the parallel and perpendicular dielectric nematic constants.

The spontaneous polarization is assumed to derive only from flexoelectric effects. Therefore, $P_s$ is written in terms of **Q** as [19]:

$$P_s = \bar{e}\, \nabla \boldsymbol{Q} \qquad \text{[e.q. 3.3.9]}$$

Where the $i_{th}$ component of $P_s$ is:

$$(P_s)_i = \bar{e} \frac{\partial Q_{ij}}{\partial x_j} \qquad \text{[e.q. 3.3.10]}$$

And $\bar{e}$ is the average flexoelectric coefficient, which is expressed as

$$\bar{e} = \frac{e_{11} + e_{33}}{2 S_{eq}} \qquad \text{[e.q. 3.3.11]}$$

Where $e_{11}$ and $e_{33}$ are the splay and bend flexoelectric coefficient of the nematics. Using [e.q. 3.3.6] and [e.q. 3.3.9], the electric density energy $F_e$ can be expressed as:

$$F_e = -\int (\epsilon_0 \boldsymbol{\epsilon} \mathbf{E} + \mathbf{P_s}) d\mathbf{E} = -\frac{\boldsymbol{\epsilon}_0}{2} (\boldsymbol{\epsilon} \boldsymbol{E}) \cdot \boldsymbol{E} - \boldsymbol{P}_s \cdot \boldsymbol{E}$$

$$F_e = -\frac{\epsilon_0}{2} (\epsilon_i |\nabla U|^2 + \epsilon_a \nabla U \cdot \boldsymbol{Q} \nabla U) + \bar{e}\, \nabla \boldsymbol{Q} \cdot \nabla U \qquad \text{[e.q. 3.3.12]}$$

### 3.3.4. Surface energy

The boundary conditions at the liquid crystal interfaces are taken into account by the surface term $F_s$. For rigid anchoring, this is equivalent to impose the Dirichlet condition on the surface:

$$\boldsymbol{Q} = \boldsymbol{Q}_s \qquad \text{[e.q. 3.3.13]}$$

Where $\mathbf{Q}_s$ is the prescribed order tensor promoted by the surface. In this case the boundary conditions are fixed and $F_s$ does not play any role. For weak anchoring, we must take into account the interaction between the nematic molecules close to the substrate and the substrate itself. In this case the form of the interaction energy is given by

$$F_s = \frac{W_s}{2} tr(\boldsymbol{Q} - \boldsymbol{Q}_s)^2 \qquad \text{[e.q. 3.3.14]}$$

Where $W_s$ is the anchoring strength and $\mathbf{Q}_s$ is the value of the tensor order parameter preferred by the surface. Equation 3.3.14 is the generalization of the classical Rapini-Papoular anchoring energy using the tensor formalism [20].

## 3.4. System of dynamical equations

The dynamical equations for calamitic nematic liquid crystals can be determined by means of a variation principle originally put forward by Rayleigh [23]. For a conservative system, this principle asserts that the Rayleigh dissipation function evolves at a minimum rate, relatively to all its virtual values. This results in the balance of energy variations given by [24,25]:

$$\delta \mathcal{D} + \delta \dot{\mathcal{F}} = 0 \qquad \text{[e.q. 3.4.1]}$$

Where $\mathcal{D}$ is the Rayleigh dissipation function and $\dot{\mathcal{F}}$ is the rate of change of the free energy. Brimicombe and Raynes [21] demonstrated both experimentally and theoretically that nematic liquid crystals confined in a $\pi$-cell in a splay symmetric configuration do not

experience backflow during switching to a vertical configuration, due to the symmetry of both states. As a consequence, the dissipation density function $\mathcal{D}$ is expressed in the positive-definite quadratic form of a time derivative of **Q**:

$$\mathcal{D} = \int_V D dV = \int_V \gamma tr\dot{\boldsymbol{Q}} dV \qquad \text{[e.q 3.4.2]}$$

Where V is a volume, and $\gamma$ is related to Leslie's rotational viscosity.

The variation of the dissipation function can be determined from eq. 3.4.2 and its density is

$$\frac{\partial D}{\partial \dot{q}_\iota}\delta\dot{q}_\iota = 2\gamma tr(\dot{\boldsymbol{Q}}\frac{\partial \boldsymbol{Q}}{\partial q_i})\delta\dot{q}_\iota \qquad \text{[e.q. 3.4.3]}$$

Where $\dot{q}_\iota$ is the time derivative of $q_i$.

The rate of the change of the free energy density is

$$\delta\dot{\mathcal{F}} = \left[\frac{\partial F}{\partial q_i} - \frac{\partial}{\partial x_j}\left(\frac{\partial F}{\partial q_{i,j}}\right)\right]\delta q_i \qquad \text{[e.q. 3.4.4]}$$

Considering infinite anchoring strength, and therefore Dirichlet boundary conditions for the liquid crystal, the surface contribution to the energy density is neglected since the boundary conditions are fixed. Assuming summation over repeated indices, the generalized Euler-Lagrange equation, gives the dynamical evolution of the system as a solutions of the PDE equation system:

$$\frac{\partial D}{\partial \dot{q}_\iota} + \frac{\partial F_t}{\partial q_i} + \frac{\partial F_e}{\partial q_i} + \frac{\partial F_d}{\partial q_i} - \frac{\partial}{\partial x_j}\left(\frac{\partial F_d}{\partial q_{i,j}}\right) - \frac{\partial}{\partial x_j}\left(\frac{\partial F_e}{\partial q_{i,j}}\right) = 0 \; i = 1 \ldots 5 \qquad \text{[e.q. 3.4.5]}$$

Summation over repeated indices is assumed, and the subscript "j" denotes differentiation with respect to the spatial coordinate $x_j$ .

Moreover, the electric field **E** inside the cell must satisfy, in the static case with no free charges, the electrostatic Maxwell equations,

$$\nabla \cdot \boldsymbol{D} = 0 \qquad \text{[e.q. 3.4.6]}$$

$$\nabla \times \boldsymbol{E} = 0 \qquad \text{[e.q. 3.4.7]}$$

E.q. 3.4.7 is automatically satisfied, because the electric field is conservative. E.q. 3.4.6 is then the governing equation for the electric potential *U*,

$$0 = \nabla \cdot \boldsymbol{D} = \nabla \cdot (-\boldsymbol{\epsilon}_0 \boldsymbol{\epsilon} \nabla U + \boldsymbol{P}_s) = 0 \qquad \text{[e.q. 3.4.8]}$$

Solving Eq. 3.4.8 is equivalent to minimizing the electric energy density, [e.q. 3.3.12], with respect to *U*. By making the electric potential *U* continuous through the cell, we ensure the standard conditions for the electrostatic: At material boundaries, the component of the electric field parallel to the interface is continuous and the normal component of the displacement field is also continuous. Typically boundary conditions for the potential *U* are (i) fixed voltage on the electrodes; (ii) spatial normal derivative of the potential equal to zero on the outer boundaries of the supporting substrate where no electrodes are present. The first case corresponds to Dirichlet conditions, which are implemented forcing the potential value on the electrodes by matrix operations. Neumann conditions, corresponding to the second case, are naturally satisfied with the finite element method by assuming that the electric energy is totally confined in the liquid crystal material as well as in the substrate regions. In addition to Dirchlet and Neumann conditions on **Q** and *U*, we have also used a periodic boundary condition on the lateral boundaries of the domain.

## 3.5. The Finite Element Method

The system of equations 3.4.5 has been solved by implementing a finite element method (FEM) inside a π-cell submitted to a sinusoidal electric field. The basic idea of FEM is to divide the domain of integration in small sub-regions (elements) and to approximated the solution over each elements by an interpolation of known functions (shape functions) with the unknown weighting coefficients on the nodes of each elements. The unknown coefficients are then determined numerically by minimizing a functional, i.e. [e.q. 3.4.5].

Suppose to divide the study region Ω in M element regions with *N* nodes. The local element has a specific shape (in our 1D case we will use linear elements) and in general each element domain will have *m* nodes and *m* interpolation functions (considering first order interpolation functions) as well. In each element domain (e.g. $e^{th}$ element) the local **Q**-tensor distribution can be interpolated by its *m* local node values using *m* local basic function as:

$$\tilde{q}_i^e = \sum_{j=1}^{m} a_{ij}^e W_j^e \qquad i = 1\ldots5 \qquad \text{[e.q. 3.5.1]}$$

Where $a_i^e$ and $W_j^e$ are the j[th] node value and the interpolation function associated to the $e^{th}$ local element for the $i_{th}$ element of the **Q**-tensor matrix, respectively. The form of $W_j^e$ is well defined, while the symbol $\tilde{q}_\iota$ denotes an approximate solution of $q_i$.

Similarly, the residual $R^e$ in each element domain $\Omega^e$ can be weighted by the element basis functions as

$$R_i^e = \frac{\partial \tilde{D}^e}{\partial q_i} + \frac{1}{\gamma}[F]_{q_i}^e \qquad \text{(i=1,…,5)} \qquad \text{[e.q. 3.5.2]}$$

Where

$$[F]_{\tilde{q}_i}^e = \frac{\partial \tilde{F}_t}{\partial q_i} + \frac{\partial \tilde{F}_d}{\partial q_i} + \frac{\partial \tilde{F}_e}{\partial q_i} - \frac{\partial}{\partial x_j}\left(\frac{\partial \tilde{F}_d}{\partial q_{i,j}}\right) - \frac{\partial}{\partial x_j}\left(\frac{\partial \tilde{F}_e}{\partial q_{i,j}}\right) \qquad \text{[e.q. 3.5.3]}$$

The exact solution occurs only when $R_i^e$ is equal to zero for each element. Due to the above approximation, the residual always leads to a nonzero value.

The residual $R_i^e$ can be minimized in each element by weighting it by the interpolation functions $W_i^e$ that are the same shape functions used to interpolate $\tilde{q}_i^e$ (Galerkin's method) , as:

$$\int_{\Omega_e} R_i^e \, W_i^e \, d\Omega^e = 0, \qquad i=1,\ldots,5 \text{ and } j=1,\ldots,m. \qquad \text{[e.q. 3.5.4]}$$

Substituting $\tilde{q}_i^e$ in the above equation and expanding it with a time difference scheme leads to

$$(q_i^e)^{t+\Delta t} = (q_i^e)^t + \Delta t [A^e]^{-1}(b^e), \qquad i=1,\ldots,5 \qquad \text{[e.q. 3.5.5]}$$

Here […] denotes a matrix and (…) denotes a vector. For the $i_{\text{th}}$ element of the tensor order parameter, one obtains that

$$A_{lm}^e = \int_{\Omega_e} W_l^e W_m^e d\Omega^e \qquad \text{[e.q. 3.5.6]}$$

$$b_m^e = -\int_{\Omega_e} \frac{1}{\gamma}[F]_{\tilde{q}_l}^e W_m^e d\Omega^e \qquad \text{[e.q. 3.5.7]}$$

As a result, the matrix $A^e$ is symmetric, and its element values depend only on the geometry and the interpolation functions. $A^e$ only needs to be calculated at the first iteration step and can be stored for the subsequent iteration steps. By applying the assembling process typical of a FEM procedure, the global matrix $A$ and the global vector $b$ can be obtained from the element matrix $A^e$ and the element vector $b^e$.

## 3.6. Liquid crystal cell equivalent capacitor

The electrical behavior of a liquid crystal cell can model as a parallel circuit of a resistor and a capacitor [29]. The resistance and capacitance values depend on the cell dimensions and liquid crystal material. The resistance value is normally high and can be consider constant but, because of the liquid crystal dielectric anisotropy, the capacitance value depends on the applied electric field, which modifies the liquid crystal molecules tilt angle.

Because of the liquid crystal permittivity behavior with temperature, the equivalent capacitance value depends not only on the applied electric field, but also on the environmental temperature.

In our work, we assume that the cell contains no free charges and that its conductivity is effectively zero [3]. For this reason, we will approximate the electric response of the nematic liquid crystal cell as a variable capacitor; neglecting the parallel resistor.

It is known, that the equivalent capacitor $C_{lc}$, it is proportional to the pixel area, and the effective dielectric constant of the liquid crystal. Also it is inversely proportional to the thickness of the cell, *d*:

$$C(t) = \frac{A}{d} * \langle \bar{\bar{\varepsilon}}_{Lcd} \rangle_E \qquad \text{[e.q. 3.6.1]}$$

Where, *A* is the area of the liquid crystal cell, *d* is the π-cell thickness , $\langle \bar{\bar{\varepsilon}}_{\mathrm{Lcd}} \rangle_{\mathrm{E}}$ is the effective dielectric constant of the liquid crystal, that depends on the applied electric field *E*. The dielectric properties of a liquid crystal capacitor is determined by the average orientation of the director of the nematic liquid crystal molecules. In this case, the vertically applied electric field reorients the liquid crystal molecules along its direction, thereby changing the apparent dielectric constant of the cell from the lower value $\varepsilon_\perp$, that corresponds to the starting splay configuration, to the higher vale $\varepsilon_\parallel$, that corresponds to the final bend configuration.

The effective dielectric constant of a liquid crystal cell can defined as:

$$\langle \bar{\bar{\varepsilon}}_{Lcd} \rangle_E = \frac{1}{d} \int_0^d \frac{1}{\bar{\bar{\varepsilon}}(z,t)} dz \qquad \text{[e.q. 3.6.2]}$$

For a 1-D approximation,

$$\bar{\bar{\varepsilon}}(\mathrm{z},\mathrm{t}) = \varepsilon_0(\Delta\varepsilon^*(-\mathrm{q}_1(\mathrm{z},\mathrm{t}) - \mathrm{q}_4(\mathrm{z},\mathrm{t}) + \varepsilon_{\mathrm{iso}}) \qquad \text{[e.q. 3.6.3]}$$

Where, $\Delta\varepsilon^* = \frac{\Delta\varepsilon}{\mathrm{Seq}}$ is the scaled dielectric anisotropy; $\varepsilon_{\mathrm{iso}} = \frac{\varepsilon_\parallel + 2\varepsilon_\perp}{3}$ is an average permittivity. $\varepsilon_\parallel$ and $\varepsilon_\perp$ are the permittivities parallel and perpendicular to the molecular axis z. $S_{eq}$ is the equilibrium order parameter, defined as [e.q. 3.3.5].

From [e.q. 3.6.1] and [e.q. 3.6.3], one can obtain the total liquid crystal equivalent capacitor:

$$C_{lc}(t) = \frac{\varepsilon_0 A}{d} \frac{1}{\frac{1}{d}\int_0^d \frac{1}{\varepsilon_0(\Delta\varepsilon^*(-q1(z,t)-q4(z,t)+\varepsilon_{iso})} dz} \qquad \text{[e.q. 3.6.4]}$$

From e.q. 3.6.4, the equivalent capacitor depends on the **Q**-tensor elements $q_1$(z,t) and $q_4$(z,t).

We can use a generalization of Deuling's argument [33] to calculate the electric current flowing across the cell, assuming that the cell does not contain free charges and that its conductivity is effectively zero (i.e. dielectric regime).

We obtain the current density through the cell as:

$$J = \frac{1}{d}\frac{d}{dt}(U.\langle\bar{\bar{\varepsilon}}_{Lcd}\rangle_E) \qquad \text{[e.q. 3.6.5]}$$

## 3.7.Cells construction

In section 4.2 we show experimental results of our investigations on the modulated electric field induced order reconstruction in π-cell. The main experimental investigations were performed measuring the electric current flowing through the sample when connected in series with a electric resistance and a sinusoidal electric power, see Fig 3.8.1. In this section we explain the principles of cells construction used for our investigations. All experiments in this thesis have been carried out by using the cell geometry presented in Fig 3.7.1.

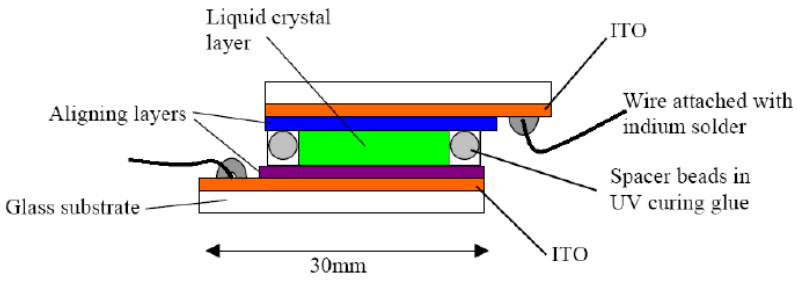


**Fig 3.7.1 Schematic diagram of a typical liquid crystal cell**

The nematic layer is contained between two glass substrates: on the inner surfaces of these substrates is deposited an optically thin layer of Indium Tin Oxide (ITO), which acts as a transparent electrode, on top of which there is an aligning layer. The cell fabrication process was always carried out in a clean room environment to minimize the risk of the structure being contaminated by dust. The glass substrates have 1.1mm thickness, and 30mm length and 20mm width. The transparent ITO electrodes are pre-deposited on the

glass substrates and have a resistivity of about 50Ω. Aligning layers to promote a particular alignment direction at the two surfaces are deposited onto the ITO.

### 3.7.1. Photolithography: pixels processing

To manufacture the pixels (to obtain select lines) the ITO layer was pattern with photolithography.

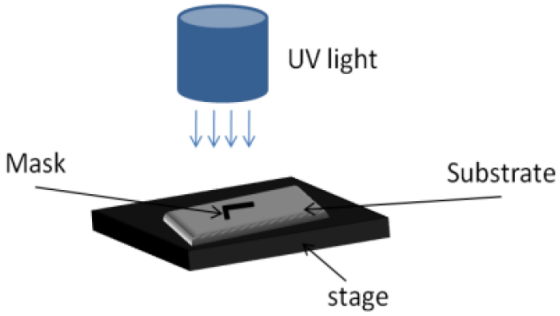


**Fig. 3.7.1.1 Resist process treatment by UV**

The procedure start by cleaning the substrate: the cleaning is done by spraying distilled water and then by spinning to dry the surface. After that, a puddle of resist is put on the center of the substrate, followed by spinning, that is, the substrate holder is rotated at high speed in order to spread the resist on all the surface to obtain a thin film.

The resist is exposed to UV radiation: the mask (containing a master copy of the pattern) is put on the substrate and an optical system projects the pattern from the mask, see Fig. 3.7.1.1. The developing of the photoresist is done by immersion of the substrate in the developer MF-321. The etching step removes the conductor where the photoresist has been developed creating the conductive stripes for pixels. The ITO layer is wet etched in an acid solution. The cleaning steps in the photolithography process are performed by spraying distilled water on the substrate, followed by drying with hot air.

### 3.7.2. Alignment techniques: Rubbed Polyimide

It is known [10, 11], that it is possible to orient the liquid crystal on a rubbed surface. Generally, the rubbing of an inorganic polyimide leads the polymer chains to be stretched and oriented along the rubbing direction. There chains also impose the orientation of the liquid crystal at a certain tilt angle [12]. In this thesis, the polyimide used for this technique was LQ1800 dissolved in 1-metyl-2-pyrrolidinone with concentration 20%. The alignment

related process consists of coating, baking, and rubbing of the polyimide LQ1800 is spin coated onto glass substrates at 3000rpm for 120s. This produced a uniform layer on the substrate. After spin coating, the obtained film is baked in the oven at 140°C for 60 minutes, followed by others 60 minutes at 250°C to evaporate the solvent completely and to iridize the polyamide acid to make a hard thin film. After the backing procedure, the polymer is cooled.

The polyimide surface is then buffed using a rubbing machine, composed of a velvet cloth attached to a rotating drum, under which the substrate moves. The rubbing pressure is adjusted by changing the gap between the cylinder and the substrate. The glass substrates are fixed to the stage by air suction. The rubbing direction on the substrate can be controlled by rotating the plates on the stage. The stage moves back and forward at a constant velocity and after the entire area is buffed, the cylinder moves away, and the stage returns to the initial position. The controllable parameters of the rubbing machine are the gap between the substrate and the cylinder, the cylinder rotation speed, the stage movement velocity, and the number of times each substrate goes through the rubbing process.

### 3.7.3. Cell assembling

A cell is assembled by putting spacer beads, immersed in a UV glue, on the edge of the two sandwiched substrates. It is then exposed to a UV lamp for 45 minutes to cure the glue. The thickness of the cell depends on the diameter of the beads. The assembling of the two substrates is either parallel or antiparallel with respect to the rubbing direction.

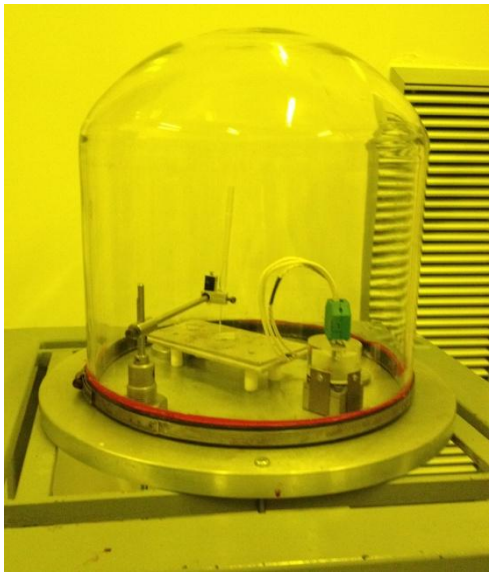

Fig. 3.7.3.1 Filling process in a vacuum chamber

When the cell is dried, we filled the cells in the vacuum chamber by capillarity on a heat-stage held at a temperature above the isotropic transition point of the nematic, see Fig. 3.7.3.1. Once filled, the cell is cooled to room temperature. Finally, we attached wires at the exposed ITO surfaces using an indium solder to allow to apply an electric field perpendicular to the substrates.

### 3.7.4. Pretilt angle measurement

The pretilt angle was measured at room temperature in anti-parallel rubbed cell. We have used the rotating crystal method [13]. It is based on measurement of the optical phase shift as a function of rotation angle. Fig. 3.7.4.1, shows the experimental setup.

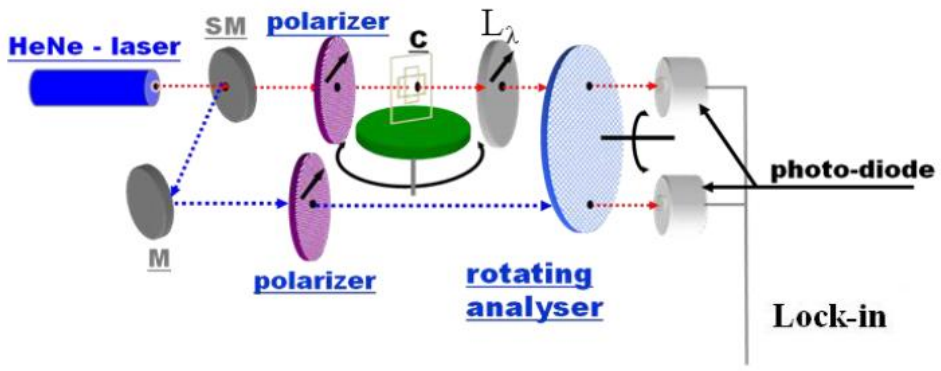


Fig. 3.7.4.1 Pretilt angel measurement experimental setup

The incident beam from a He-Ne laser (λ = 632 nm) is split by a semi-silvered mirror SM into two beams (reference and signal). The reference beam passes through a linear polarizer with its axis at 45° with respect to the optical axis of the sample. The signal beam also linearly polarized parallel to the reference beam, passes through the sample and then through a quarter wave (λ/4) plate $L_\lambda$. Both the signal and the reference impinge on a rotating analyzer (rotation frequency 90Hz) and are recorded by two photodiodes connected to a lock-in amplifier which measures the phase difference.

The experimental optical path difference measured for a scan of the incidence angle φ from -30° to 30° is fitted by the equation 3.7.1, using d and $\theta_s$ as unknown variables [13].

$$\delta = \frac{2\pi d}{\lambda}\left(\frac{n_o^2 - n_e^2}{n^2} sin\theta_s cos\theta_s sin\varphi + \frac{n_o n_e}{n^2}\sqrt{n_e^2 - sin^2\varphi} - \sqrt{n_o^2 - sin^2\varphi}\right) \quad \text{[eq. 3.7.1]}$$

$$n^2 = n_o^2 cos^2\theta_s + n_e^2 sin^2\theta_s$$

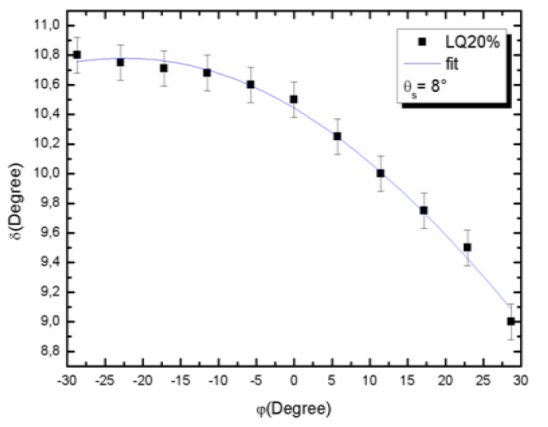


**Fig. 3.7.4.2 Phase shift δ as a function of the rotation angle φ for a rubbing LQ1800 (20%)**

Where $n_o$ and $n_e$ are respectively the ordinary and extraordinary optical refraction index of light, $\theta_s$ is the pre-tilt angle, $d$ the cell thickness and $\varphi$ the incidence angle. Fig. 3.7.4.2, show the optical phase shift δ as a function of the rotation angle $\varphi$. The pre-tilt angle of LQ20% is 8° with respect to the surface plane.

## 3.8. Experimental Set up

We built a π-cell by using two plates already covered with Indium Tin Oxide (ITO) film. The ITO electrodes were patterned by a photolithographic treatment to make on each plate two ITO strips. The strips on the two plates assembled to form four regions each one has an area of about $1mm^2$. The oblique symmetrical anchoring on the two plates was attained

by spin coating using a solution 20% of polyamide acid LQ1800 (from Hitachi) in 1-methyl-2-pyrrolidione and rubbing in parallel direction. The cell thickness was fixed *d*=2,5 µm by spacers at the board of the pixel and the pre-tilt angle of this fabricated cell was approximately 8°. The cell was filled with the nematic liquid crystal 5CB (from MERK) by capillarity in a vacuum chamber in isotropic phase. The cell was placed under polarizing optical microscope between crossed polarizer in such a way that the director projection onto the glass was parallel to the axis of the polarizer. Optical images were acquired with a charge-coupled device CCD camera.

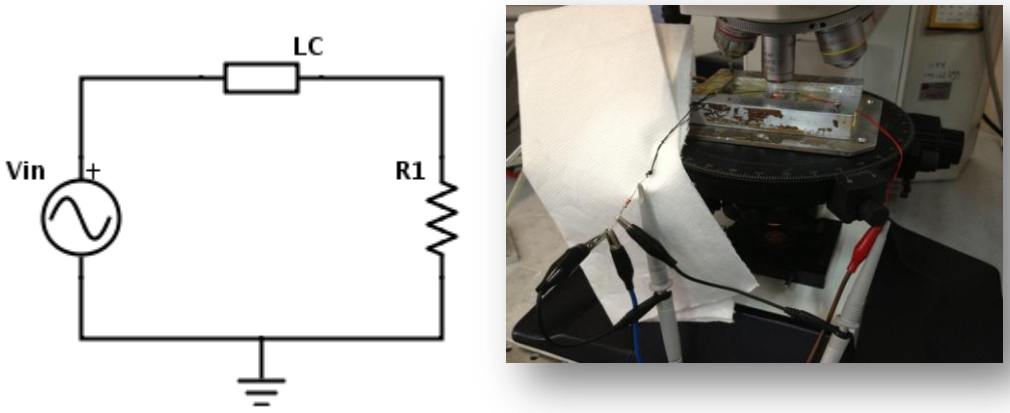


**Fig 3.8.1 Experimental Electric circuit**

Fig 3.8.1 shows the experimental electric circuit set up used for the electric current measurement. A modulate voltage, $V_{in}$, was applied to the cell which was connected in series with a 10kΩ electric resistance, $R_1$: its voltage "*Vr*" allows to measure the electric current that flows through the sample. The electric current was measure from the voltage across the resistor by means of a digital oscilloscope (Agilent infiniium 54830D MSO 1GHz, 4GSa/s). The electric current data was process later on by using Matlab program routine.

# 4. Results and discussions

In this chapter we present our results of the induced biaxial distortion inside a π-cell when submitted to a sinusoidal electric field. In the first section, we discuss about the theoretical time evolution of the biaxial distortion induced in a nematic π-cell submitted to an external sinusoidal electric field. For symmetric and asymmetric cases; We will show that the induced biaxial distortion presents a modulation similar to that of the applied signal. In fact, we have observed both numerically and experimentally, that the induced biaxial distortion inside the cell, is related to the applied field frequency and amplitude, presenting an oscillatory behavior.

Furthermore, when the applied signal period is smaller than the nematic relaxation time, the order reconstruction will take place after a suitable number of undulations such that the accumulated distortion inside the cell reach the necessary energy. At last, we will present an study of the dynamical electric field threshold dependency on the applied frequency.

In the second part, we discuss our numerical and experimental observation of the electric current flowing across an electrical resistor connected in series with a nematic π-cell when submitted to an external sinusoidal electric field. We found that the induced biaxial distortion inside the cell, will reflex on the electric current, creating different shape's distortions.

## 4.1 Biaxial Order Reconstruction induced by sinusoidal electric field

### 4.1.1. Introduction

In order to better understand the order reconstruction in a π-cell submitted to an external electric field, a numerical model, based on finite element method [6, 42, 43], has been developed. A π-cell of 1 μm thickness has been discretized with one-dimensional elements with Dirichlet anchoring conditions on the boundary plates. The time-dependent nematic configuration is the solution of the five coupled Euler-Lagrange equations [e.q. 3.4.5] joined with an additional partial differential equation [e.q. 3.4.8] for taking into account the effect of the applied sinusoidal electric field, $V_{in}(t)$ [e.q. 4.1.1]. In particular the sinusoidal electric field has been modeled with the following equation:

$$V_{in}(t) = Usin(2\pi ft) \qquad \text{[e.q. 4.1.1]}$$

where the frequency, *f*, varies in a range $f$ [1kHz, 100kHz], and the amplitude, *U*, assumes values between [4V , 30V]. The electric field is applied perpendicularly to the cell, along the *z-axis*, and its time duration is fixed to $\tau$= 1ms. The time step size used for the minimization of the system of equations [e.q. 3.4.5] was δt=0.1μs. Moreover an adaptive mesh technique has been used in order to discretize the one-dimensional domain of integration: a finer mesh around the biaxial region (minimum element size was set to 0.1nm) and coarser in the rest of the domain (with a maximum mesh size of 10nm). For a symmetric π-cell, the initial splay configuration is obtained fixing the lower surface angle to $\theta_l$=10° and the upper surface angle to $\theta_u$=-10°; $\theta$ is measured with respect to the surface. For asymmetric π-cell, the initial splay configuration is obtained fixing the lower surface angle to $\theta_l$ = 10° and varying the upper surface angle from 0° to -10° in steps of 1°.

### 4.1.2. Biaxial distortion induced by a sinusoidal electric field

#### *4.1.2.1 Biaxial undulations*

An electric field applied perpendicular to a π-cell forces the nematic molecules to reorient, parallel to the applied field and perpendicular to the boundary plates ($\Delta\varepsilon a>0$). Due to boundary conditions, the nematic molecules align everywhere parallel to the electric field except for three thin regions: one in the middle of the cell and two on the surface layers, where, for strong anchoring conditions, the nematic director keeps its initial quasi-planar orientation. The maximum distortion arises in the center of the cell: a biaxial region of thickness comparable with the biaxial coherence length $2*\xi_b$ starts growing to connect the homeotropic upper and lower textures with the central planar orientation.

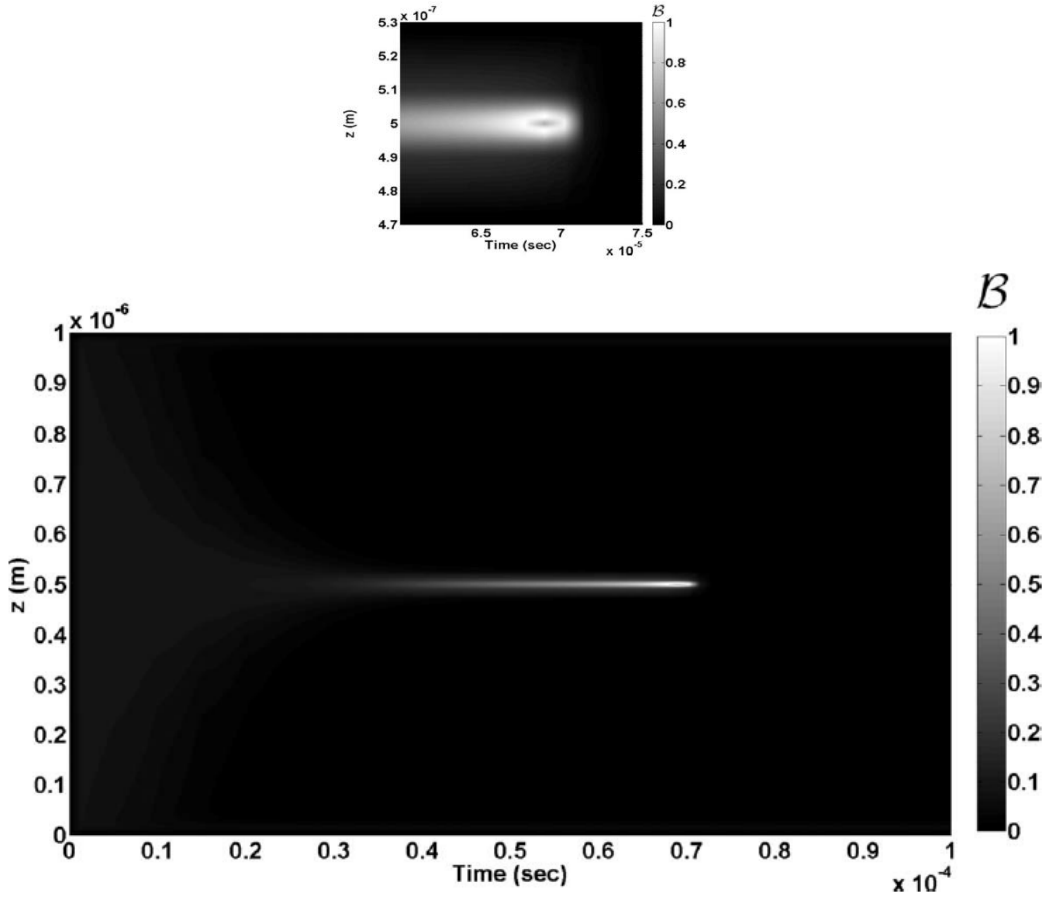


**Fig. 4.1.2.1 One-dimensional dynamical representation of biaxiality inside a π-cell submitted to an external rectangular electric pulse and an enlargement of the figure around t= 70μs [6]**

It has been proved [6] that for a rectangular electric field, the temporal evolution of the induced biaxial order behaves as shown in Fig. 4.1.2.1. The white color represents the maximum value of the biaxiality, $b = 1$, while the black color corresponds to $b= 0$. All the

other possible values of biaxiality are linearly mapped as gray levels between white and black.

The biaxiality remains almost equal to $b=0.1$ close to the boundaries plates where the strong anchoring prevents reorientation and it grows in the center of the cell where a biaxial wall is formed. At t=70μs the nematic configuration in the center of the cell becomes purely biaxial with $b=1$ and the transition to the bend texture takes place, see also the enlargement of Fig. 4.1.2.1 (top panel), at around t =70 μs . The biaxial region surrounding the center has a size comparable with $2*\xi_b$ and looks like the crater of a volcano, where b is zero inside and around the crater [6, 30, 42].

The focus of this work is to study the order reconstruction phenomenon when a sinusoidal electric field is applied to a nematic π-cell. We have observed that the resulting distortion is no longer continuous, as shown in Fig. 4.1.2.1, but it presents a modulation which is two times the frequency of the applied sinusoidal electric field, as shown in Fig. 4.1.2.2.

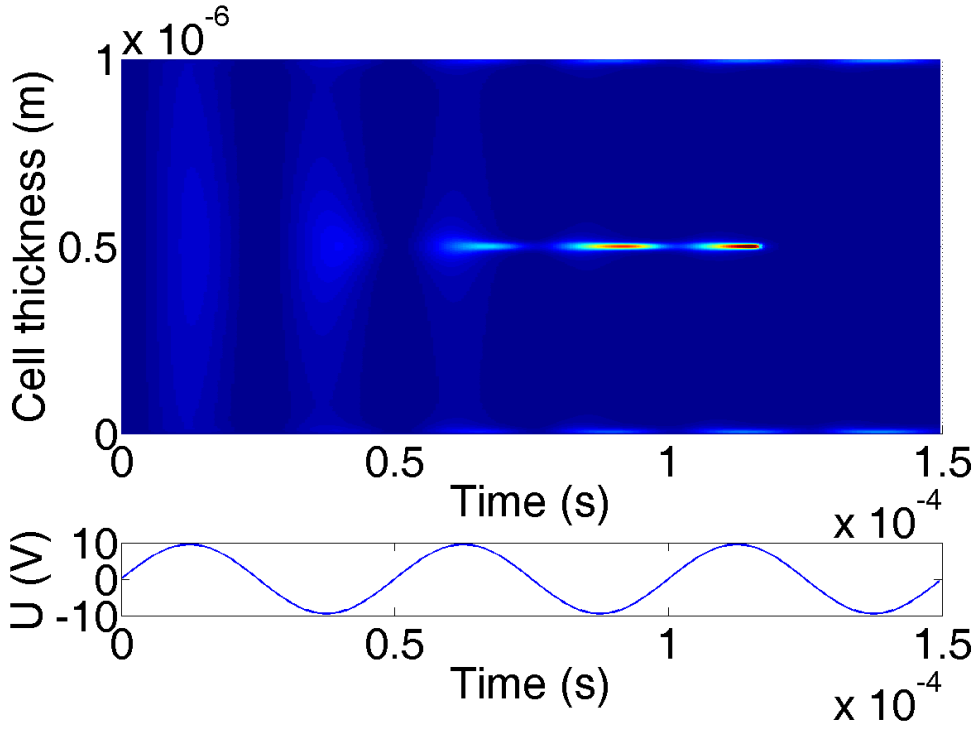


**Fig. 4.1.2.2 Top panel: One – dimensional dynamical representation of biaxiality inside a π-cell submitted to an external sinusoidal electric pulse. For *f*=20kHz and *U*=9.5V, cell thickness *d*=1μm. Bottom panel: applied sinusoidal electric field**

Fig. 4.1.2.2 shows a typical one-dimensional temporal evolution of the induced biaxial order inside a π-cell submitted to an external sinusoidal electric field, with frequency *f* =

20kHz and amplitude $U$= 9.5V. The red color represents the maximum value of the biaxiality, $b$=1, while the blue color corresponds to $b$=0. All other possible values of biaxiality are linearly mapped between red and blue.

The transient biaxial undulations depend on the amplitude and frequency of the applied field. One can observe that each maximum magnitude of the applied signal correspond a maximum biaxial distortion in the middle of the cell. Moreover, the induced biaxial distortion will grow and will vanish above a certain amplitude value, thus creating biaxial undulations.

Close to the boundaries, where the strong anchoring prevents reorientation, the maximum value of $b$ is 0.35. The biaxial undulations at the boundaries remains as long as the electric field is applied.

In the middle plane, the induced distortion increase at each half cycle of the external electric field. The first two undulations are spread along the cell thickness. From the third undulation the distortion concentrates in the middle plane of the cell. The last biaxial undulation, when the order reconstruction takes place, behaves similar to the induced biaxiality in the case of a rectangular electric pulse, that is, presents a volcano-structure comparable in size with the biaxial coherence length, $2*\xi_b$, where $b$ is zero inside and around the crater.

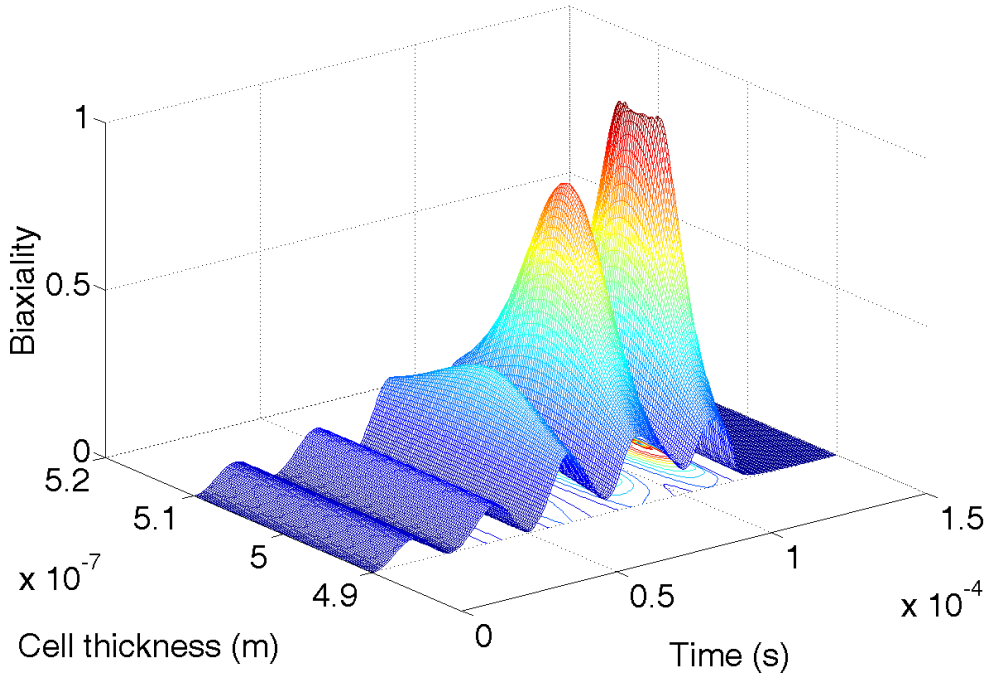


**Fig. 4.1.2.3 3D - Enlargement of Fig. 4.1.2.2, around z ϵ [0.49µm, 0.51µm] and t ϵ [0, 0.150ms]. Dynamical representation of biaxiality inside a *π*-cell submitted to an external sinusoidal electric pulse for *f*=20kHz and *U*=9.5V. Cell thickness *d* = 1µm**

In the center of the cell, due to the signal periodicity, in each undulation the electrically induced textural distortion has not time to be fully recovered and it is accumulated in subsequent periods. The resulting effect is that when the accumulated distortion is so high, the nematic phase reduces its symmetry by the appearance of biaxial order to lowering the distortion.

In fact, evaluating the relaxation time for the nematic phase to recover the elastic distortion, we obtain $\tau_f$= 1.1 ms [e.q. 4.1.2.1]. In this work, the applied sinusoidal electric field has been evaluated for a frequency range $f \epsilon$ [1kHz, 100kHz]. The period value for these frequencies goes from $T$= 1ms for $f$=1kHz, to $T$=0.01ms for $f$=100kHz, all periods smaller than the nematic relaxation time, $\tau_f$. In the case $f$ = 1kHz, where the signal period is close to the nematic decay time, the accumulation rate is expected to be low, since the molecules has enough time to release the induced energy before the appearing of the next oscillation.

The following equation was applied to calculate the nematic relaxation time:

$$\tau_f = \frac{\gamma_1 d^2}{\pi^2 K} \qquad \text{[e.q. 4.1.2.1]}$$

Where $d$ is the cell thickness, $\gamma_1$ is related with Leslie's rotational viscosity and $K$ is a mean value of the bend and twist Frank elastic constant. Estimated values for the material parameter can be obtained from literature [1, 7, 38]: $K$≈3-12N, $\gamma_1$≈0.1Pa. We consider $d$=1μm.

#### 4.1.2.2 Stored Distortion Energy: Q-tensor eigenvalues time evolution

The evolution in time of the distortion energy could be analyzed by studying the temporal evolution of the eigenvalues of the **Q**-tensor order in the center of the cell, as shown in Fig. 4.1.2.4 for $f$ = 20kHz and $U$= 9.5V. Assuming that the **Q**-eigenframe corresponds to the laboratory frame of reference, then $\lambda_1$, $\lambda_2$, and $\lambda_3$ are associated with the eigenvector pointing along the $x$, $y$ and $z$ directions respectively.

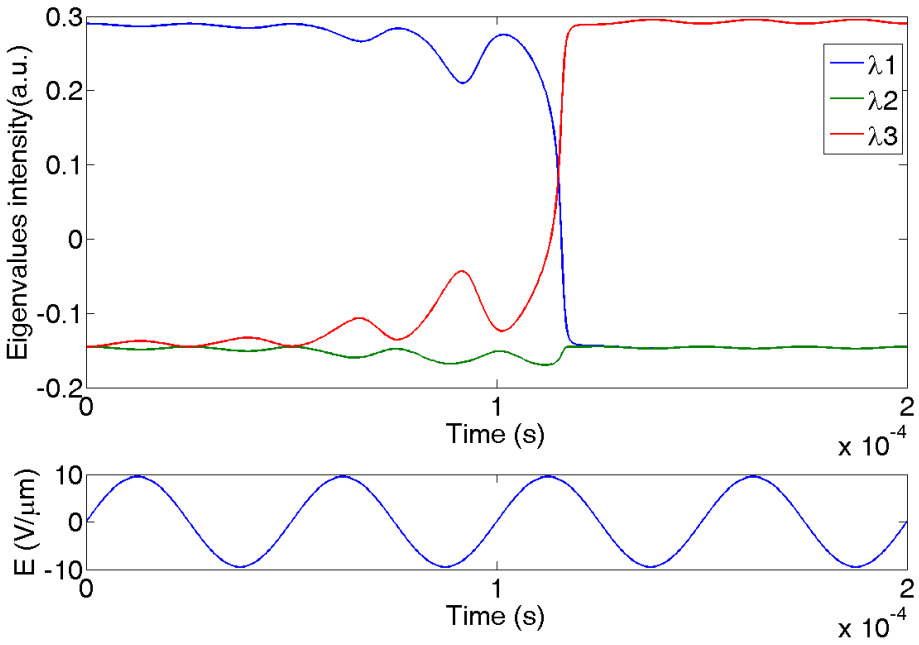


**Fig. 4.1.2.4 Temporal evolution of the eigenvalues $\lambda_1$,$\lambda_2$ and $\lambda_3$ of the Q-tensor order in the center of the cell ($d$=1μm), for the investigated sinusoidal electric field, $f$=20kHz, $U$=9.5V in the time interval 0<t<0.2ms**

In Fig. 4.1.2.4, at t= 0, the largest eigenvalue $\lambda_1$, indicates that, in absence of applied fields, the nematic director lies, on average, along the $x$-direction, parallel to the cell plates and perpendicular to the $z$-axis. Applying a vertical sinusoidal electric field with frequency $f$ = 20kHz and amplitude $U$= 9.5V, $\lambda_1$ starts to decrease and at the same time, $\lambda_3$ starts to

increase, as expected from literature [3]. We can observe that the order reconstruction takes place at t=0.115ms, when $\lambda_1$ and $\lambda_3$ exchange.

It is worth noting that at t > 0, $\lambda_2$ starts to decrease and its sign is opposite to $\lambda_3$. In fact by algebra definitions [31], it is known that for a traceless tensor, the sum of its eigenvalues must be zero, $\lambda_1 + \lambda_2 + \lambda_3 = 0$. This behavior, though present, is not so evident for the rectangular electric pulse case [3]. The physical meaning is that the system tries to compensate the biaxial distortion. In fact, $\lambda_1$ and $\lambda_3$ are, respectively, the eigenvalues along the *x* and *z*-axis. They respond directly to the applied field influence, while $\lambda_2$ tries to maintain the minimal energy configuration opposing the other two eigenvalues variations. This is clear in Fig. 4.1.2.4 for all the considered time interval, even after that the order reconstruction takes place.

Furthermore, the time evolution of the eigenvalues follows a sinusoidal behavior; that is, their maxima variations correspond in time to the maxima and minima of the applied sinusoidal signal. For the tensor symmetric reflection, the eigenvalues variation increases at each half cycle. In fact, in nematic materials $\boldsymbol{n}$=$\boldsymbol{-n}$, where $\boldsymbol{n}$ is the nematic director.

Fig. 4.1.2.4 also shows the progressive accumulation of the distortion energy in the middle plane of the cell. During the first cycle of the applied electric field, the stored energy is low and all the eigenvalues $\lambda_1$, $\lambda_2$ and $\lambda_3$ practically return to their original value at t=0. Starting from the second cycle, they do not return to their initial values, instead their variation increases due to the accumulation of energy distortion inside the system.

### 4.1.3. Biaxial Order Reconstruction: Sinusoidal Electric Field Threshold, Eth

The application of a sinusoidal electric field on a symmetric π-cell induces for each oscillation a nematic distortion which increases over time, as discussed in the previous section. The stored distortion energy increases with time and when the distortion is strong enough and the induced electric coherence length, $\xi_E$, is comparable with the biaxial coherence length, $\xi_b$, the distortion is lowered by the biaxial order reconstruction and the splay-bend transition occurs.

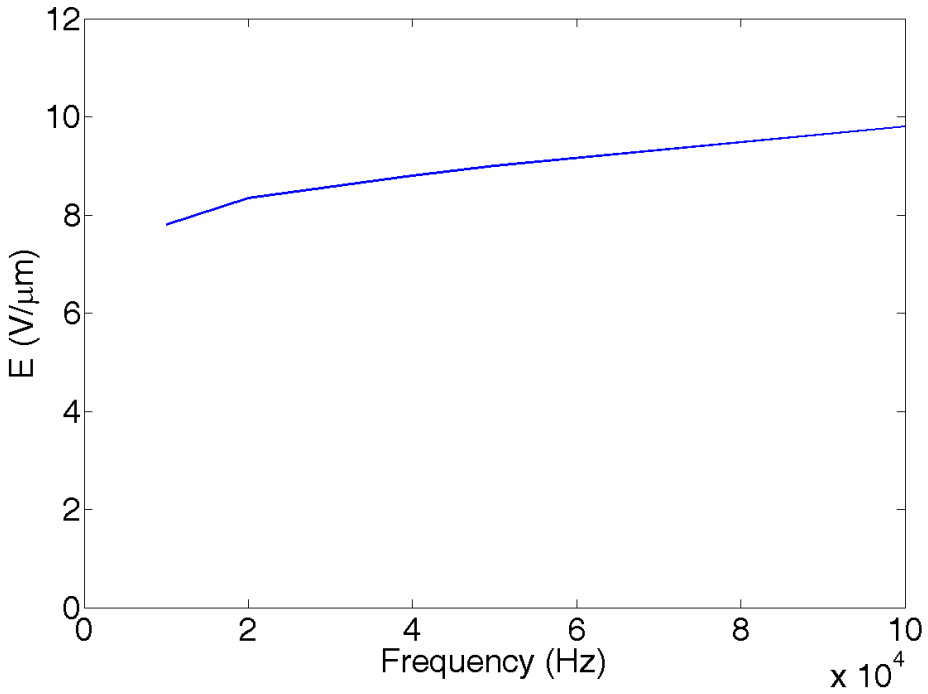


**Fig. 4.1.3.1 Numerical $E_{th}$ versus frequency $f$ for a π-cell**

Figure. 4.1.3.1 shows the numerical order reconstruction threshold data $E_{th}$ as a function of the applied frequency, $f$. For higher $f$, an increase of $E_{th}$ is observed. Hence, the electric field threshold will depend on the applied frequency and amplitude. As at higher frequencies correspond shorter time periods, a slightly higher $E_{th}$ is required to reach the necessary distortion energy in the cell and hence to concentrate enough biaxial order in the middle plane to induce the order reconstruction as explained in the following.

The oscillating electric field has two maxima of intensity for each period. The electric field induces the nematic distortion in the cell and this distortion is largest when the field intensity is at its maximum. Therefore also the nematic distortion oscillates with two maxima for each period of the sinusoidal external electric field. The sinusoidal behavior of

the electric field allows an elastic relaxation of the nematic texture between two maxima of the electric intensity and hence the excitation of the nematic matrix follows an alternation of increasing induced distortions, when the electric field grows, and spontaneous visco-elastic relaxations, when the field intensity decreases, with a period which is two times the period of the electric sinusoid. As the visco-elastic relaxation time is about 1 ms, at $f$=1 kHz we do not observe any distortion energy storing. The system has enough time to relax all the distortion induced by a semiperiod of the electric sinusoid. As the frequency of the external electric field increases, the semiperiod is shorter and for a fixed amplitude of the electric field, the electric energy furnished in a semiperiod to the system decreases. The storing effect allows to reach the order reconstruction threshold for frequencies $f$ >1 kHz at longer times if enough oscillations take place. Even if helped by the energy storing effect, the electric threshold tends to increase with the frequency, as expected, as we know from previous studies on electric rectangular pulses that the field intensity grows when the pulse duration decreases. Shorter times always require higher electric fields to induce the order reconstruction.

### 4.1.4 Induced biaxial Undulations

The biaxial distortion energy required to induce the order reconstruction in the middle of the cell is reached after a suitable number of induced biaxial undulations, that depends on the frequency and on the amplitude of the applied external signal.

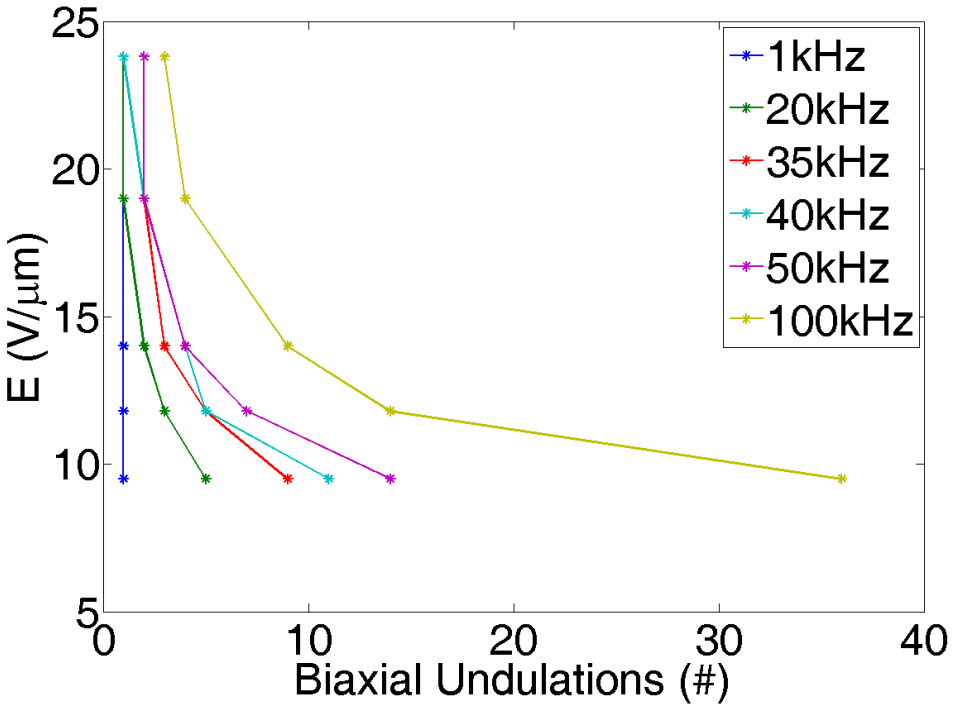


**Fig. 4.1.4.1 Numerically evaluated number of undulations required to reach the order reconstruction threshold for a fixed electric field *E* inside a π-cell for different frequencies**

Fig. 4.1.4.1 shows the numerical results for different frequencies $f$ = 1kHz, 20kHz, 35kHz, 40kHz, 50kHz and 100kHz, of the applied electric amplitude, $E$, versus the number of biaxial undulations induced inside a 1μm thick π-cell to obtain the order reconstruction.

For a fixed frequency it is possible to observe that an increasing of the amplitude corresponds to a smaller number of induced undulations, because the stored distortion accumulates faster and the order reconstruction takes place sooner. The minimum number of required undulation is one, though the time $t$ when the order reconstruction takes place is shorter for higher electric amplitudes, see Fig. 4.1.5.1.

The electric field intensity cannot grow saving the nematic order, because the applied electric amplitude is also related to the electrical induced nematic melting. For intense electric amplitudes the induced electric coherence length, $\xi_E$, becomes in fact comparable

with the nematic coherence length, $\xi_n$, inducing the nematic melting. In any case, the biaxial transition takes always place before the melting as $\xi_b > \xi_n$ .

### 4.1.5 Biaxial Order Reconstruction time: dependency on Frequency and Amplitude

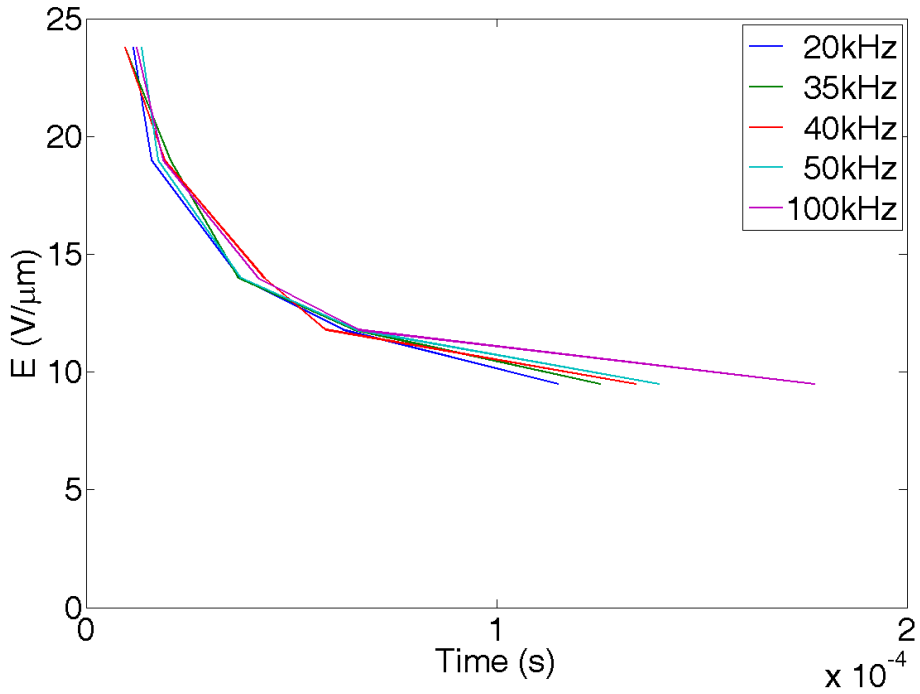


**Fig. 4.1.5.1 Numerically evaluation of the time required to reach the order reconstruction threshold for a fixed electric field *E* inside a π-cell for frequencies *f*=20kHz, 35kHz, 40kHz, 50kHz, 100kHz**

Fig. 4.1.5.1 shows the biaxial order reconstruction time required to obtain the order reconstruction for a fixed electric amplitude $E$ at frequencies $f$ = 20kHz, 35kHz, 40kHz, 50kHz and 100kHz. One can observe that the order reconstruction takes place at comparable times for a fixed electric intensity if the field is strong enough. At low field, just above the transition threshold, a high frequency electric field induces the order reconstruction at a longer time with respect to lower frequencies. Furthermore a higher amplitude of the applied electric field always corresponds to a faster order reconstruction.

Fig.4.1.5.2 shows the biaxiality time evolution for $U$ = 9.5V, for two different frequencies: $f$ = 100kHz, and $f$ = 20kHz. For $f$ = 20kHz, 5 biaxial undulations are present and the order reconstruction occurs at t = 0.115ms. For 100kHz, 36 biaxial undulations are required to achieve the order reconstruction, that occurs at t = 0.177ms. This can be explained because the distortion induced by the external electric field in each period is smaller at high

frequencies. As a consequences the required number of undulations to store enough energy in the cell and hence to achieve the order reconstruction increases.

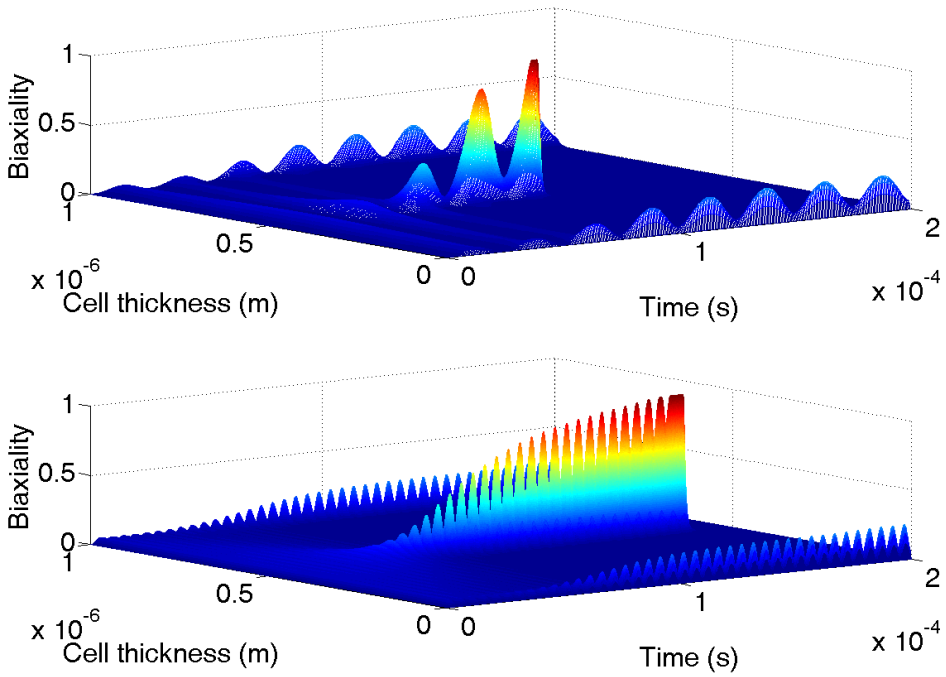


**Fig. 4.1.5.2 Biaxiality time evolution for U = 9.5V, *f* = 100kHz (bottom panel) versus f = 20kHz (top panel)**

### 4.1.6 Numerical results: Symmetric π-cell under an external sinusoidal electric field.

The influence of the applied sinusoidal electric field, for a fixed frequency $f$ = 20kHz is shown in Fig. 4.1.6.1. The analysis has been done for different amplitudes of the vertical applied electric field: (a) 4.8V/µm below $E_{th}$, (b) 8.3 V/µm below $E_{th}$ (c) 8.34 V/µm = $E_{th}$ (d) 11.9 V/µm above $E_{th}$, (e) 14 V/µm above $E_{th}$,(f) 19 V/µm above $E_{th}$,(g) 23.8 V/µm above $E_{th}$. The cell thickness was fixed to $d$=1µm.

The application of the electric field for t > 0s changes the initial splay configuration inside the π-cell. Assuming strong anchoring energy on both surfaces, the surface molecules will held their positions, whereas the nematic director in the bulk will tend to realign along the electric field ($\Delta\varepsilon_{5CB} > 0$). Depending on the amplitude of the external electric field, the induced biaxiality in the middle of the cell will behave differently.

Generally, increasing the amplitude of the applied external field, $E$, the biaxial features become progressively faster, and the number of biaxiality undulation decreases, as shown in Fig. 4.1.4.1 and Fig. 4.1.5.1.

For a suitable amplitude, $E \geq E_{th}$, one can observe that the biaxial distortion increases progressively till a maximum frustration is reached, allowing the nematic to relax its energy locally by the appearance of the order reconstruction which let to transit from the initial quasi splay texture to the final bend.

The biaxial distortion at the upper and lower cell plates also depends on the applied electric amplitude. It increases as the amplitude increases, and the induced undulations persists as long as the external electric field is applied, see 3D representation in Fig. 4.1.6.1 (a), (b), (c), (d), (e), (f) and (g). Due to the strong anchoring condition, the order reconstruction cannot take place on the cell boundary surfaces.

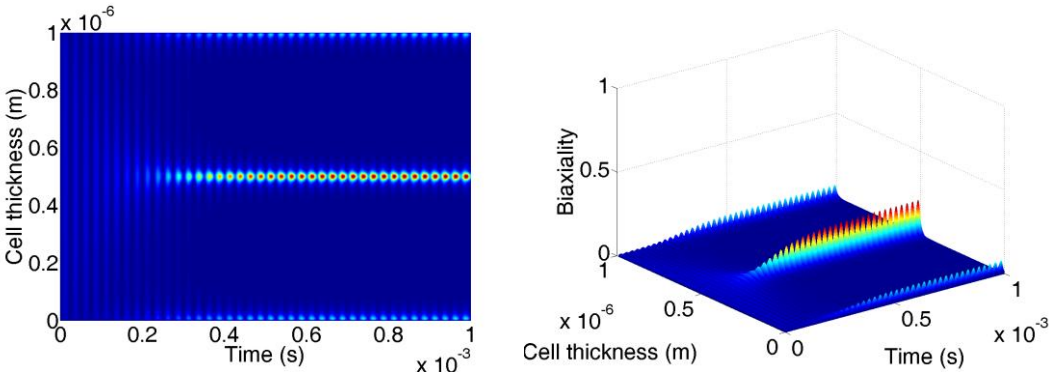


*(a) f=20kHz, E = 4.80V/μm < Eth: no order reconstruction.*

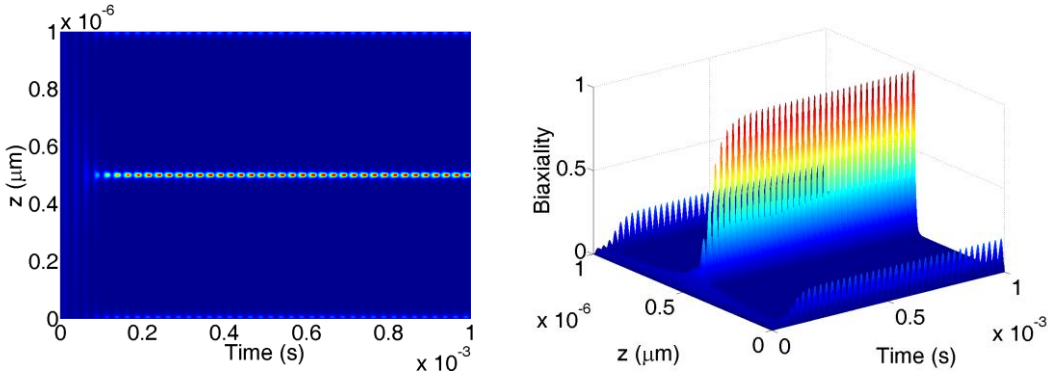


*(b) f=20kHz, E = 8.30V/μm < Eth, no order reconstruction*

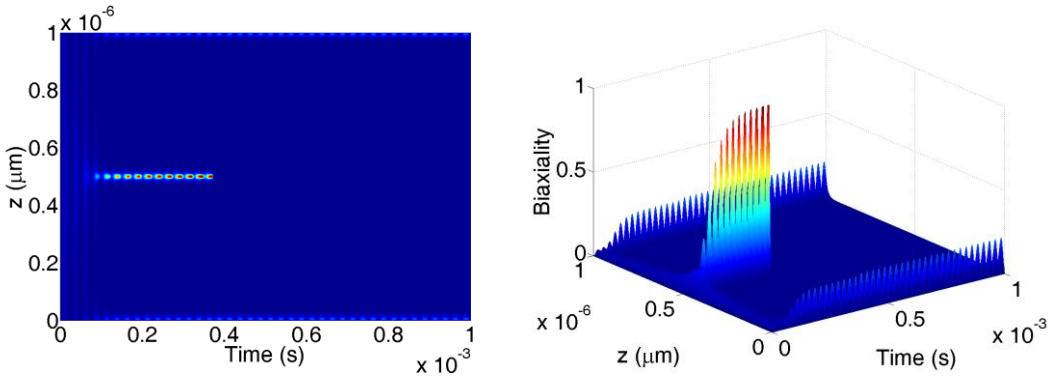


*(c) f=20kHZ, E = 8.34V/μm = Eth. Tb = 0.369ms. Threshold electric field.*

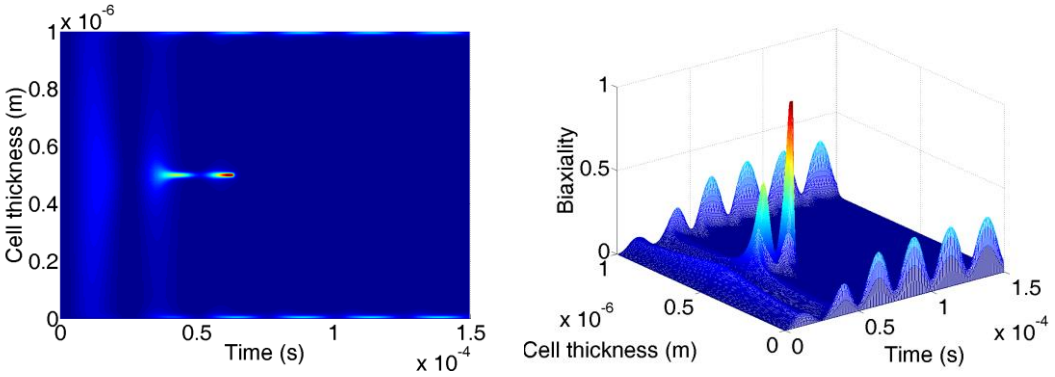


*(d) f=20kHz, E = 11.90 V/μm. Tb = 0.065ms.*

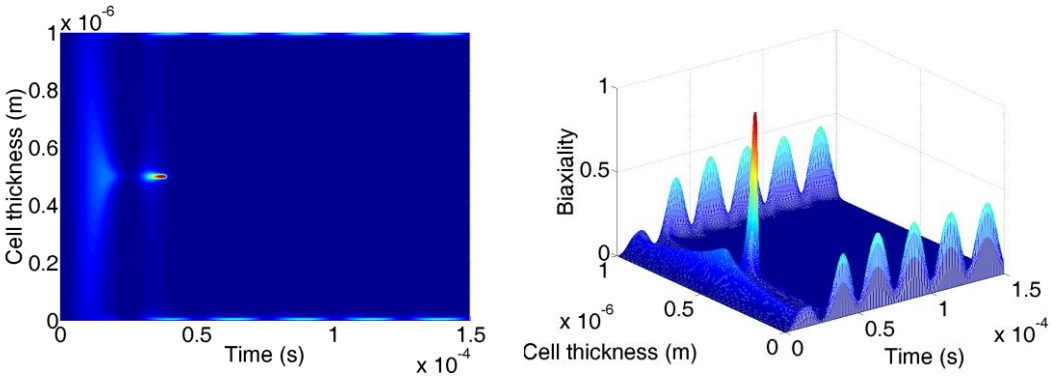


*(e) f=20kHz, E = 14.00 V/µm. Tb = 0.037ms.*

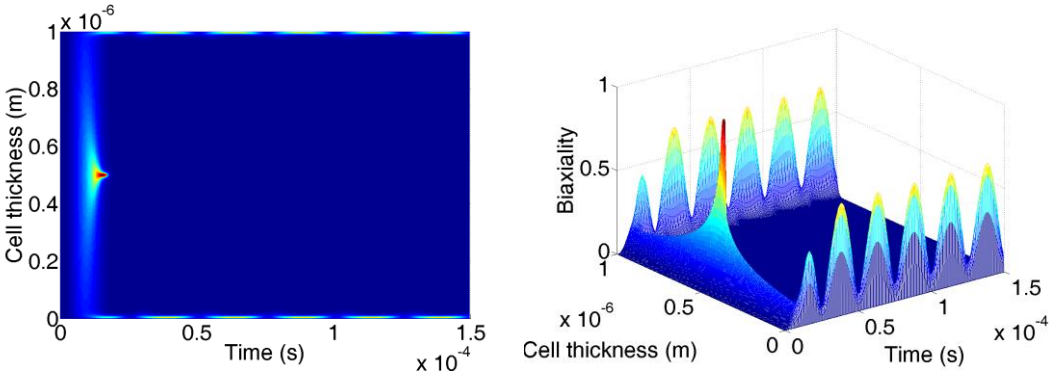


*(f) f=20kHz, E = 19.00 V/µm. Tb = 0.016ms.*

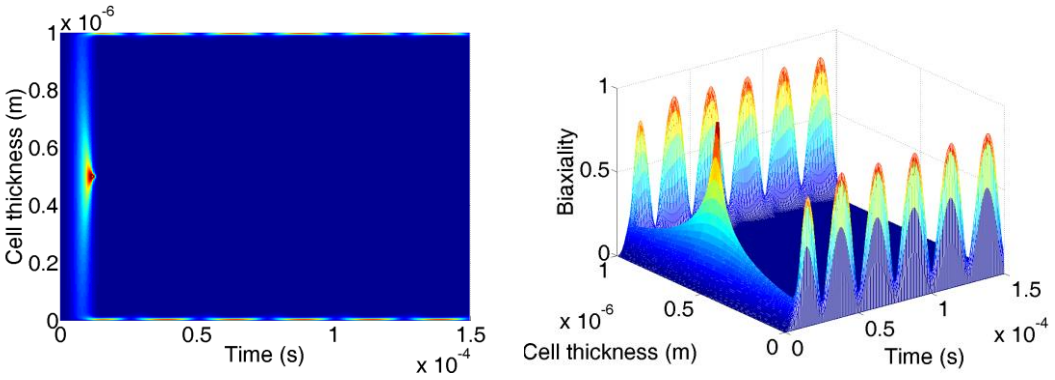


*(g) f= 20kHz, E = 23.80 V/µm. Tb = 0.012ms.*

**Fig. 4.1.6.1 Biaxial order evolution in time for sinusoidal electric field amplitudes of 4.8 (a), 8.3(b), 8.34(c) and time interval $0<t<1$ms; 11.9(d), 14 (e), 19 (f), 23.8(g) and time interval $0<t<100$µs. The red color is associated to the maximum value of the biaxiality, while the blue color is associated to the uniaxial phase. For the left panel, the vertical axis represents the cell thickness, while the time is represented along the horizontal axis. For the right panel, the vertical axis represent biaxiality, while the plane *x-y* represents the cell thickness and the time. Cell thickness is $d = 1$µm.**

Fig. 4.1.6.1 (a), $E$= 4.8V/µm, shows the theoretical evolution of the biaxiality when the field is well below $E_{th}$. In this case, when the field is switched on, the liquid crystal molecules start to reorient parallel to the applied field and a biaxial distortion start to create

in the center of cell. Since $E << E_{th}$, the biaxial distortion is not strong enough to induce the order reconstruction. In fact, the induced biaxiality in the middle of the cell increases from $b$=0 to $b$=0.22, far below the necessary $b$=1. When the electric field is switched off, the induced distortion disappears completely and the π-cell returns to the initial splay configuration.

Fig. 4.1.6.1 (b), $E$=8.30V/μm, slightly below $E_{th}$=8.34V/μm, presents a different biaxial time evolution with respect to the previous case $E$=4.8V/μm (a). In this case, the applied amplitude is strong enough to induce a well defined biaxial distortion in the middle of the cell, $b$= 0.98, very close, but slightly lower than the value required for the order reconstruction. In the right panel of Fig. 4.1.6.1 (b), one can observe that the induced distortion at the beginning increases progressively in the middle of the cell, but then, after about 8 undulations, the induced biaxiality reaches a steady state lower than the order reconstruction threshold.

Fig. 4.1.6.1 (c), $E_{th}$=8.34V/μm, just at the order reconstruction threshold. In this case the stored distortion is able to induce the splay-bend transition after 15 biaxial undulations and hence the order reconstruction takes place at t=0.369ms.

In Fig. 4.1.6.1 (d) $E$ = 11.90V/μm > $E_{th}$, i.e. with an electric field about 40% stronger than the transition threshold, the biaxial order reconstruction is reached after only 3 biaxial undulations. During the first undulation, the biaxial distortion is spread along all the $z$-axis, while during the second undulation the distortion starts to spread along the $z$-axis and then get concentrated in a region of width $2*\xi_b$, when t=0.036ms, close to the maximum amplitude of the applied field. The last undulation presents well defined and concentrated biaxial region in the middle of the cell, the accumulated distortion is very strong inducing the nematic to relax its energy through the order reconstruction. The biaxial order reconstruction occurs at t=0.0625ms.

Fig. 4.1.6.1 (e), $E$ = 14V/μm > $E_{th}$ , i.e. with an electric field about 70% stronger than the transition threshold. In this case, two biaxial undulations are present. During the first one, the biaxial distortion spreads all along the $z$-axis, while during the second one, it is concentrated in a small region of width comparable to $2*\xi_b$. The order reconstruction takes place at t=0.037ms, at shorter time than the lower external electric fields.

Fig. 4.1.6.1 (f), for $E$= 19V/μm > $E_{th}$, larger than two times the threshold, only one biaxial undulation is present. The biaxial distortion starts spreading along the $z$ direction, but becomes progressively an ellipsoid when the biaxiality is above $b$=0.6. In this case, the splay-bend transition occurs at t=0.019ms, and the crater of the biaxial volcano occurs at t =0.016ms. The biaxial cluster ($b$= 0,37) last from t= 0.01ms to t= 0.017ms. The biaxiality distortion at the cell plates, reach a maximum value $b$=0.6.

Fig. 4.1.6.1 (g), for $E$=23.8V/μm > $E_{th}$, close to three times the threshold, there is only one biaxial undulation. Due to the intense amplitude, the biaxial order saturates and it becomes confined in a very short time interval and. The splay-bend transition is completed within 0.014ms from the pulse start and the biaxial order is definitively squashed along the $z$-axis (the volcano crater form at t=0.0115ms). The biaxiality along the $z$-axis goes from 0.357μm ($b$=0.36, light blu) to 0.642μm, corresponding to a width of $28*\xi_b$, starting at t= 0.008ms until 0.013ms. The inner red zone ($b$=0.66) goes from 0.464μm to 0.541μm, which corresponds to a width of $8*\xi_b$, starting at t=0.0095ms until t=0.0125ms. The biaxiality distortion at the plates reaches a quite large maximum value of $b$=0.8.

### Strong Amplitude, $E$ = 14V/μm above the transition threshold.

The influence of the applied sinusoidal electric field, for fixed amplitudes $E$=14V/μm and $E$ = 23V/μm is shown in Fig.4.1.6.2 and Fig.4.1.6.3 respectively. The analysis has been done for five different frequencies of the vertical electric field: (a) 1kHz, (b) 35kHz, (c) 40kHz, (d) 50kHz, (e) 100kHz. The cell thickness was fixed to $d$=1μm.

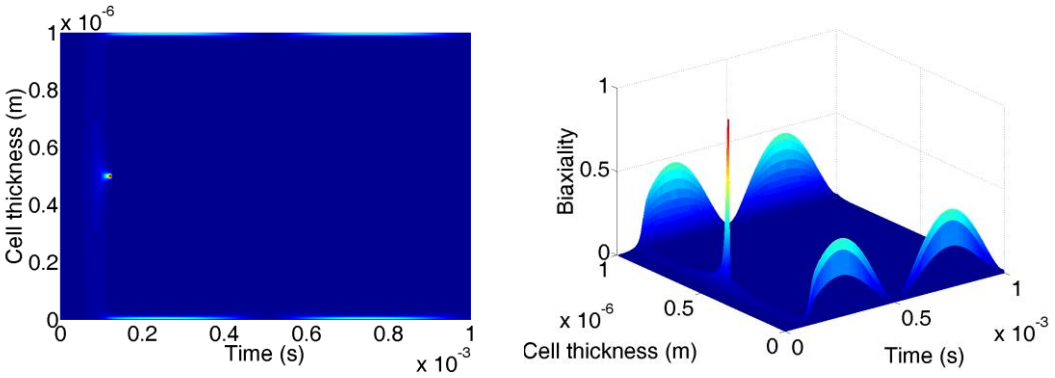


*(a) f = 1kHz, E = 14V/μm. Number of undulation = 1. Tb=0.125ms.*

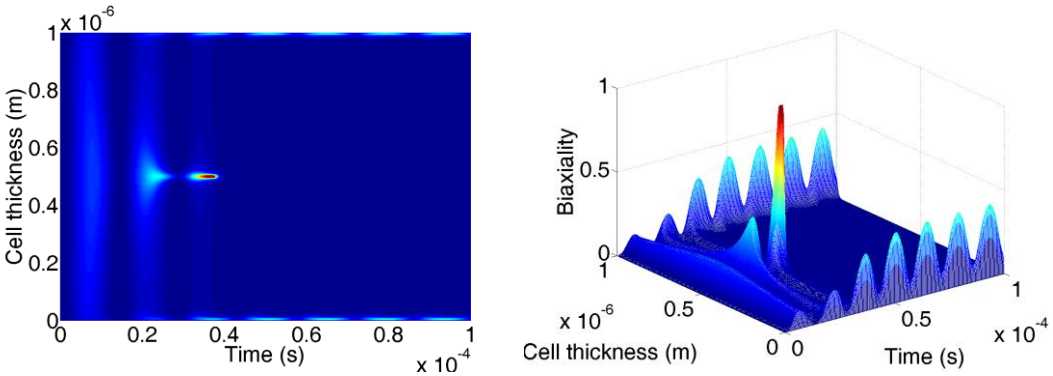


*(b) f = 35kHz, E = 14V/µm. Number of undulations = 3. Tb = 0.039ms.*

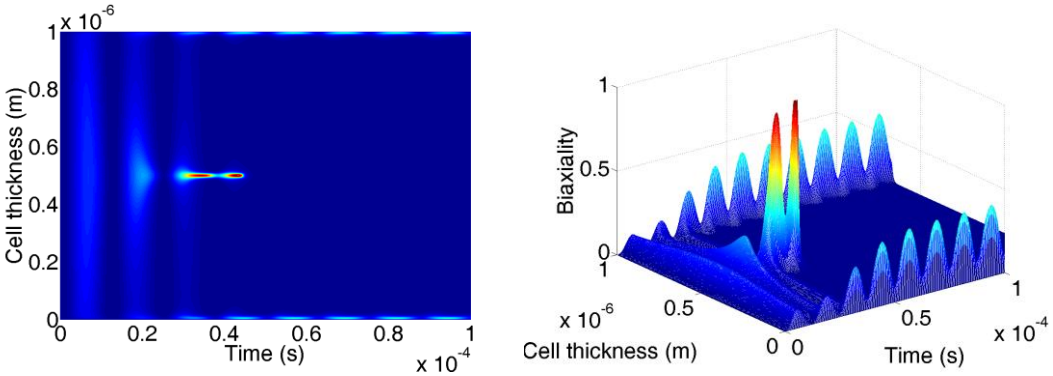


*(c) f = 40kHz, E =14V/µm. Number of undulations = 4. Tb = 0.043ms.*

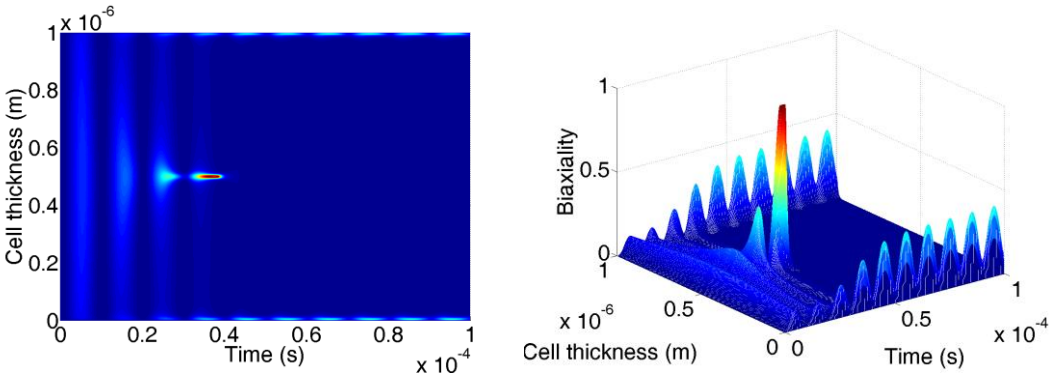


*(d) f = 50kHz, E = 14V/µm. Number of undulations = 4. Tb = 0.038ms.*

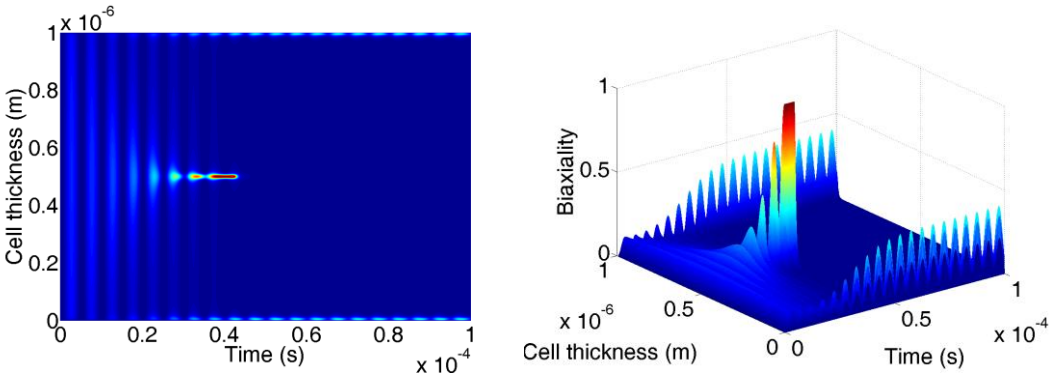


*(e) f = 100kHz, E = 14V/µm. Number of undulations = 9. Tb = 0.042ms.*

**Fig. 4.1.6.2 Biaxial order evolution in time for sinusoidal electric field amplitude *E* = 14V/µm and frequencies: (a) 1kHz, , (b) 35kHz, (c) 40Khz, (d) 50kHz and (e) 100kHz. Cell thickness *d*=1µm.**

Fig. 4.1.6.2. shows the theoretical evolution of the biaxiality when the field is above the electric transition threshold, *E*=14V/µm for different frequencies, *f*= 1kHz (a), 35kHz (b), 40kHz(c), 50kHz(d) and 100kHz(e). One can observe that the number of undulations increase for an increasing frequency, for (a) *f* = 1kHz the order reconstruction takes place at the first undulation, while it takes place after 3, 4, 4 and 9 undulations for 35kHz, 40kHz, 50kHz and 100kHz respectively. As discussed in previous sections of this chapter, the required number of undulations to store enough energy in the cell increases because the distortion induced by the external electric field in each period is smaller at high frequencies.

In Fig 4.1.6.2 for (b), (c), (d) and (e) the order reconstruction takes place at about t=0.040ms. For (a) *f* = 1kHz, the larger signal period induced the order reconstruction at t=0.124ms.

For (e) f = 100kHz, the signal oscillation are so fast that the accumulated energy has not time at all to relax, and the last two undulations form a continuous one.

At the border plates, the maximum induce biaxiality is about b=0.4 independent of the frequency applied and it persists as long as the electric field is on.

### Intense Amplitude, *E* = 23.8V/µm above the transition threshold

The influence of the applied sinusoidal electric field, for an electric field amplitude *E*=23.8V/µm is show in Fig. 4.1.6.3. The analysis has been done for five different

frequencies of the vertical electric field: (a) 1kHz, (b) 35kHz, (c) 40kHz, (d) 50kHz, (e) 100kHz.

At the border plates, the maximum induce biaxiality is about b=0.8 independent of the frequency applied and it persists as long as the electric field is on.

For this intense amplitude, the biaxial order saturates and it becomes confined in a very short time interval.

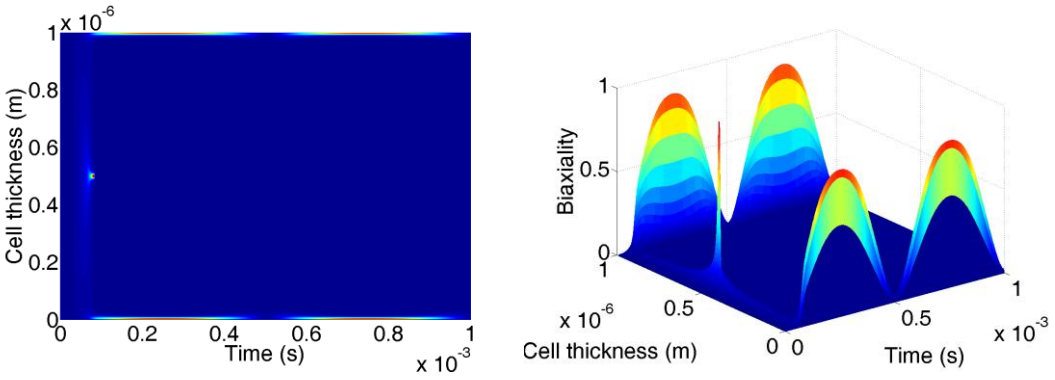


*(a)f = 1kHz, E= 23.8V/µm. Number of undulations=1. Tb=0.083ms.*

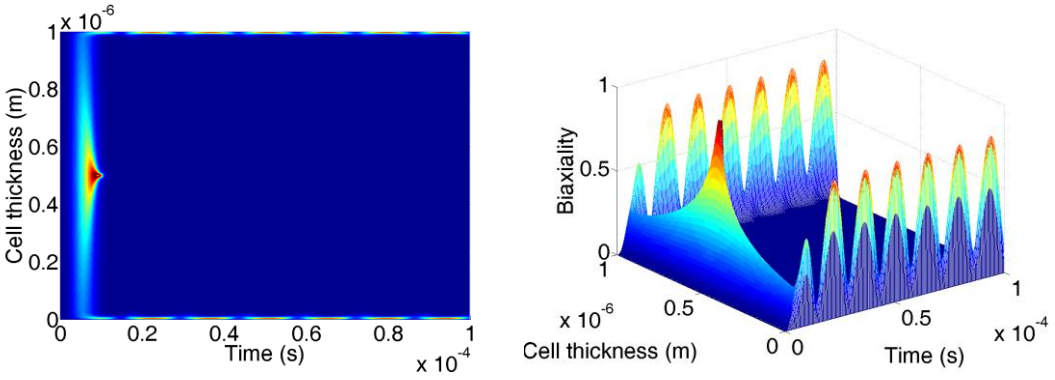


*(b )f = 35kHz, E = 23.8 V/µm. Number of undulations=1. Tb= 0.008ms.*

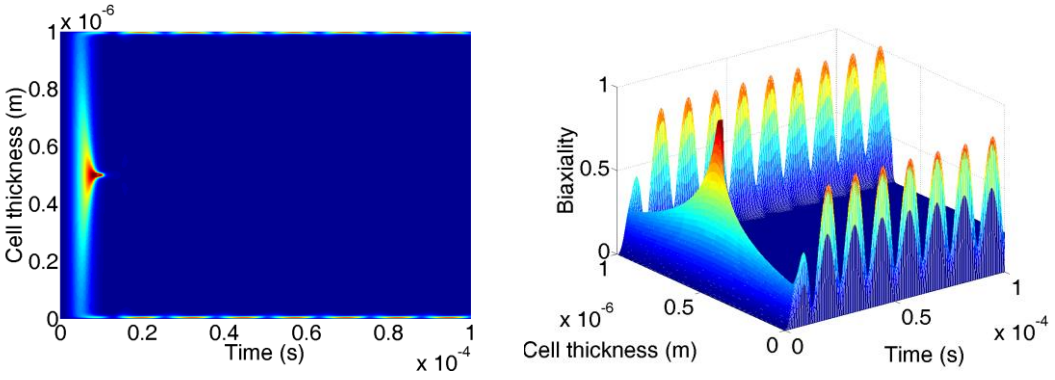


*(c)f = 40kHz, E = 23.8 V/µm. Number of undulations=1. Tb= 0.0095ms*

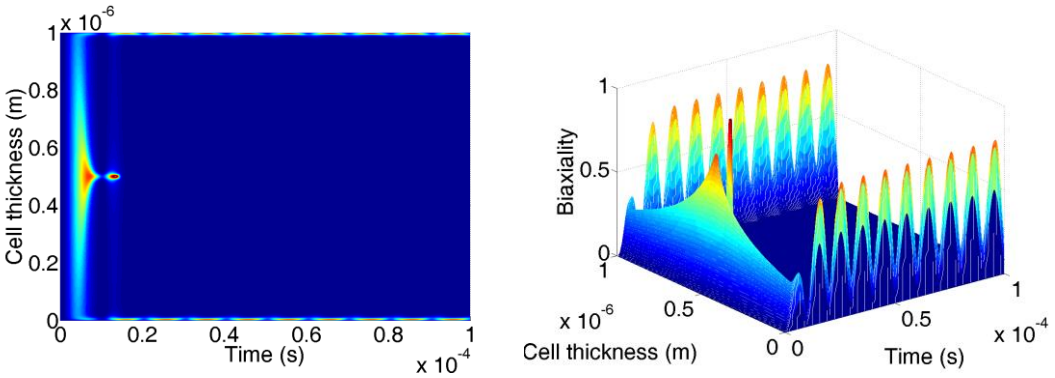


*(d) f= 50kHz , E = 23.8 V/µm. Number of undulations: 2. Tb=0.014ms*

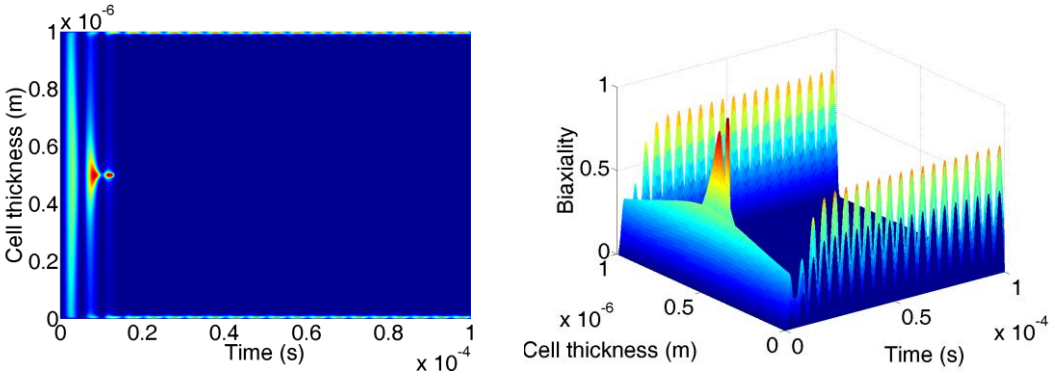


*(e)f = 100kHz, E = 23.8V/µm. Number of undulations=3. Tb= 0.012ms*

**Fig. 4.1.6.3 One-dimensional dynamical representation of biaxiality inside a 1 µm thick π-cell submitted to an external sinusoidal electric filed, for an electric amplitude *E* = 23.8V/µm, and frequencies: (a) 1kHz, (b) 35kHz, (c) 40Khz, (d) 50kHz and (e) 100kHz.**

In Fig. 4.1.6.3 (a) for *f*= 1kHz, (b) *f* = 35kHz and (c) *f* = 40kHz, only one distortion undulation is present, and the order reconstruction take places at t = 0.083ms, t = 0.008ms and t = 0.0095ms respectively. The different order reconstruction time depends on the signal period.

In Fig. 4.1.6.3 (d) *f* = 50kHz and (e) *f* = 100kHz, there are, respectively, two and three undulations. In this case, the signal periods, T/2(d) = 0.01ms and T/2(e) = 0.005ms, required a higher amplitude to induced the biaxial order reconstruction at the first undulation. As for the previous cases, the first biaxial undulation is spread along the cell thickness. The second and third one, become progressively confined in the middle of the cell. The order reconstruction takes place at t=0.014ms and t=0.012ms respectively.

It is worth noticing, that for (d) and (e) even if more than one undulation is required, the time where the order reconstruction takes place is comparable to the previous (a), (b) and (c) cases.

### 4.1.7 Numerical results: Asymmetric π-cell under an external sinusoidal electric field

Nematic liquid crystal confined in a π-cell with strong and asymmetric anchoring conditions, present two different topological textures: splay and bend. The applied asymmetry on the pre-tilt anchoring angle as well as the strong anchoring conditions allows to concentrate the largest nematic distortion close to the surface where the nematic molecules have anchoring angles approaching planar conditions. The electrically induced biaxial wall occurs near a confining surface plate and the π-bend texture grows at the expense of the starting splay texture, overcoming the topological barrier [26, 45].

The evolution of the electrically induced distortion is monitored calculating the biaxiality arising in a region close to the upper boundary plate, for different upper pre-tilt angles and imposing electric sinusoidal fields with different frequencies and amplitudes.

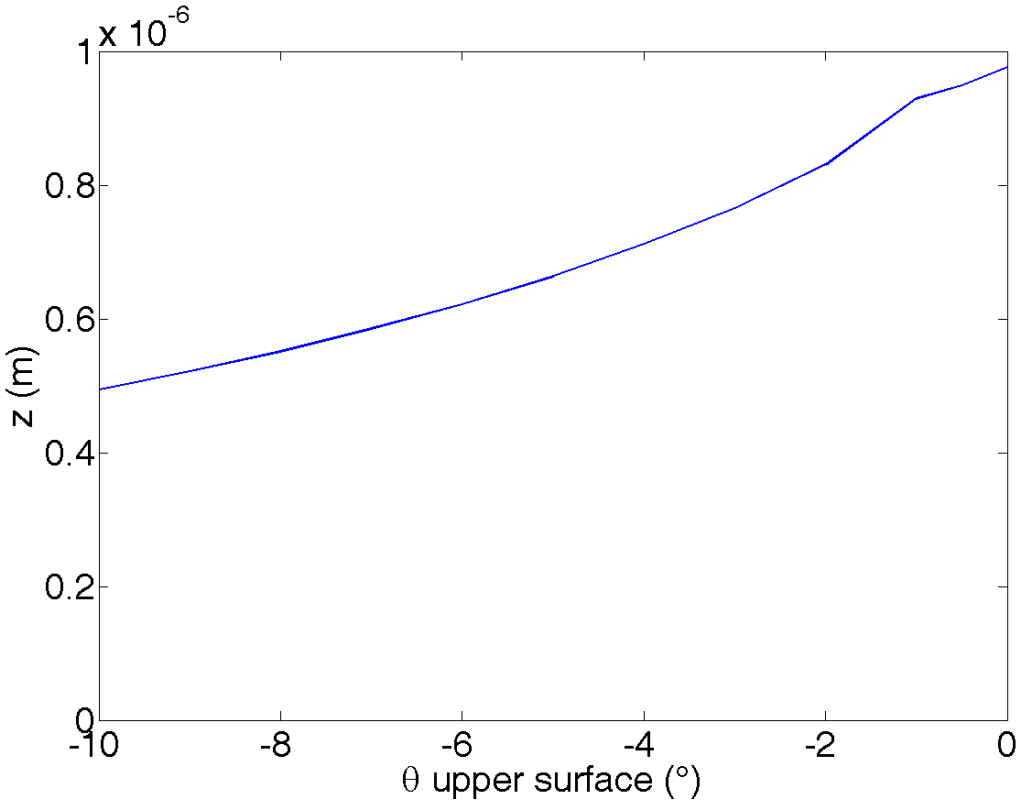


**Fig.4.1.7.1 Position of the biaxial wall along the z-axis versus the upper surface tilt angle $\theta_u$ for a fixed lower surface angle $\theta_l$=10°**

The nematic distortion tends to concentrate close the surface with smaller pretilt. Fig. 4.1.7.1 shows the position of the electrically induced biaxial wall on the *z*-axis versus the upper pretilt angle, when the upper angle was varied from 0° to -10°, with a fixed lower

angle $\theta_l$ = 10°. For upper pretilt orientations from -1° to -10°, the biaxial undulation shape is always the same of the bulk biaxial wall, whose thickness is about 10nm, corresponding to two times the biaxiality coherence length, $2*\xi_b$. When the upper surface anchoring is close to the planar one, i.e. the pretilt is close to 0°, the biaxial wall enlarges and it tends to be absorbed by the boundary surface. In this case, one cannot observe the order reconstruction for electric fields up to three times the bulk transition threshold, as shown in Fig. 4.1.7.5. For $\theta_u$=-10°, the biaxial wall concentrated in the middle plane of the cell corresponding to the symmetric π-cell case.

In general, decreasing the upper pretilt angle, $\theta_u$, if the biaxial wall will form close enough to the boundary surface, the electrically induced nematic distortion can relax by means of two different mechanisms: a fast one, involving the appearance of the order reconstruction phenomenon, practically the same than the bulk order reconstruction, and a slow one, involving the motion of the bulk biaxiality towards the low pretilt surface plate, on which it finally spreads [26, 45]. In fact, for $\theta_u$ from -2° to -10°, at suitable field amplitudes, the splay-bend transition presents a complete order reconstruction evolution similarly to what happens within a symmetric π-cell, see Fig.4.1.7.2; otherwise, for $\theta_u \approx$ -1°, the induced nematic strain is absorbed on the upper surface, where the growth of the surface biaxial layer mediates the competition between the bulk reorientation due to the high electric field and the surface local order, which cannot change due to the strong anchoring energy, see Fig. 4.1.7.3 and Fig. 4.1.7.4.

Applying higher amplitudes of the electric field, the textural switching mechanisms occur faster and, moreover, it is possible to achieve the order reconstruction transition very close to the upper surface layer, but never on the upper boundary surface.

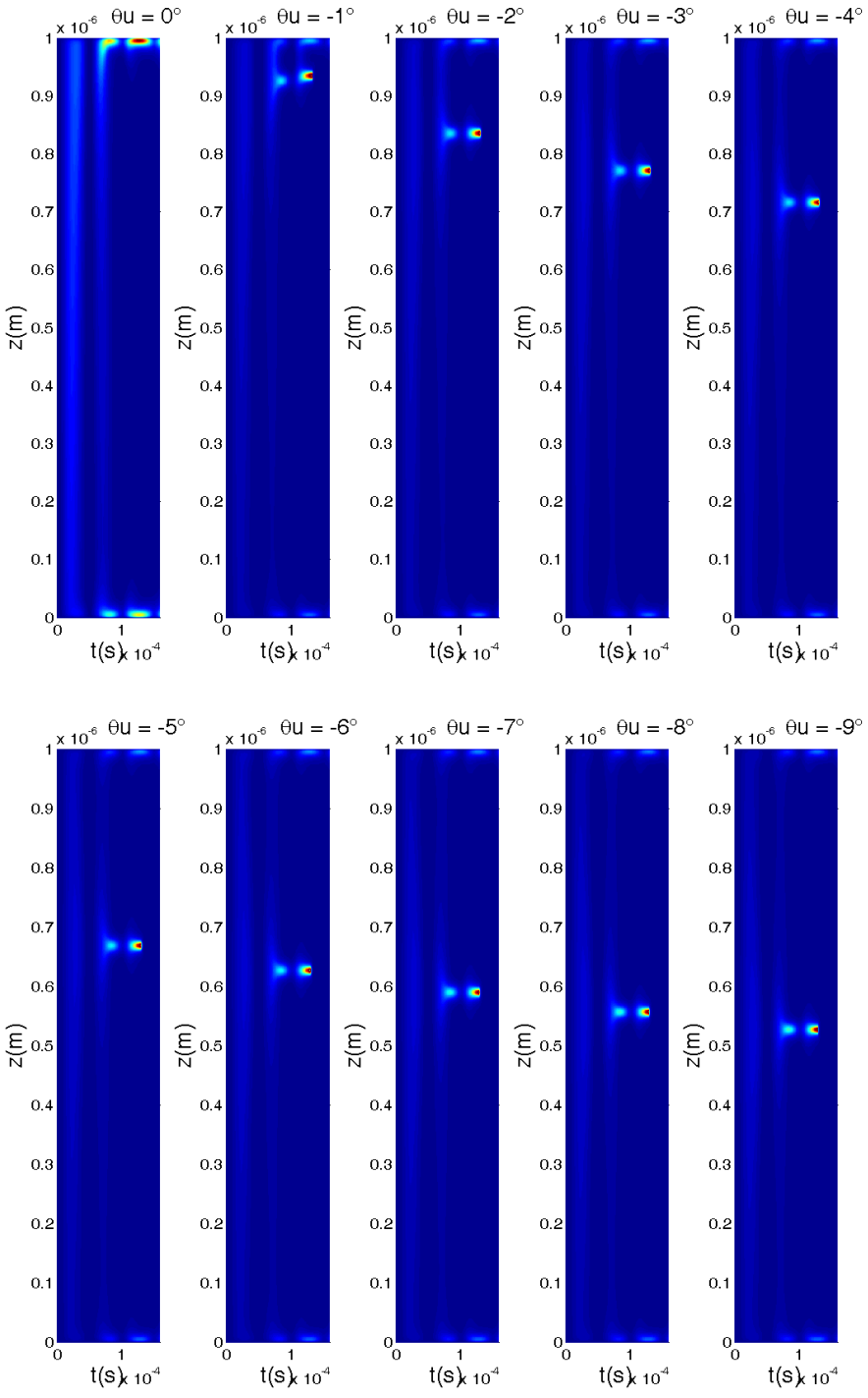


**Fig. 4.1.7.2 Theoretical time evolution of the biaxiality inside a 1µm thick π-cell when submitted to an external sinusoidal field $f$=10kHz and $U$= 8.9V; for $\theta_l$=10° and $\theta_u$ varying from 0° to -9°.**

Fig. 4.1.7.2 shows the theoretical time evolution of the biaxiality inside a π-cell when submitted to an external sinusoidal electric field with frequency $f$=10kHz and amplitude $U$ = 8.9V, for a fixed lower pretilt angle $\theta_l$=10° and different upper pretilt angle, $\theta_u$ from 0° to -9°. One can observe that the biaxiality concentrated close to the surface with smaller

pretitl angle. At this electric amplitude, the order reconstruction takes place at about the same time, t= 0.131ms for an upper pretilt angle varying from -1° to -9°, while, as expected, no order reconstruction takes place at the upper boundary plate, i.e. $\theta_u$=0°.

The evolution of the electrically induced distortion is monitored calculating the local biaxiality arising in a region close to the upper boundary plate, for different upper pretilt angles and imposing electric pulses with increasing amplitude. Each Figs. 4.1.7.3 to 4.1.7.5 shows the induced biaxiality during the application of a sinusoidal electric field with frequency $f$ = 10kHz, and amplitudes 8.1(a), 8.3(b), 8.5(c), 8.7(d) and 8.9 V/μm (e). Each figure for a different upper anchoring angle, $\theta_u$= -3°, $\theta_u$=-1° and $\theta_u$=0°, respectively.

For all the following figures, the vertical and the horizontal axes correspond, respectively, to the cell thickness in the $0 \leq z \leq 1$ μm range and to the time scale of the solution evolution in the 0 ms ≤ t ≤ 0.3 ms interval. The biaxiality is linearly mapped in between the blue (zero biaxiality) and red (maximum biaxiality) colours.

### *Biaxial distortion time evolution, Upper pretilt angle $\theta_u$ = -3°*

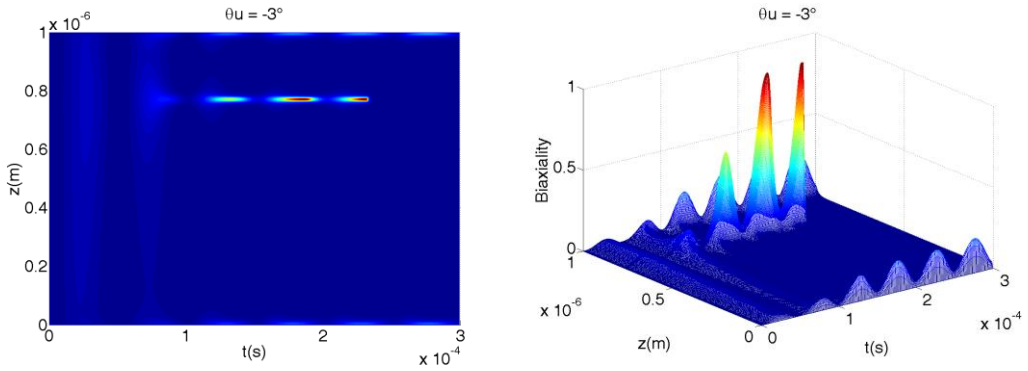


*(a) f = 10kHz, E = 8.1 V/μm, θu = -3°. #5 undulations. Tb= 0.232ms.*

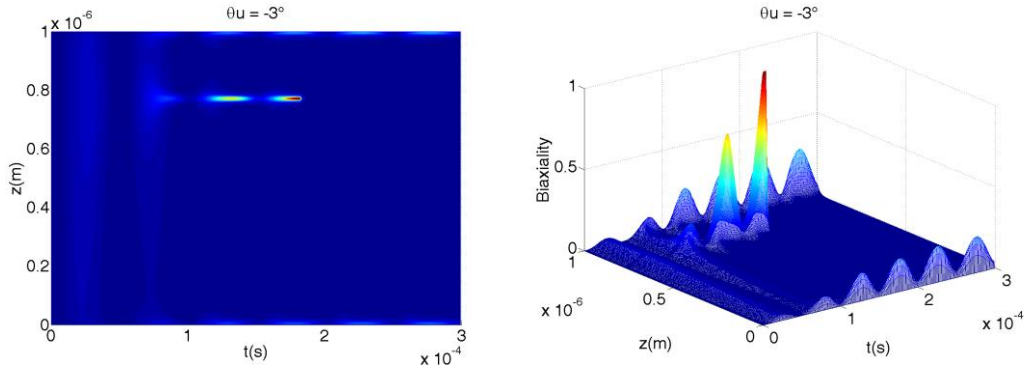


*(b) f = 10kHz, E = 8.3 V/μm, θu = -3°. #4 undulations. Tb=0.180ms.*

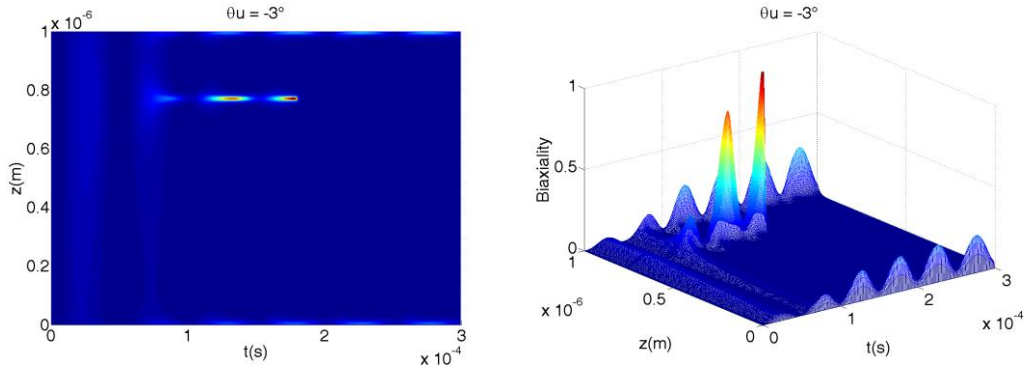


*(c) f = 10kHz, E = 8.5 V/µm, θu = -3° , #4 undulations. Tb=0.178ms.*

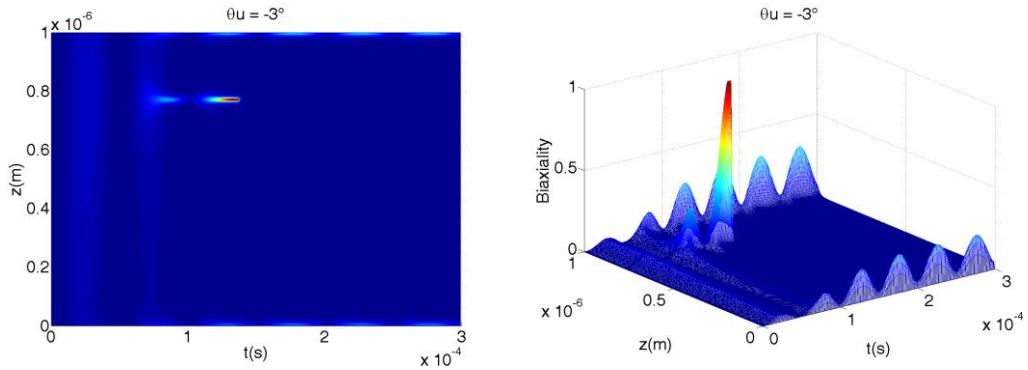


*(d) f = 10kHz, E = 8.7 V/µm, θu = -3° , #3 undulations. Tb=0.136ms.*

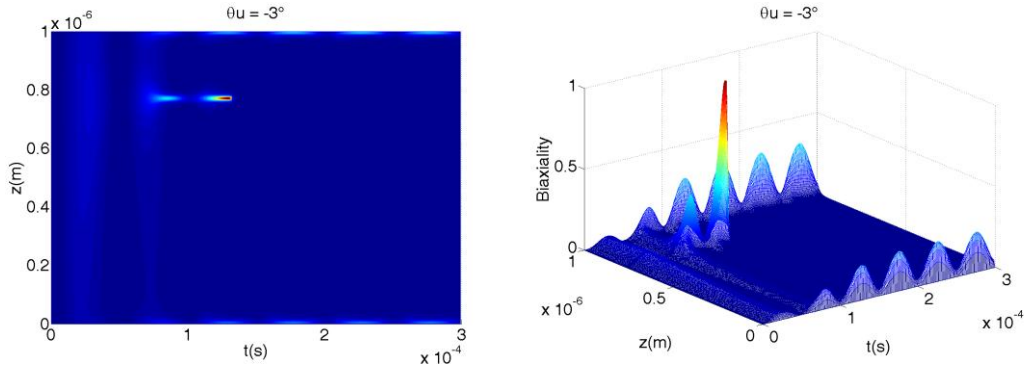


*(e) f = 10kHz, E = 8.9 V/µm, θu = -3° #3 undulations. Tb = 0.131ms.*

**Fig. 4.1.7.3 Surface contour plot of the biaxial order evolution in the time, for a sinusoidal electric field amplitudes of , 8.1 (a), 8.3 (b), 8.5(c), 8.7(d), 8.9 (e), time interval 0<t<0.3ms.. *θu = -3°***

In Fig. 4.1.7.3 from (a) to (e), one can observe that the induced biaxiality undulations concentrated along the z-axis from about z=0.76µm= to z=0.77µm, with a thickness of about10nm. The initial undulations are not evenly spread along the *z*-axis, but tend to concentrate towards the surface plate with smaller pretilt angle. Similar to the symmetric case, the order reconstruction phenomenon occurs faster for higher electric amplitudes and the numbers of undulations depends on the applied amplitude.

A t=0s, the initial nematic texture is in an asymmetric splayed configuration and the nematic molecules next to the upper surface stay almost planar to the plate. After the application of the sinusoidal electric field, for t > 0s, the molecules start to align along the field direction, and a first biaxial undulation starts to grow concentrating close to the upper surface plate. When the stored biaxial distortion is high enough, the undulations become concentrated in a region of thickness comparable with the biaxial coherence length ($2*\xi_b$), connecting the surface planar nematic texture with the competing vertical bulk nematic molecules: the strong induced nematic distortion relaxes by lowering the nematic order, i.e. the starting uniaxial phase is loosen and it is locally replaced by the growing biaxial domains.

In Fig. 4.1.7.3 (a) Five biaxial undulations are present, the first two with a maximum biaxiality of 0.137. The third one from t=0.160ms to t=0.142ms. The fourth one present a higher biaxiality with a maximum b=0.98. The last biaxial undulation starts from t=0.208ms to t=0.233ms the induced biaxial region looks like a crater of a volcano, where the biaxiality is zero inside and around the crater, the order reconstruction takes place at t=0.233ms. For t > 0.233ms the biaxial wall disappears, meaning that the initial splayed texture is replaced by a bend one. The uniaxial order is restored everywhere except for a residual biaxiality near the surface plates due to the strong anchoring energy.

In Fig. 4.1.7.3(.b), only four biaxial undulations are present. The first two are low and spread along the *z*-axis, with a maxima biaxiality b= 0.175. The third biaxial undulation, present a maxima biaxiality of 0.678. The last biaxial undulation form from 0.158ms to 0.183ms. The order reconstruction phenomenon occurs at t=0.180ms.

In Fig 4.1.7.3 (c) the applied electric field induced inside the cell four biaxial undulations. The first two distortion undulations are low and spread along the z-axis. The third biaxial undulation concentrate in space around 0.76μm and 0.77μm. The last biaxial distortion forms from t=0.157ms to t=0.18ms. The order reconstruction takes place at t=0,178ms.

In Fig 4.1.7.3 (d), only three biaxial undulations are present. The first two, as for the other cases, are not strong, the biaxiality reach a maximum value of b=0.278. The order reconstruction occurs at 0.135ms.

In Fig 4.1.7.3(e), only three biaxial undulations are present. On the third one, the order reconstruction occurs at t 0.13ms, lasting from t 0.109ms to t 0.133ms.

### *Biaxial distortion time evolution, Upper pretilt angle θu = -1°*

At lower pre-tilt angles, the order reconstruction is no longer a bulk phenomenon, but a surface one.

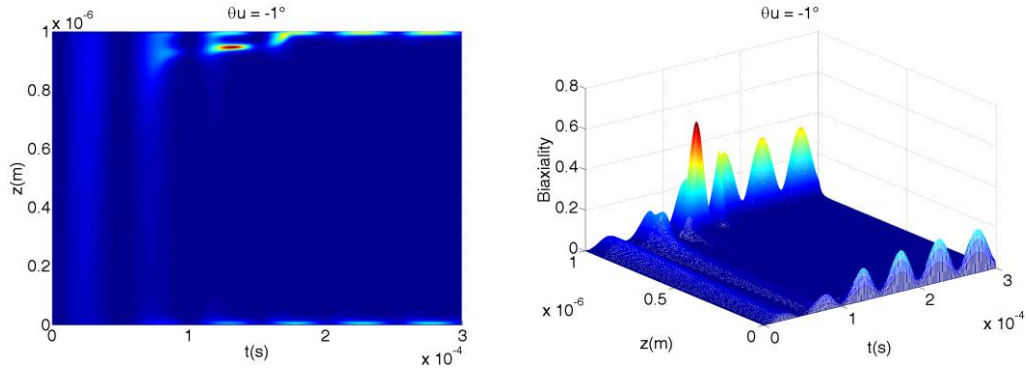


*(a) f = 10kHz, E= 8.1 V/µm, θu = -1°, # 3 undulations. No order reconstruction.*

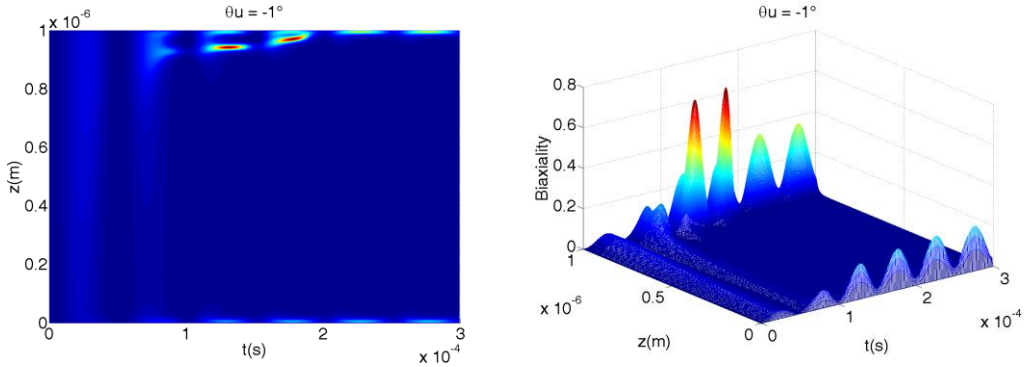


*(b) f = 10kHz, E = 8.3 V/µm, θu = -1° , #4 undulations. No order reconstruction.*

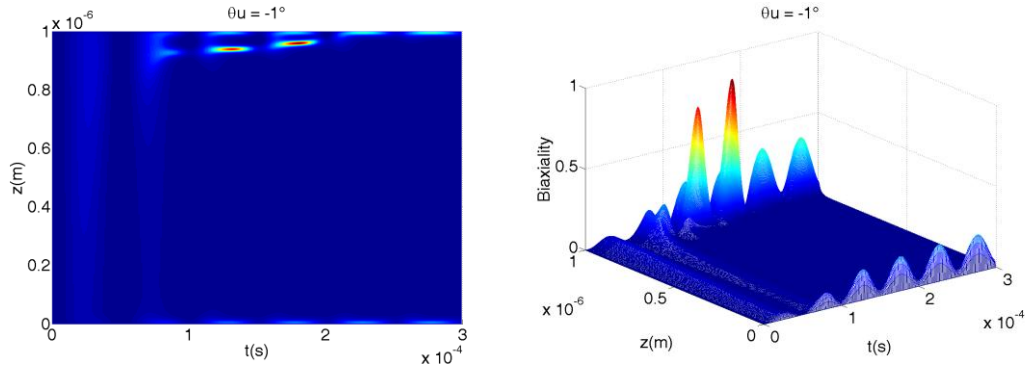


*(c ) f = 10kHz, E = 8.5 V/µm, θu = -1°, #4 undulations. No order reconstruction.*

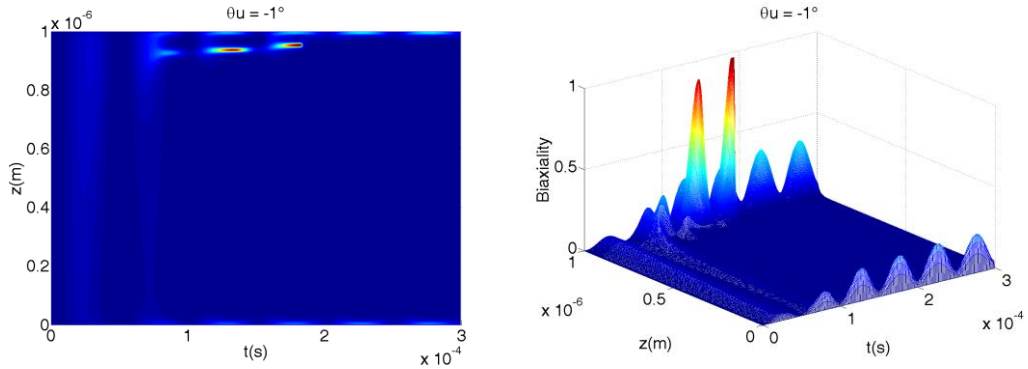


*(d ) f = 10kHz, E = 8.7 V/μm; θu = -1°, # 4 undulations. Tb = 0.182ms.*

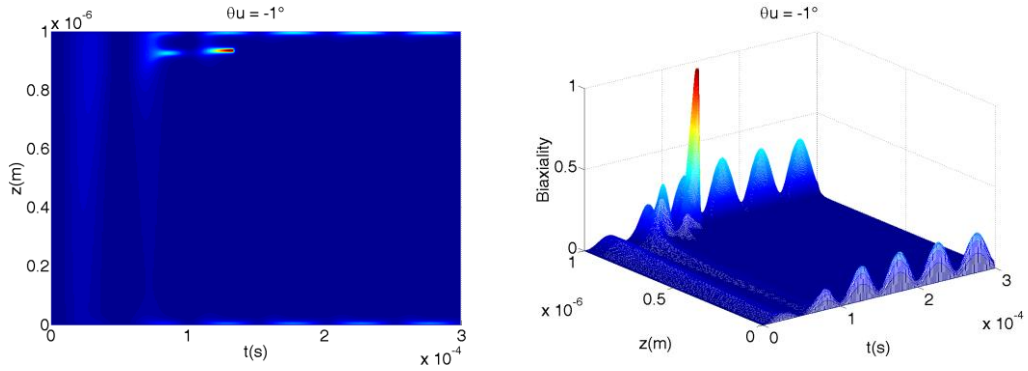


*(e) Freq = 10kHz, U = 8.9 V/μm; θu = -1°, #3 undulations. Tb = 0.132ms.*

**Fig. 4.1.7.4 Surface contour plot of the biaxial order evolution in the time., for a sinusoidal electric field amplitudes of , 8.1 (a), 8.3 (b), 8.5(c), 8.7(d), 8.9 (e), time interval 0<t<0.3ms. θu=-1°**

In Fig. 4.1.7.4, one can observe that the induced biaxial distortion undulations inside the cell tend to move towards the surface boundary with the lower pretilt angle, in this case the upper surface. For lower amplitude, the motion towards the surface is faster than the distortion energy accumulation rate, inducing the biaxial distortion to spreads on the surface with a consequent bulk topological behaviour equivalent to the splay – bend transition allowed by order reconstruction at higher voltage.

For $\theta u$ = -1°, $E$=8.1 V/μm , Fig. 4.1.7.4 (a), there are only four biaxial undulations and no order reconstruction takes place. The first two biaxial distortion are not well spatially concentrated and are spread along the $z$-axis. The third biaxial undulation form from t=0.118ms to t=0.143ms, and it is spatially concentrated from $z$=0.934μm to $z$=0.954μm, with a thickness around 20nm. The last biaxial undulation starts around t=0.163ms, but it is absorbed by the upper boundary surface at t=0.169ms, in this case there is not order reconstruction phenomenon. For the same electric amplitude, and $\theta u$ = -3° , see Fig. 4.1.7.3

(a) five biaxial undulations are present and the order reconstruction takes place at t= 0.232ms.

For $\theta u$ = -1°, $E$=8.3 V/μm, Fig. 4.1.7.4 (b), four biaxial undulations are present. The first two are spread along the $z$-axis. The third biaxial undulation starts from t=0.118ms to t=0.143ms, and it is spatially concentrated from z=0.933μm to z=0.948μm, the last biaxial undulation starts around t=0.164ms to t=0.186ms. The biaxial distortion inside the cell, moves toward the upper boundary surface, where remains as long as the electric field is applied; In this case there is not order reconstruction phenomenon. For the same electric amplitude and $\theta u$ = -3°, the order reconstruction takes place at t=0.180ms.

For $\theta u$ = -1°, E=8.5 V/μm , Fig. 4.1.7.4 (c), four biaxial undulations are present. The first two has a low spatial concentration, and they are spread along the $z$-axis. The third undulation starts from t=0.118ms to t=0.143ms, with a spatial thickness around 12nm, from z=0.932μm to z=0.944μm, the last biaxial undulation starts around t=0.164ms to t=0.190ms; with a spatial thickness around 17nm , from z=0.95μm to z=0.967μm, with a deformed shape that spatially moves toward the upper boundary surface; in this case there is not order reconstruction phenomenon. For the same electric amplitude, and an upper angle $\theta u$= -3°, the order reconstruction takes place at t=0.178ms after four biaxial undulations.

For $\theta u$ = -1°, $E$=8.7 V/μm, Fig. 4.1.7.4 (d), Three biaxial undulations are present. The first one is not spatially concentrated, presenting a low distortion energy. The second one, start from t=0.118ms to t=0.143ms, with a spatially thickness around 13nm, from z=0.93μm to z=0.943μm, the last biaxial undulation has a spatial thickness of 15nm (from 0.945μm to 0.96μm). It starts around t=0.165ms, and the order reconstruction phenomenon occurs at t=0.181ms. For the same electric amplitude, with a upper angle $\theta u$ = -3°, the order reconstruction takes place at t=0.136ms and only three biaxial undulations are required.

For $\theta u$ = -1°, $E$=8.9 V/μm , Fig. 4.1.7.4 (e), Three biaxial undulations are present. The first two distortion biaxial undulation behaves as the previous cases, they are spread along the $z$-axis. The third biaxial undulation starts from t=0.115ms to t=0.134ms, with a spatial thickness of 10nm, from z=0.93μm to z=0.94μm, the order reconstruction phenomenon occurs at t = 0.131ms. For the same electric amplitude and an upper angle $\theta u$ = -3°, Fig.

4.1.7.3 (e), the time evolution of the biaxiality inside the cell behaves in a similarly. In fact, the order reconstruction takes place after three biaxial undulation at t=0.132ms.

### *Biaxial distortion time evolution, Upper pretilt angle $\theta_u$ = -0°*

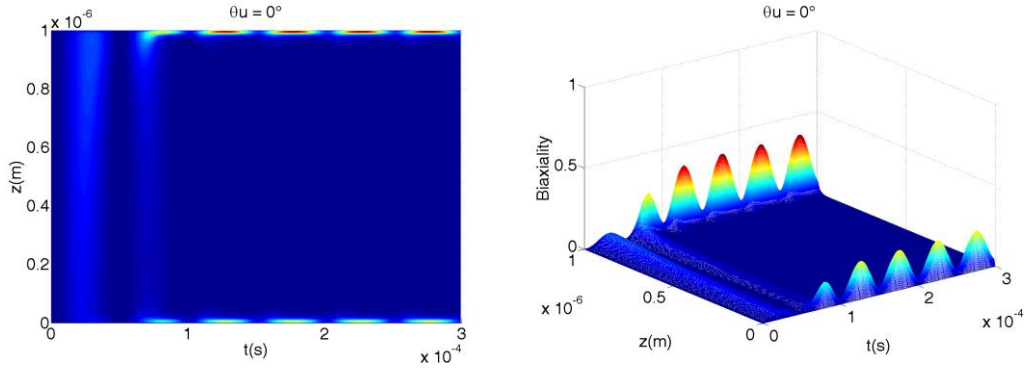


**Fig. 4.1.7.5 Surface contour plot of the biaxial order evolution in the time., for a sinusoidal electric field amplitude E=8.9V/µm, *f* =10kHz. Time interval interval 0<t<0.3ms.**

In Fig. 4.1.7.5 the time evolution for the biaxial distortion is shown for an upper angle $\theta u$ = -0° and an applied electric sinusoidal electric field $E$=8.9V/µm and $f$ = 10kHz. In this case, only two biaxial distortion undulations are induce inside the cell. They are low and spread along the *z*-axis. Both presenting a higher intensity close to the surface with lower pretilt angle, in this case the upper surface. The second undulation that start spread along the *z*-axis, gets spatially concentrated around t=0.069ms and it moves towards the upper surface; at t=0.082ms the biaxial distortion is absorbed by the upper surface plate. There is not biaxial order reconstruction phenomenon.

At the upper and lower surface, the biaxial distortion follows a sinusoidal oscillations. At the upper surface the biaxiality has a higher intensity than at the lower surface. Both remains present as long as the electric field is on.

## 4.2 Electric current in a π-cell submitted to a sinusoidal electric field

### 4.2.1 Introduction

The electric current flowing across a nematic liquid crystal cell submitted to an electric field depends on the variation of the external electric field itself but also on the variation of the liquid crystal dielectric properties, and thus it is intrinsically related to the director reorientation. This means that the electric current observations can give relevant information about the nematic dynamics. It has been also demonstrated, both experimentally and theoretically [3, 42, 43], that the electric response of a π-cell is strictly related to the nematic order dynamics and the analysis of the current signal provides relevant data about the induced biaxiality, which arises inside the cell [2,26].

The dynamical numerical model developed to describe the electrically induced biaxial order can be exploited to calculate the electric current flowing across a π-cell. Lombardo et al [2, 6] have developed a numerical procedure for calculating the electric current flowing across a π-cell during the application of a rectangular electric pulse. The numerical results obtained are in agreement with experimental measurements.

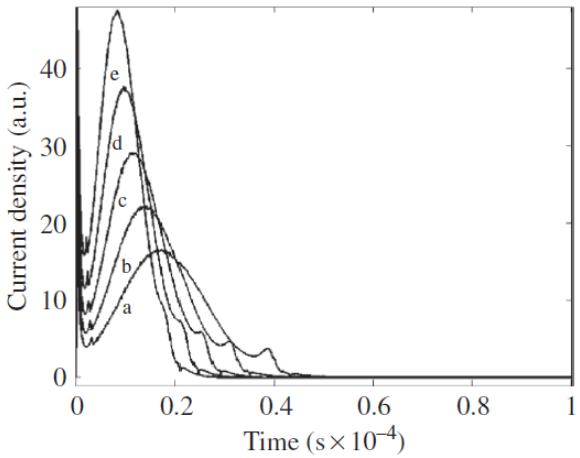


**Fig. 4.2.1.1 Plot of the electric current density flowing across the cell in the 0 ms ≤ t ≤ 0.1 ms time interval for applied rectangular electric field amplitudes of 10V µm-1 (a) , 11 V µm-1 (b) , 12 V µm-1 (c) , 13 V µm-1 (d) and 14 V µm-1 (e). [4]**

Fig. 4.2.1.1 shows the calculated electric current which flows across the cell during the application of rectangular electric pulses [4]. The first broad structure is related to the dielectric molecular reorientation along the electric field direction, as the considered liquid crystals has a positive dielectric anisotropy, while the second peak is associated with the

vanishing nematic order in a thin biaxial wall in the middle of the symmetric π-cell [6,12,13]. Increasing the amplitude of the electric pulse, the current changes behavior, as shown by the curves (a) – (e). Due to the stronger coupling between the molecular orientation and the external electric field and to the elastic response of the nematic system, the first peak becomes sharper and faster, while the order reconstruction peak takes place sooner, as the amplitude of the applied electric field is increased, till it merges inside the first peak.

The application of a sinusoidal electric field inside the π-cell induces a temporal modulation of the biaxial order. We aim to analyze the dynamics of the nematic distortion by numerically calculating the electric current which flows across the cell during the splay-bend transition. The numerical results will be compared with experimental observations.

### 4.2.2 Equivalent capacitor for a π-cell

It is well known, that a liquid crystal cell can be considered, from an electric point of view, as a variable capacitor in which the dielectric properties depend on the initial orientation and reorientation of the nematic texture due to the applied field. Therefore, the transition from splay to bend involves the variation of the nematic texture and, as a consequence, the change of the overall dielectric properties of the π-cell. In fact, the equivalent dielectric constant of the cell varies from the lower value, $\varepsilon_{\perp}$ , associated to the starting slightly splayed orientation, to the higher value, $\varepsilon_{\parallel}$ , when the transition to the bend texture is achieved. In particular, during the splay-bend transition, both the current phase and its amplitude change, whereas, when the transition is completed, the electric current will present a sinusoidal shape with a constant amplitude and a constant lead phase -90° with respect to the applied sinusoidal voltage.

The transition from the splay texture to the bend one, through the order reconstruction phenomenon, induces a fast alignment of a thin biaxial region (i.e. $2*\xi_b$ ~ 10nm), along the applied electric field, in a short period of time in the order of 1μs. The macroscopic effect is that a sudden increment of the equivalent capacitance occurs. This capacitance change determines an electric current flowing inside the π-cell. To better understand this statement, we can consider the electric current definition [34]:

$$I_c(t) = \frac{d}{dt}\left(C_{lc}(t) \cdot V_{lc}(t)\right) \qquad \text{[eq. 4.2.2.1]}$$

$$I_c(t) = V_{lc}(t)\frac{dC_{lc}(t)}{dt} + C_{lc}(t)\frac{dV_{lc}(t)}{dt}$$

E.q. 4.2.2.1 shows that the electric current flowing across the cell exists only in presence of variations of the external applied voltage and/or of the internal capacitance. It is known that the capacitance of a liquid crystal cell is proportional to the pixel area and to the effective dielectric constant of the LC and it is also inversely proportional to the thickness of the cell, *d*. Hence the cell capacitance can be written as:

$$C_{lc}(t) = \frac{A}{d} * \langle \bar{\bar{\varepsilon}}_{Lcd} \rangle_E \qquad \text{[eq. 4.2.2.2]}$$

It is also known that the effective dielectric constant of the liquid crystal, in 1-D approximation, can be defined by:

$$\langle \bar{\bar{\varepsilon}}_{Lcd} \rangle_E = \frac{1}{\frac{1}{d}\int_0^d (\varepsilon_0(\Delta\varepsilon^*(-q1(z) - q4(z) + \varepsilon_{iso}))^{-1} dz} \qquad \text{[eq. 4.2.2.3]}$$

From eq. 4.2.2.2 and eq. 4.2.2.3, one obtains that the total capacitance is expressed as:

$$C_{lc}(t) = \frac{\varepsilon_0 A}{d} \frac{1}{\frac{1}{d}\int_0^d \frac{1}{\varepsilon_0(\Delta\varepsilon^*(-q1(z,t) - q4(z,t) + \varepsilon_{iso})} dz} \qquad \text{[eq. 4.2.2.4]}$$

From [e.q. 4.2.2.4], one can deduce that the electric current flowing across the π-cell depends on the algebraic sum of two elements of the **Q**-tensor, $q_1(z, t)$ and $q_4(z, t)$. Moreover, from the **Q**-tensor order definition, taking the laboratory axes to be such that the directors **n** and **m** lies along the *x* and *z* axes respectively, the **Q**-tensor eigenvalues can be written as: $\lambda_1(z,t) = q_1(z,t)$, $\lambda_2(z,t) = q_4(z,t)$ and $\lambda_3(z,t) = -q_1(z,t) - q_4(z,t)$. Thus, one can consider that the electric current is inversely proportional, in time, to $\lambda_3(z,t)$ variations through the cell thickness. Since $\lambda_3$ is associated with the eigenvector along the *z*-axis, it describes the electrically induced biaxiality inside the cell through the eigenvalues exchange. For this reason, we expect that the electric current reflects the induced nematic distortion.

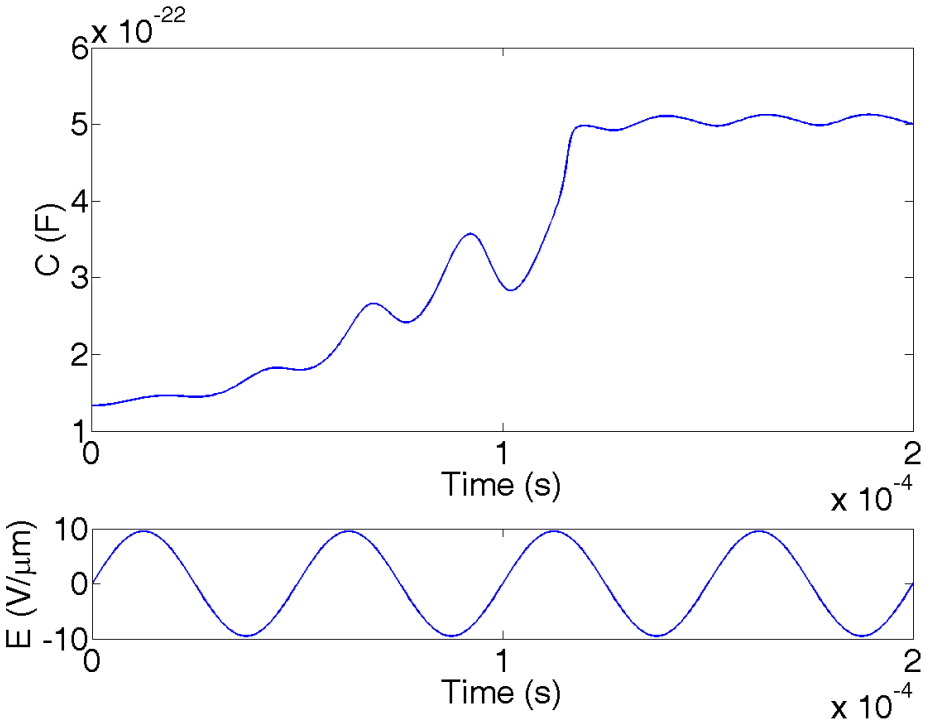


**Fig. 4.2.2.1 Numerically calculated time evolution of the capacitance $C_{lc}$ (top) versus applied voltage $V_{lc}$ (bottom) across a 1 µm thick π-cell when submitted to a sinusoidal electric field with $f$ = 20kHz and $U$ = 9.5V**

Fig. 4.2.2.1 shows a typical 1 µm thick liquid crystal cell equivalent capacitance time evolution in presence of a suitable external sinusoidal electric field. $C_{lc}$ evolves from a minimum value close to $10^{-22}$ F to a maximum one of about $5x10^{-22}$ F. The maximum value is reached at t=0.117ms, when the splay-bend transition determined by the order reconstruction phenomenon is completed.

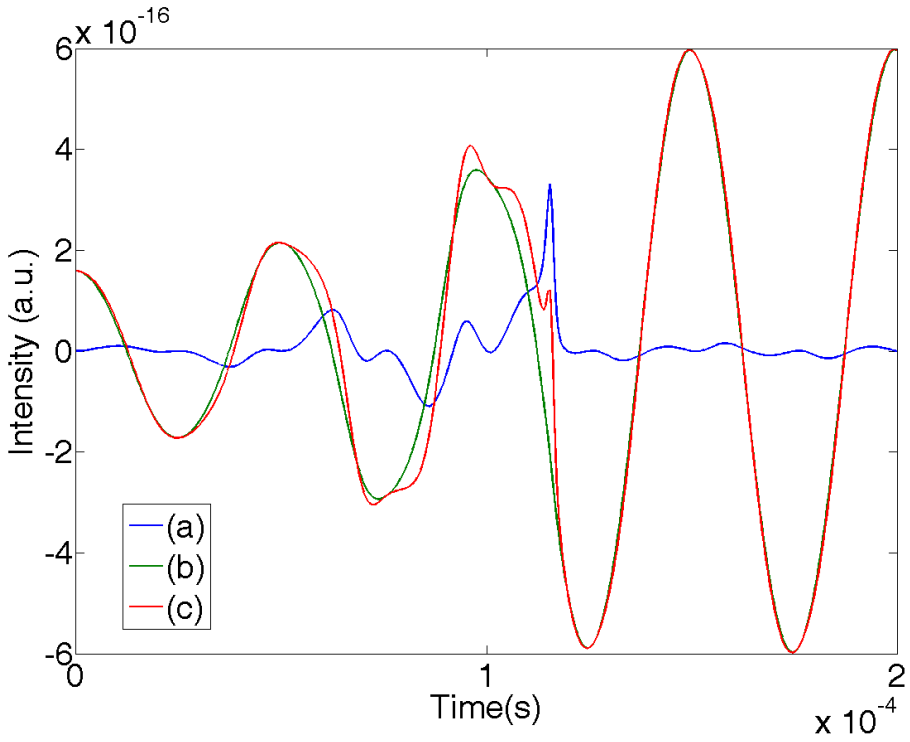


**Fig. 4.2.2.2 Numerical calculated time evolution of $V_{lc}\frac{dC_{lc}}{dt}$ (a) , $C_{lc}\frac{dV_{lc}}{dt}$ (b) and $I_{lc}$ (c) across a $\pi$-cell when submitted to a sinusoidal electric field $V_{lc}$ with $f$ = 20kHz and $U$ = 9.5V**

Fig. 4.2.2.2 shows the electric current (c) evaluated by using the eq. 4.2.2.1. Lines (a) and (b) represent the two different contributions to the electric current due to respectively the variation of the electric capacity and to the variation of the applied voltage. It is evident that the fast variations of the overall electric current mainly depends on the fast changes of the electric capacity induced by the re-orientation of the nematic molecules.

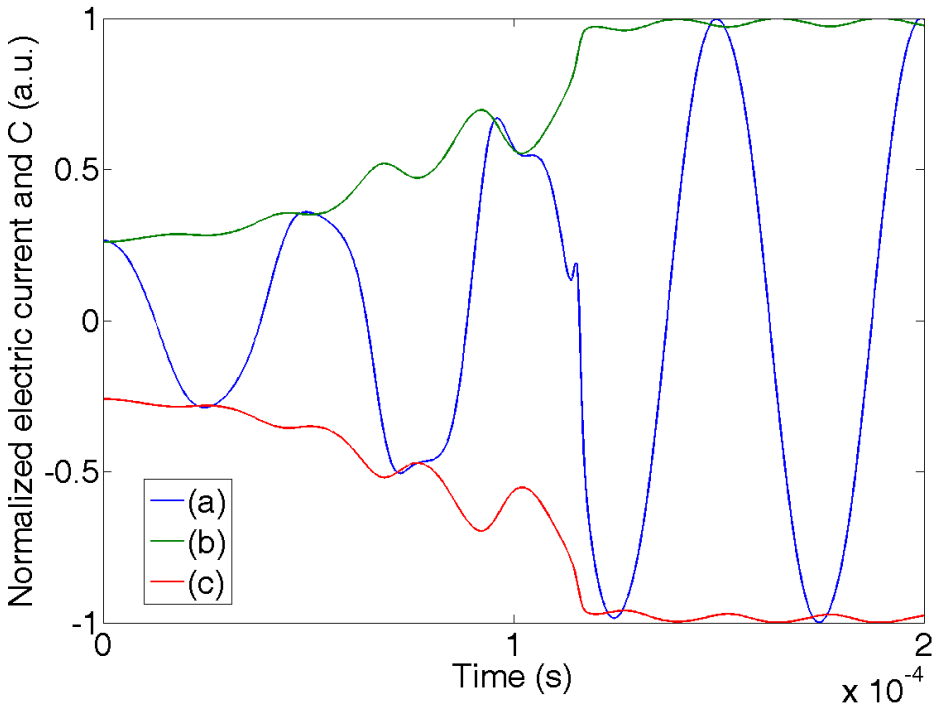


**Fig. 4.2.2.3 Numerically evaluated time evolution of the electric current flowing across the cell (a), and the variable cell capacitance $C_{lc}$(b) and its negative correspondent $-C_{lc}$(c) for an applied sinusoidal electric field with $f$ = 20kHz and $U$=9.5V**

Fig. 4.2.2.3 shows the superposition in time of the normalized numerical electric current, which flows across the π-cell when submitted to a sinusoidal electric field, together with the liquid crystal equivalent capacitance $C_{lc}(t)$ and its negative correspondent $-C_{lc}(t)$. One can see that the amplitude of the periodic electric current follows the equivalent liquid crystal capacitance evolution.

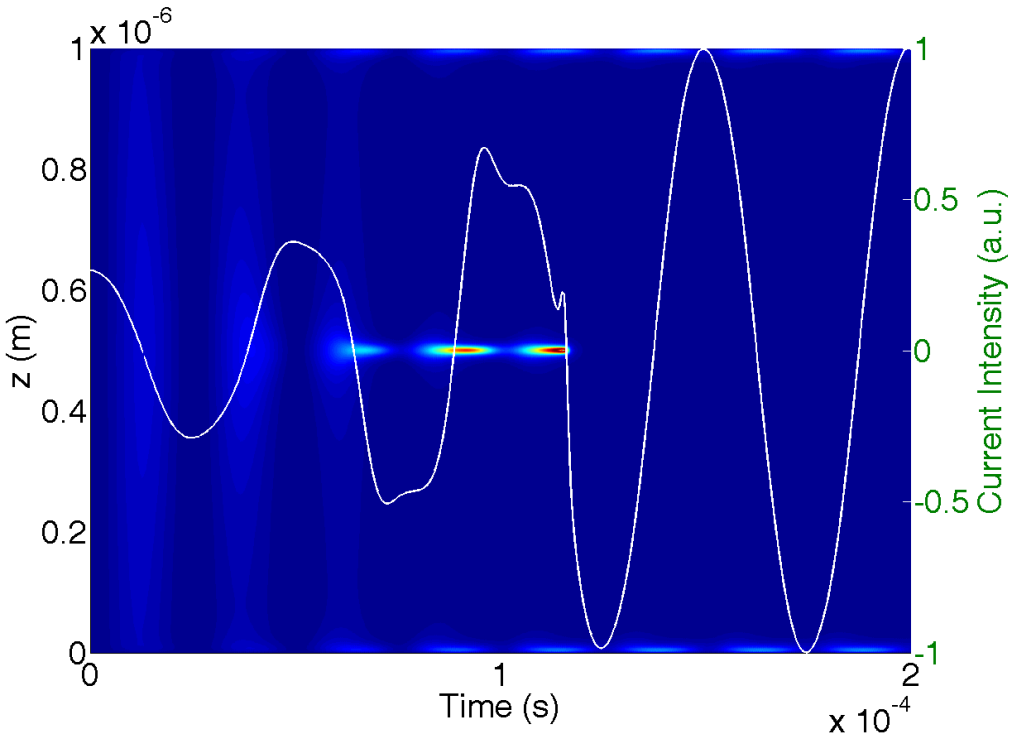


**Fig. 4.2.2.4 Biaxiality and electric current time evolutions in a π-cell cell for an applied sinusoidal electric field with *f*=20kHz and *U*=9.5V. The local biaxiality is mapped by colors: from blue, *b*=0 for the uniaxial order, to red, *b*=1 for the full biaxial order.**

In Fig. 4.2.2.4, the theoretical time evolution of biaxial nematic order inside the cell is superposed to the numerically evaluated electric current in the case of an applied sinusoidal field with frequency $f$ = 20kHz and amplitude $U$ = 9.5V. The time evolution of the induced biaxiality presents 5 undulations, that correspond, in time, with the occurrence of the maximum amplitude of the applied electric field. The electric current, shows peaks with different shapes and distortions. During the first cycle, the electric current presents an initial modulation without evident distortion as the biaxiality is yet distributed on all the cell thickness. During the second cycle, it presents an irregular shape with two peaks with different structure. During the third cycle, a small structure appears at t=0.115ms. This distortion, as we can see in Fig. 4.2.2.5, is related to the breaking of the biaxial wall in the middle of the π-cell by means of order reconstruction. We note that the fast variations of the electric current occur when the biaxiality is larger than $b$=0.4 and the fastest one appears in correspondence of the order reconstruction phenomenon. In fact, its length corresponds to the biaxial volcano – crater due to the fast vertical realignment from planar orientation to the vertical one of nematic molecules in the middle plane of the π-cell.

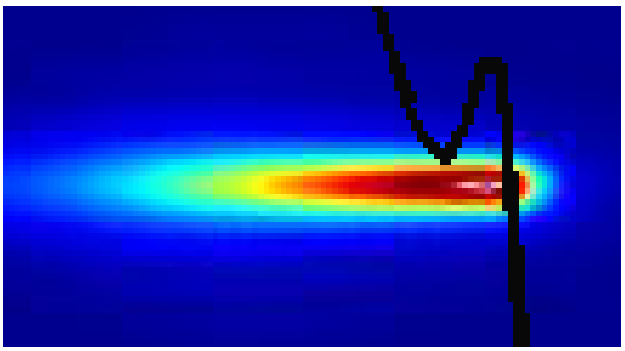

**Fig. 4.2.2.5 Enlargement of Fig. 4.2.2.4 showing the time evolution of biaxial order when the order reconstruction takes place. The electric current peak (black line) corresponds to an applied sinusoidal field *f* = 20kHz, *U*= 9.5V. The represented time interval is about 10μs.**

At time t=0.117ms, when the order reconstruction phenomenon is completed and the nematic texture has relaxed in the bend one, i.e. all the nematic molecules are practically aligned along the vertically applied electric field, the electrically equivalent liquid crystal capacitance presents a greater value than the corresponding capacitance associated to the starting splay texture, since $\varepsilon_{\parallel} > \varepsilon_{\perp}$. Therefore, after the splay-bend transition, the equivalent capacitance can be considered constant and the electric current variations are practically now due only to the external electric voltage oscillations. The electric current presents a sinusoidal shape, with a lead phase of -90° with respect to the applied electric voltage, as shown in Fig. 4.2.2.6.

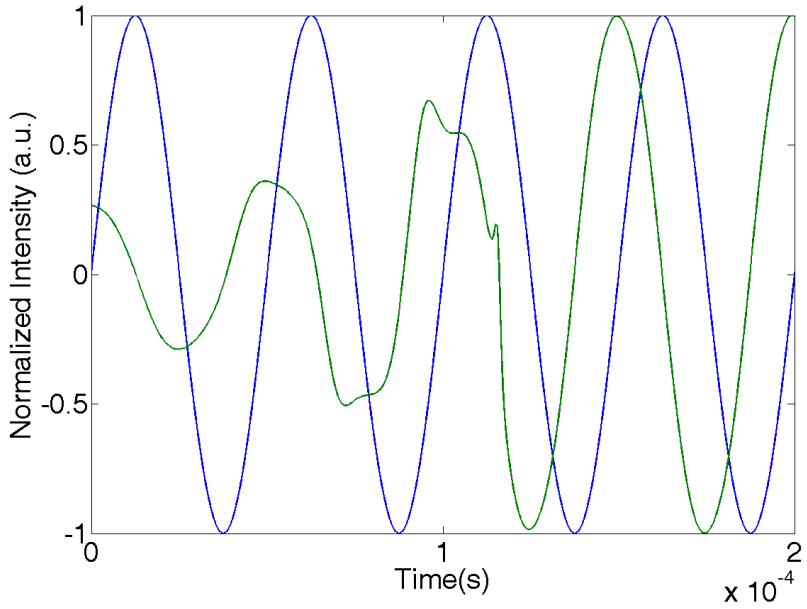


**Fig. 4.2.2.6 Electric current and electric field time evolutions in a π-cell cell for an applied sinusoidal electric field with *f* = 20kHz and *U* = 9.5V**

In the following subsection we will present numerical results of the electric current time evolution when, for a fixed frequency, the amplitude varies.

### 4.2.3 Theoretical electric current and biaxiality in a π-cell

We now analyze a π-cell submitted to an external sinusoidal electric voltage oscillating at $f$=20kHz, when its amplitude varies from 4.8 V to 23.8V. Three different cases can be considered:

#### Case 1: Amplitude $U < U_{th}$=8.34 V

When the applied sinusoidal electric field is below the electrical biaxial threshold, $U_{th}$=8.34 V, the electric current presents the characteristic shape of a sinusoid with a modulated amplitude, as shown in Fig. 4.2.3.1. The amplitude modulation is due to the progressive dielectric reorientation of the nematic molecules along the vertically applied field throughout the cell thickness, with the exclusion of the middle plane where all the starting splay distortion tends to be concentrated, as previously shown in Fig. 4.1.6.1 (a) and (b).

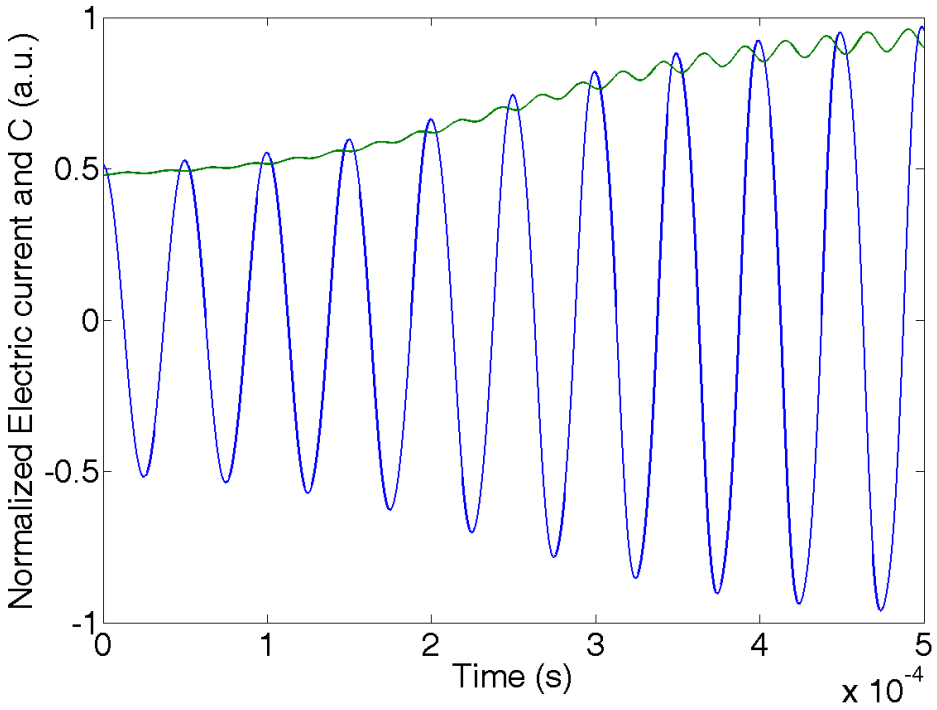


**Fig. 4.2.3.1 Electric current and $C_{lc}$ versus time for $U$=4.8V, $f$=20kHz**

When the applied electric field amplitude is lower but close to $U_{th}$ , the induced local biaxiality assumes values larger than 0.4, not enough strong to induce the order

reconstruction, but able to distort the shape of the electric current, as shown in Fig. 4.2.3.2. These deformations always appear in correspondence of the strongest values of the concentrated biaxiality.

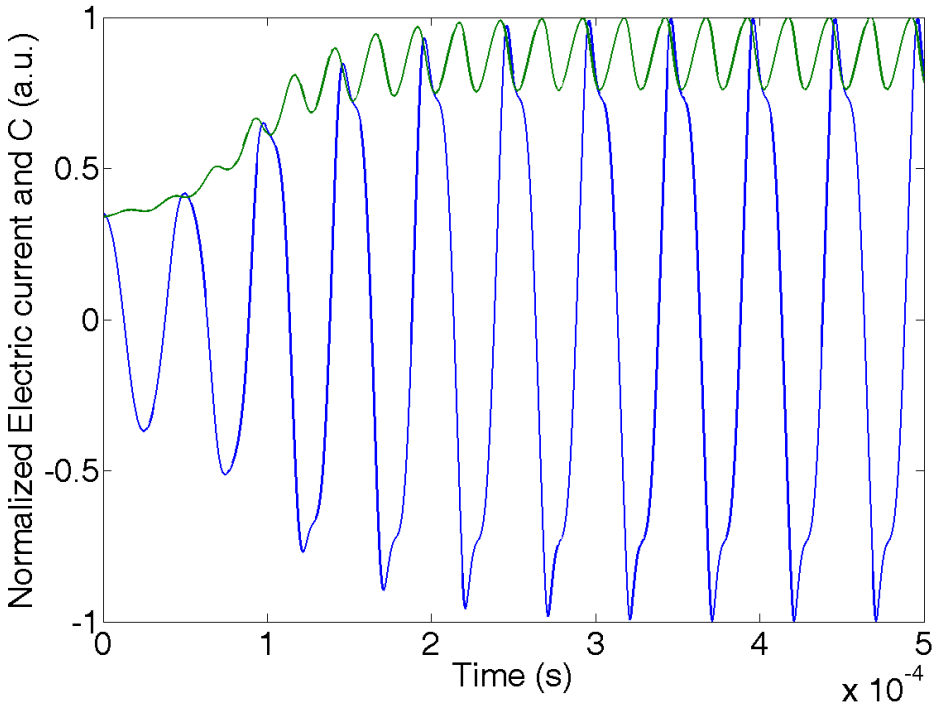


**Fig. 4.2.3.2 Electric current and $C_{lc}$ versus time for $U$=8.3V, close to $Uth$ = 8.34V, $f$ = 20kHz**

In this case, the biaxial wall does not break even if the maximum value of biaxiality is about $b$=0.98. The electric current flowing across the cell presents peaks deformations separated by the time interval between two adjacent dynamical biaxial clusters as shown in Fig. 4.2.3.3. They are present as long as the oscillating electric field is applied. When the field is switched off, the π-cell comes back to the original splay state. We can observe that the peaks deformation becomes progressively stronger till a steady state, when the distortion energy inside the system stabilizes.

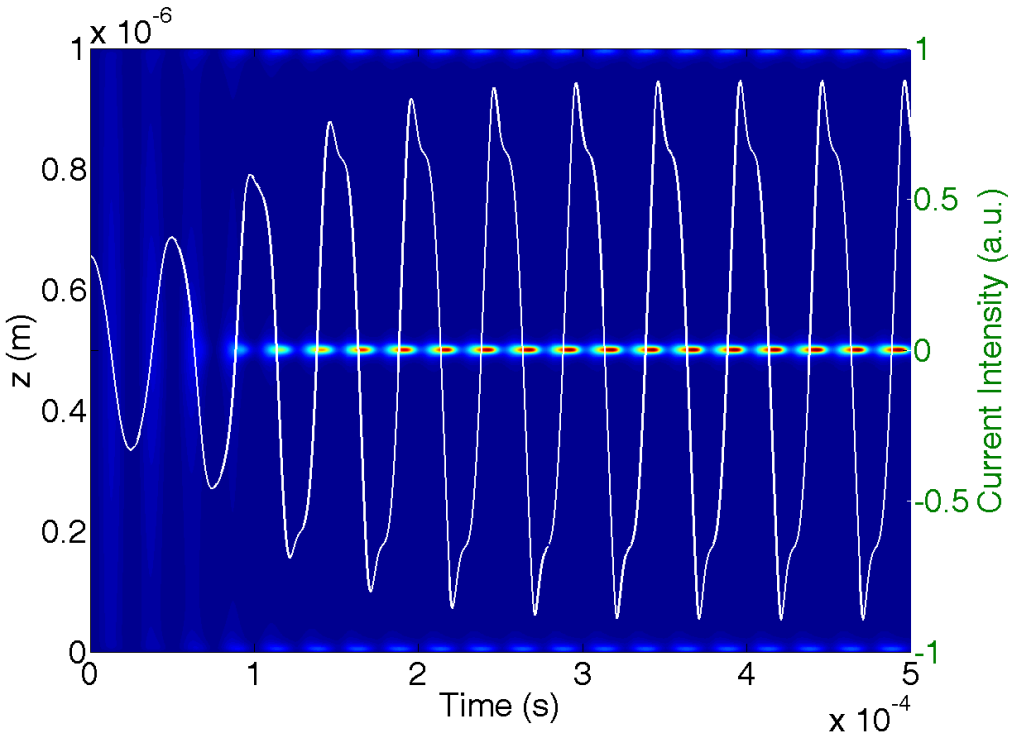


**Fig. 4.2.3.3 Superimposition of the time evolution of the biaxiality and the corresponding electric current which flows inside a π-cell submitted to an external electric field *U*=8.3V, close to *Uth* = 8.34V, *f*=20kHz**

### Case 2: Amplitude $U = U_{th} = 8.34$ V

As discussed in section 4.1.2, the amplitude of the electric threshold for a fixed frequency and temperature depends on the number of oscillations of the external electric voltage, which stores more and more bulk biaxial distortion till it is strong enough to induce the biaxial order reconstruction within the π-cell.

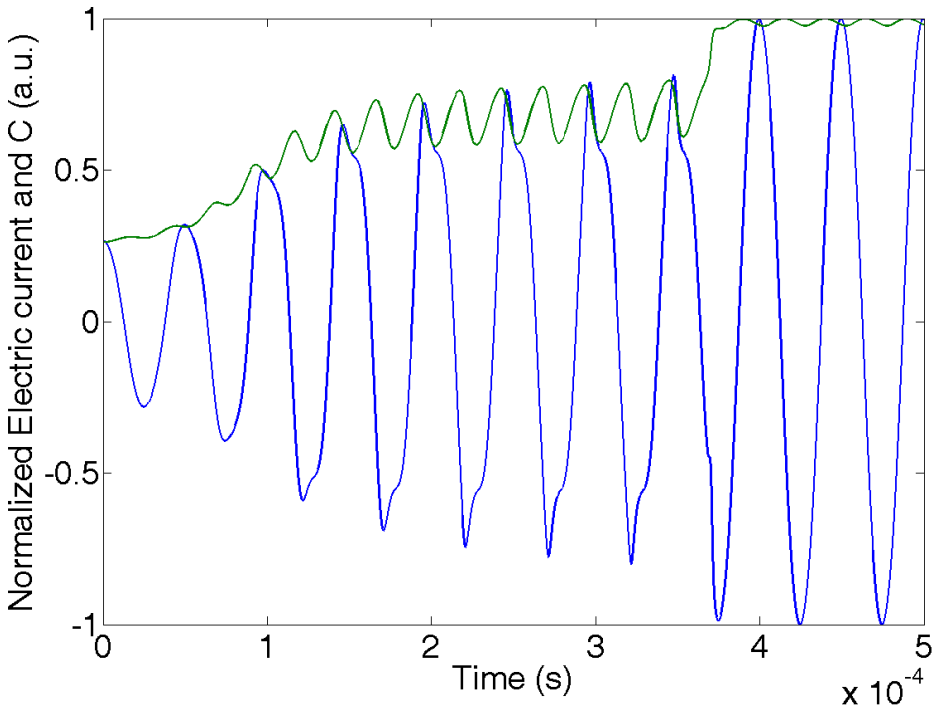


**Fig. 4.2.3.4 Electric current and $C_{lc}$ versus time for $U_{th}$ = 8.34V, $f$ = 20kHz, i.e. at the threshold for the order reconstruction.**

Fig. 4.2.3.4 shows the numerically evaluated electric current and the equivalent capacitance $C_{lc}$ in the case of an applied sinusoidal field with frequency $f$ = 20kHz and amplitude $U_{th}$ = 8.34V, at the threshold for the order reconstruction. One can observe three different behaviors in time, as also shown in Fig. 4.2.3.5. From 0<t<0.1ms the biaxial distortion inside the cell is spread on all the cell thickness and both the electric current and the capacitance does not present distortions. In the interval 0.1<t<0.369ms the induced distortion increases progressively and the electric current peak deformations become larger. At t= 0.369ms the order reconstruction takes place and after this phenomenon the electric current becomes a sinusoid with constant phase and amplitude.

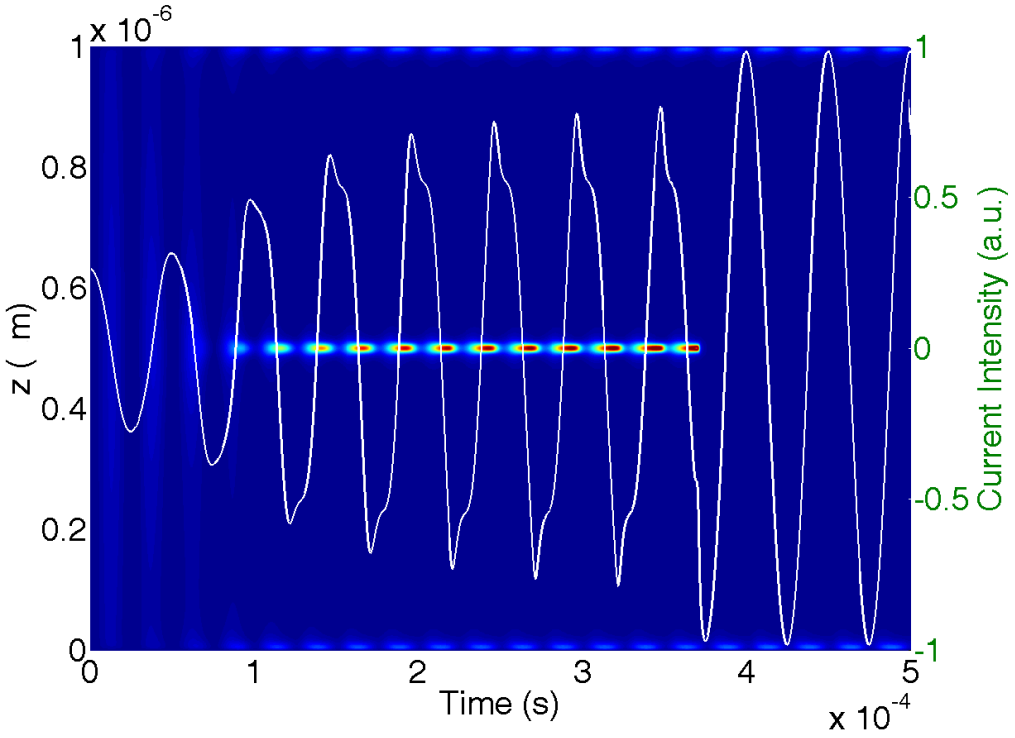


**Fig. 4.2.3.5 Super-imposition of the time evolution of the biaxiality and the corresponding electric current which flows inside a $\pi$-cell submitted to an external electric field $Uth$=8.34V, $f$=20kHz**

Fig. 4.2.3.5 shows the time evolution of the biaxial nematic order inside the cell and the superposed electric current versus time always in the case of an applied sinusoidal field with frequency $f$ = 20kHz and amplitude $U_{th}$ = 8.34V, at the order reconstruction threshold. We can observe, that there are 15 biaxial undulations in the bulk before that the splay-bend transition takes place. During the first 4 undulations, the biaxiality is spread along all the *z*-axis and it is not strong enough to induce peak deformations in the electric current shape. Starting from the fifth biaxial undulation, the biaxial order concentrates close to the middle plane of the cell and it is also sharper in time. The external oscillating electric field is storing elastic distortion in the middle of the cell. When this distortion energy is large enough, the order reconstruction takes place and the nematic texture passes from the splay configuration to the bend one. One can observe two signatures of this transition: a small peak appears in the electric current signal at t=0.369ms and the amplitude of the electric current oscillations reaches its maximum value and it stabilizes at this steady state.

### Case 3: Amplitude U > $U_{th}$

When the external electric field has an amplitude higher than the threshold, $U > U_{th}$, as discussed in section 4.1.2, the number of undulations necessary to accumulate enough distortion energy to induce the order reconstruction in the middle of the cell decreases as $U$ increases. For intense amplitudes, only one biaxial undulation is sufficient to induce the splay-bend transition and the electric current presents shapes similar to what is represented in Fig. 4.2.3.6 and in Fig. 4.2.3.7.

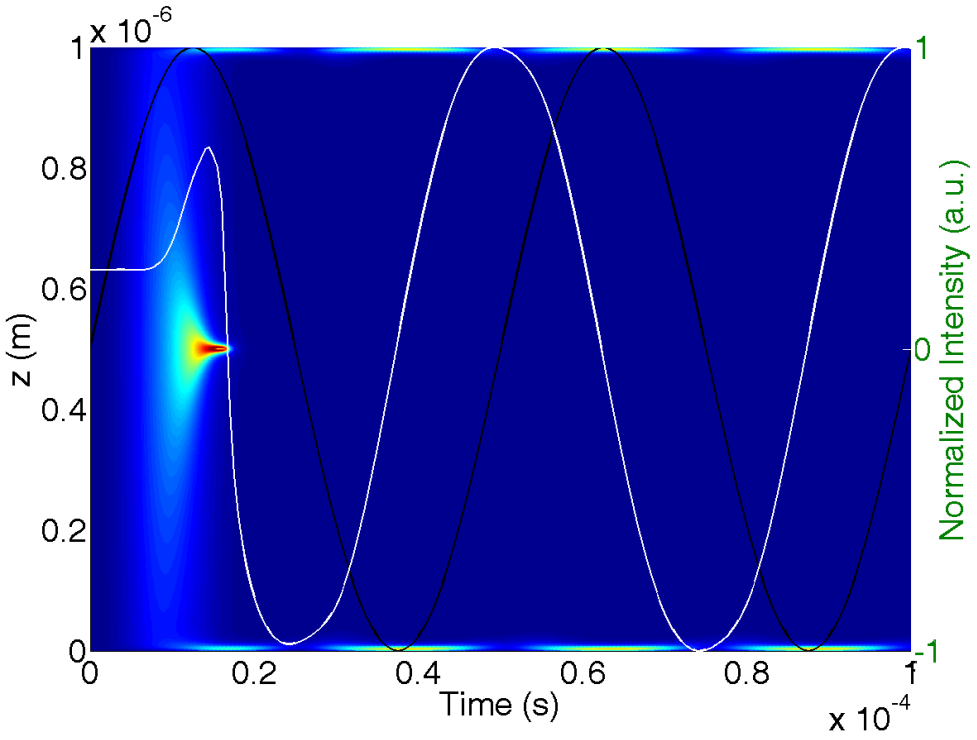


**Fig. 4.2.3.6 Superposition in time of the biaxiality, the electric current(white curve), and the applied electric field *U*=19V > *Uth*, *f*=20kHz (black curve)**

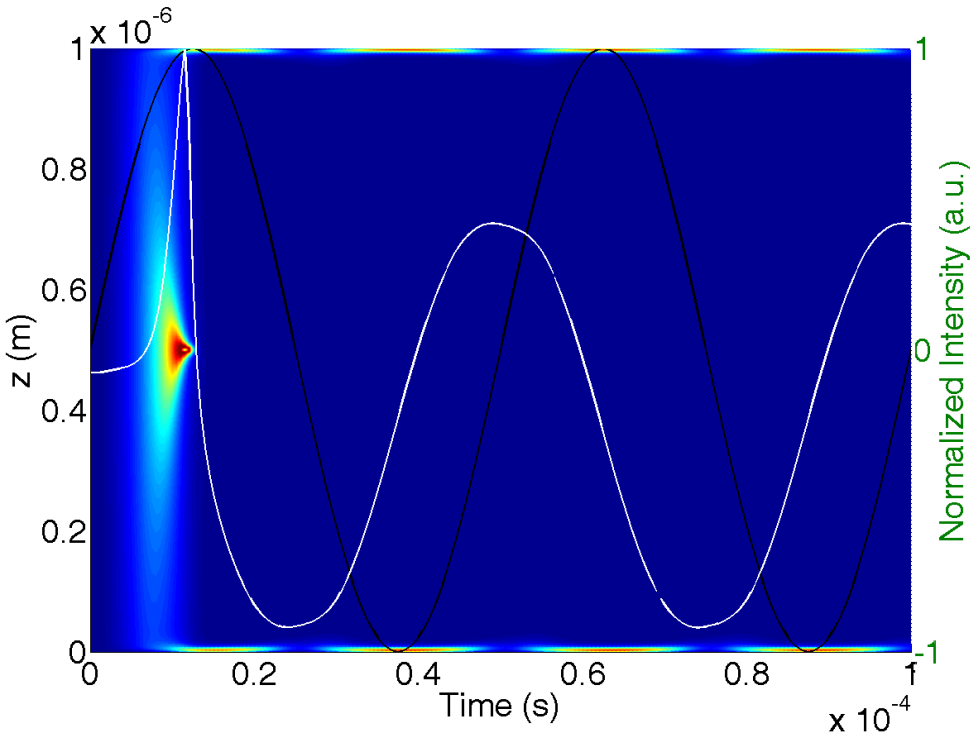


**Fig. 4.2.3.7 Superposition in time of the Biaxiality, electric current (white curve), and applied electric field *U*=23.8V (*U* > *Uth* ), *f*=20kHz (black curve)**

In Fig. 4.2.3.6 and Fig. 4.2.3.7, the amplitudes of the external electric field is largely above $U_{th}$=8.34V, $U$=19.00V and $U$=23.80V respectively, and in both cases the order reconstruction occurs within the first half cycle of the applied signal, inducing only one biaxial undulation. In both cases, the biaxiality concentrates in a very short time in the middle of the cell and an higher amplitude implies a narrow time window and a faster order reconstruction. Due to the intense applied field, the molecules alignment is very fast and the effect of the wall breaking remains mixed within the general dielectric reorientation in all the cell thickness. The consequence is that, as the two phenomena occur at the same time scale, from an experimental point of view the electric current observations will provide only one characteristic time.

### 4.2.4 Experimental Observations

In this section, we will present our experimental results for a nematic liquid crystal π-cell submitted to a sinusoidal electric field. The main experimental investigations were conducted by measuring the electric current flowing across a π-cell during the application of an external sinusoidal electric field. In order to improve the knowledge of the order reconstruction mechanism, the experimental observations will be compared with numerical results.

Measurements has been performed using 4-cyano-4'-n-penthylbiphenyl liquid crystal; brand K15 from Merck (also known as 5CB). This compound exhibits strong positive dielectric anisotropy, which determines a strong coupling with the applied electric field. We obtained the symmetric π-cell by using the procedures presented in section 3.7 of this dissertation. The oblique symmetrical anchoring on the two boundary plates was obtained by polymeric (PI 20%) coating, this results in a strong anchoring with a small pre-tilt angle of about 8°.

To measure the electric current flowing across the cell during the electric field application, the cell was connected in series to an electric resistor, $R_1$ =10kΩ. We measured the amplitude of the electric current flowing in the circuit by measuring the dropped voltage $V_r$ across this resistor.

We applied a modulate electric field, $V_{in} = Usin(2\pi ft)$, with variable amplitude U ∈ [10V, 70V], frequency $f$ ∈ [10kHz, 100kHz] and fixed duration τ=1ms. All measurement have been carried out at room temperature.

To observe textural changes, the sample was directly observed by means of a polarized microscope. The plate of the microscope was rotated to align the optical axis of the sample in the starting splay configuration at 45° with respect to the optical axis of the crossed polarizers. This is a well known condition of maximum intensity for the transmitted light in presence of a birefringent sample. Therefore the director configuration during the splay-bend transition can be optically characterized by mean of direct optical observations: the splay state appears as a dark domain, while the bend state is bright under crossed polarizers.

### *4.2.4.1 Experimental electric current in a π-cell*

In Fig 4.2.4.1.1, we present experimental results for a symmetric π-cell of thickness about 2.8 µm. The typical behavior of the electric current flowing across a π-cell during the application of a sinusoidal electric field of frequency $f$ = 20khz with different amplitudes is shown.

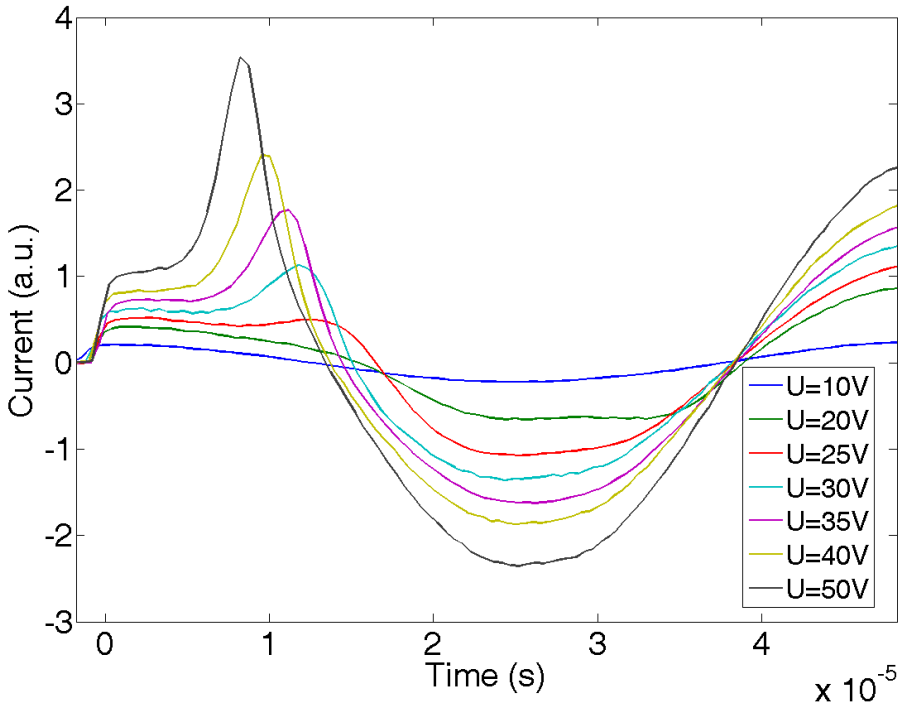


**Fig 4.2.4.1.1 Experimental measured electric current flowing across a π-cell submitted to a sinusoidal electric field, with $f$ = 20khz and $U$ = 10, 20, 25, 30, 35, 40, 50V. Cell thickness $d$=2.8 µm**

Observing the sample under a crossed polarized microscope, the splay to bend transition can be optically detected by the local optical change from the starting dark state to a bright one. Varying the applied amplitude, we found the electric field threshold, for $f$=20kHz, to be $U_{th}$ = 25V, corresponding to $E_{th}$= 8.86V/µm. As we can see in Fig 4.2.4.1.1, for such electric field the first half cycle of the electric current presents an irregular shape with two different structures. The first structure is related to the initial response when the electric field is switched on. The second structure is related to the order reconstruction.

In Fig 4.2.4.1.1, for $U$=10V and $U$=20V, i.e. electric field amplitudes below the order reconstruction threshold, $U < U_{th}$, as expected, no splay-bend transition has been observed.

In this case, the applied voltage amplitude is not strong enough to concentrate enough biaxiality in the middle plane of the cell to induce the order reconstruction. For $U$ = 20V, the first cycle presents a distorted shape related to an induced biaxiality, which spreads all along the cell thickness. The second cycle presents two different structures, that according to our numerical simulations, appear when the biaxiality is concentrated in the middle of the sample. Nevertheless the electric induced biaxiality is not high enough to induce the splay-bend transition.

For amplitudes above the threshold, $U > U_{th}$, that is $U$ = 30V, 35V, 40V and 50V, the nematic molecules are submitted to a fast alignment along the electric field direction and the measured electric current presents an irregular shape only at the first half cycle. The sharp structure is related to the molecule reorientation and the order reconstruction phenomenon, which appear together, see Fig. 4.2.3.6 and Fig. 4.2.3.7. This structure becomes faster for higher amplitudes and its magnitude is proportional to the applied voltage. In this case the general dielectric reorientation is mixed with the order reconstruction phenomenon and only one peak can be observed.

Fig 4.2.4.1.2 shows the numerical evaluated (green curve) and the experimental measured (blue curve) electric current versus time. The experimental electric current presents a higher peak at the first half cycle, and presents a smaller distortion at the second one; the current becomes a sinusoid with constant amplitude at about t=0.030ms. In the numerical case, the electric current presents a smaller first structure and a well visible deformation at the second half cycle. The order reconstruction occurs at t=0.033ms.

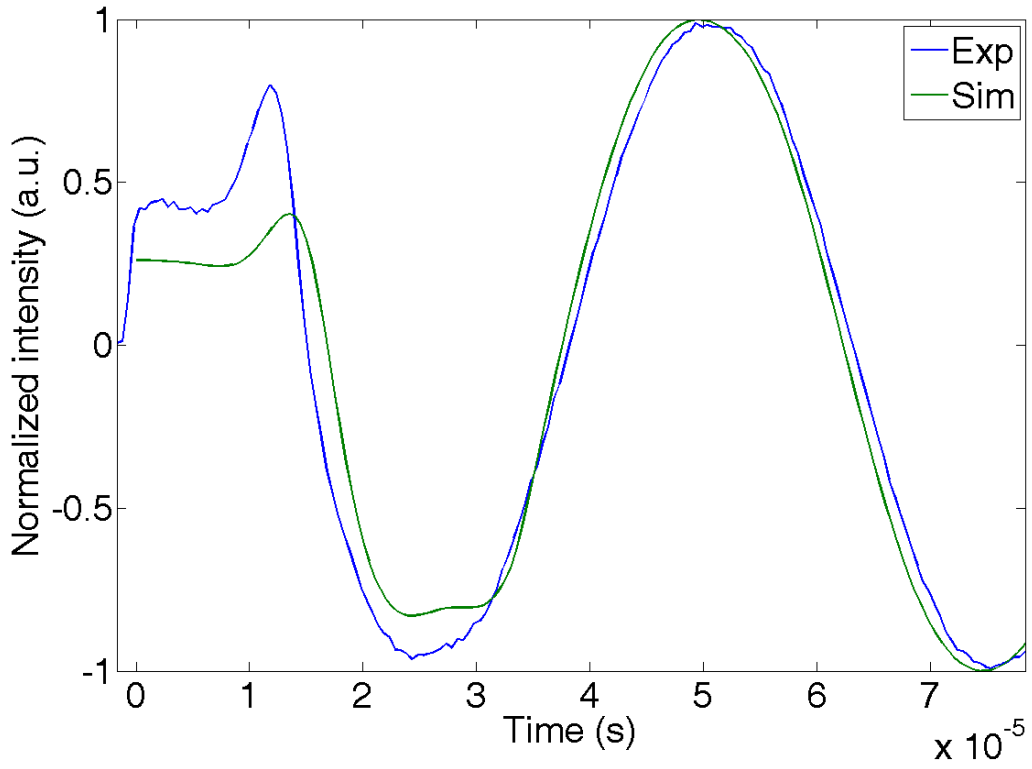


**Fig 4.2.4.1.2 Numerical evaluated electric current (green curve) superposed to the experimental measured electric current (blue curve). Both for an applied sinusoidal electric field U = 30 V, f = 20kHz, cell thickness d=1.5µm**

### *4.2.4.2 Order reconstruction threshold, $E_{th}$: dependency on the applied frequency*

In this subsection we present our studies on the dependence of the order reconstruction threshold $E_{th} = U_{th}/d$ on the applied signal frequency. A typical plot of $E_{th}$versus $f$ is shown in Fig 4.2.4.2.1. The electric field threshold, $E_{th}$ , was optically found observing the splay – bend transition under a polarized optical microscope, while increasing the applied amplitude *U* from 10V to 40V in steps of 1V, for different frequencies, *f*.

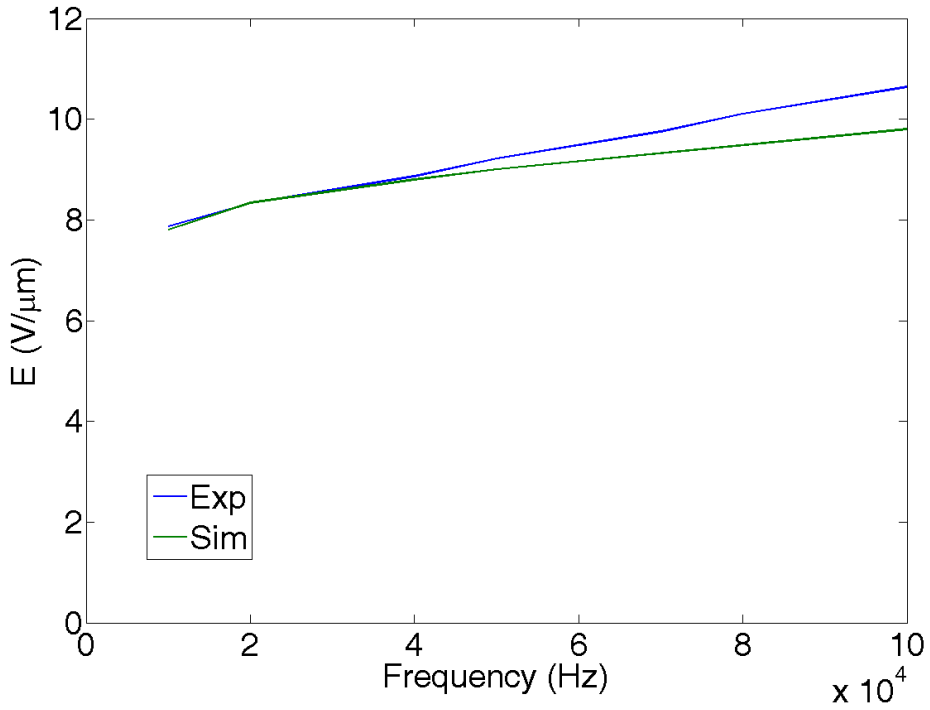


**Fig 4.2.4.2.1 Theoretical and experimental Eth versus frequency *f* , for a *π*-cell with normalized thickness *d* = 1µm.**

Fig 4.2.4.2.1 shows the experimental order reconstruction threshold data as a function of the applied frequency, *f*. For higher *f*, an increase of $E_{th}$ is observed, which corresponds to a dynamical threshold. $E_{th}$ increases to force a fast evolution of the order reconstruction in the imposed shorter signal period. As discussed in section 4.1.2, for a smaller signal period, a higher electric amplitude is necessary to accumulate the required distortion energy to induce the splay-bend transition through the biaxial order reconstruction.

### *4.2.4.3 Order Reconstruction dependency on the applied frequency and amplitude*

The dependency of the order reconstruction on the applied frequency and amplitude is reported in the following. A typical plot of the applied amplitude versus the order reconstruction time for different frequencies is shown in Fig 4.2.4.3.1. We measured the time at which the order reconstruction takes place by means of the electric current flowing across the cell, as discussed in sections 4.2.2. and 4.2.3; where we discussed how the current peaks are related to the order reconstruction.

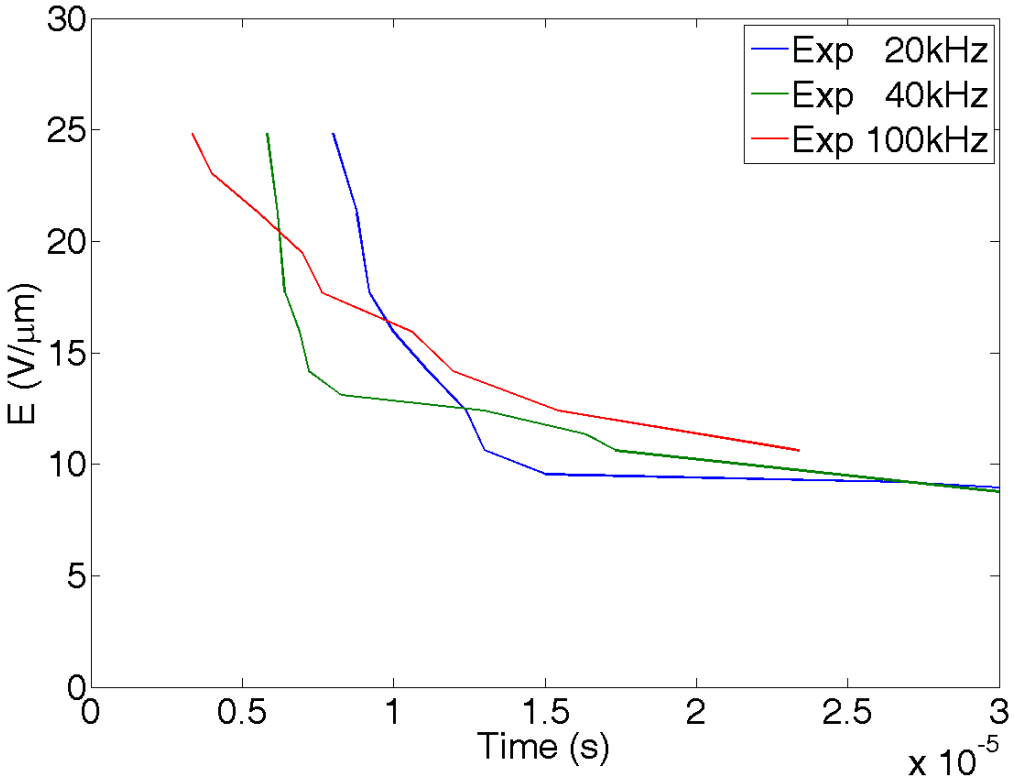


**Fig 4.2.4.3.1 Experimental applied electric amplitude *E* versus order reconstruction time for *f* = 20kHz, 40kHz, 100kHz. Cell thickness *d* = 2.8µm**

In Fig 4.2.4.3.1, we can observe, as discussed in section 4.1.5, Fig. 4.1.5.1, that for a fixed frequency, an increasing amplitude corresponds to a faster order reconstruction.

On the other hand, for very intense, strong and low applied electric amplitudes, the order reconstruction will behave differently. We must take into account the induced energy, that depends both on the amplitude and the signal period, and the energy accumulation rate, that depends on the frequency, the relaxation time, and the number of induced biaxial undulations.

For very intense amplitudes, at least three times the order reconstruction threshold, a higher frequency will induce a faster order reconstruction. In this case, the induced energy is high enough for the order reconstruction to take place at the first half signal period, independently from the frequency, thus there's not influence of the accumulation rate, neither of the relaxation time. In first approximation, this case corresponds to the rectangular electric field, with an application time equals to half the signal period, $\tau = T/2$ .

Fig 4.2.4.3.2 shows the experimental electric current flowing across the cell for an applied very intense amplitude $E$ = 25 V/μm for two different frequencies, $f$ = 20kHz and $f$ = 100kHz. We can observe that the order reconstruction peak occurs faster for $f$= 100kHz than for $f$= 20kHz.

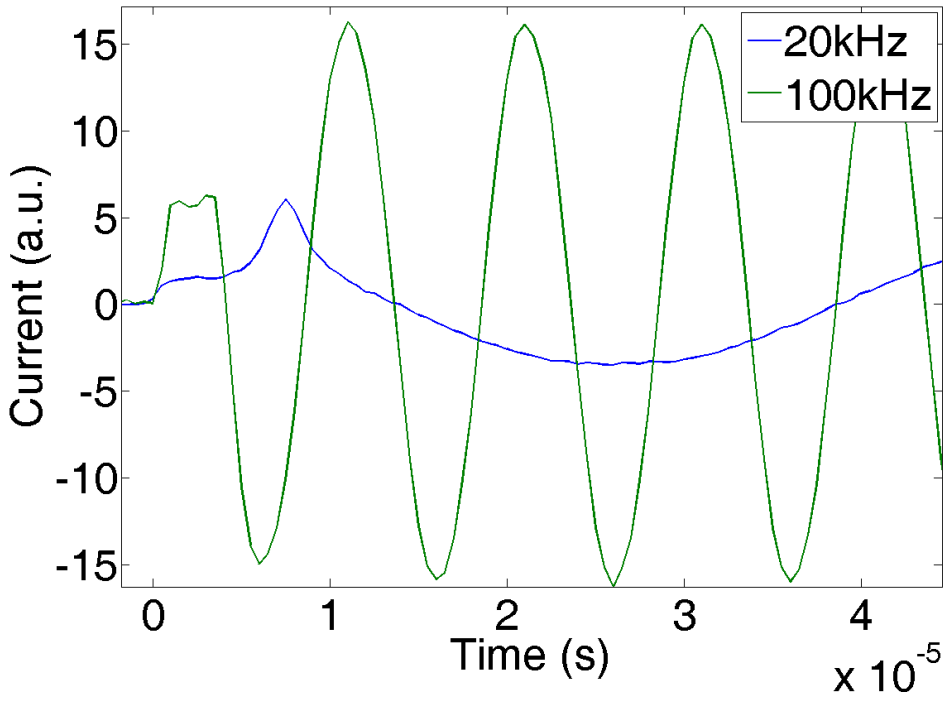


**Fig 4.2.4.3.2 Electric current across a π-cell for an applied sinusoidal electric field, amplitude $E$ = 25V/μm and two different frequencies $f$=20kHz, $f$ = 100kHz.**

For strong amplitudes, in the order of two times the order reconstruction threshold, the splay-bend transition takes place with a comparable delay with respect to the switching on of the external electric field. In this case, the induced energy and the accumulation rate compensated each other; the necessary distortion energy is reached in the same time because higher frequencies present a smaller induced energy by period but a higher numbers of undulation; meanwhile lower frequencies induce a lower number of stronger distortions.

Fig 4.2.4.3.3 shows the experimental electric current flowing across the cell for an applied amplitude E=15V/μm and frequencies $f$=20kHz and $f$=100khz. We can observe that for $f$=20kHz the order reconstruction takes place during the first cycle at about t = 0.012ms, where a peak related to the order reconstruction is well evident. For $f$=100kHz, the order reconstruction takes place at the same timing, but at the second cycle. Now there is not any

evident peak but a small deformation in the current curve. Also in this case, at t= 0.012ms, the electric current becomes a perfect sinusoid and both from optical observations and from our numerical results one knows that the order reconstruction had occurred.

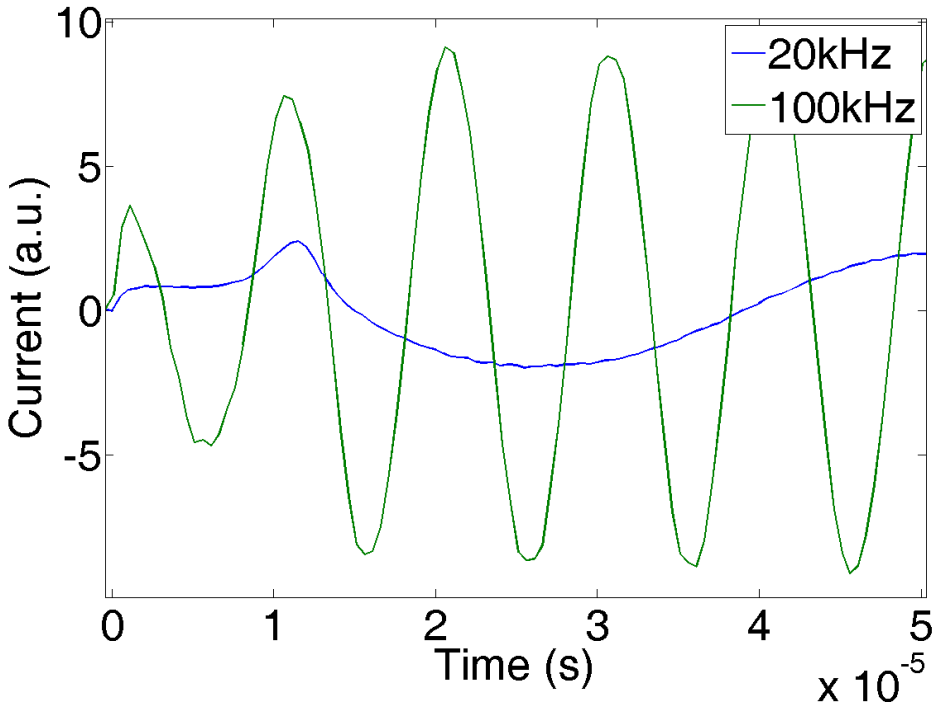


**Fig 4.2.4.3.3 Electric current across a π-cell for an applied sinusoidal electric field, amplitude *E* = 15 V/µm and two different frequencies *f*=20kHz, *f*=100kHz.**

For low electric amplitudes, at the order reconstruction threshold, the splay-bend transition is influenced by other phenomena, as a non uniform breaking of the biaxial wall or by the moving of defects towards the boundary plates.

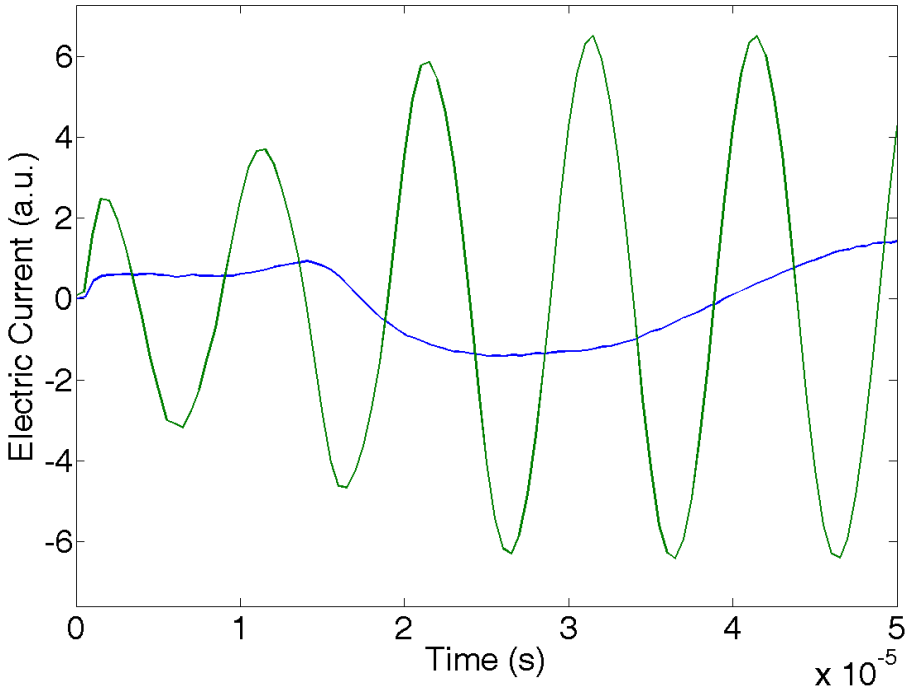


**Fig 4.2.4.3.4 Electric current across a π-cell for an applied sinusoidal electric field, amplitude *E* = 10 V/μm and two different frequencies *f*=20kHz, *f* = 100kHz.**

Fig. 4.2.4.3.4 shows the experimental electric current flowing across the cell for an applied amplitude $E$=10V/μm and frequencies $f$=20kHz and $f$=100khz. We can observe that for $f$=20kHz the order reconstruction takes place during the first cycle at about t = 0.016ms, where a peak related to the order reconstruction is evident. For $f$=100kHz, the order reconstruction takes place at the third cycle, at about t =0.022ms. Now there is not any evident peak but a small deformation in the current curve. The induced distortion energy by period is smaller in this case, thus more time is required for the order reconstruction to takes place.

# 5. Conclusion and Future work

The main focus of this thesis has been the development of an advanced numerical model to simulate the behavior of nematic liquid crystals when subjected to strong fields. A full Landau de Gennes **Q**-tensor description has been used in order to describe the nematic phase. A numerical algorithm was implemented applying the FEM method based on Galerkin's formulation, to minimize the free energy of the nematic system for specific boundary conditions.

We computed the evolution of the biaxiality and the electric current flowing across a symmetric and asymmetric π-cell after the application of external sinusoidal electric field with variable frequencies and amplitudes. We studied the dependence of the dynamical transition threshold, the induced distortion accumulation rate, the numbers of induced undulations, on the applied frequency and amplitude.

For a better and complete understanding of the order reconstruction dynamics, we performed experimental measurements of the electric current flowing across a nematic π-cell when subjected to an external sinusoidal electric field. The experimental observation were compared to our numerical results.

We observed that the induced biaxial distortion is modulate with a frequency that is two times that of the applied signal. Furthermore, the accumulation rate of the induced distortion inside the cell depends on the applied electric amplitude and frequency and on the nematic relaxation time.

By measuring the electric current flowing across the cell, the evolution in time of the induced biaxial distortion inside a π-cell submitted to an external sinusoidal electric field can be studied. In fact, we observed, both numerically and experimentally, that the shape deformations on the electric current cycles are related with the internal induced biaxiality, and the electric current can be used as an indirect measurement method of the splay-bend transition. Furthermore, the time when the order reconstruction phenomenon takes place can be determined as the time when the electric current reach a steady state. In fact, we observed that before the order reconstruction, both the phase and amplitude of the electric

current are variable, while right after the electric current becomes a sinusoid with constant amplitude and a phase lead of -90° respect the applied signal.

The time when the order reconstruction takes place, as for the case of a rectangular electric pulse, will depend on the cell thickness, but, due to the external signal periodicity, a different number of oscillations will be present for different cell thicknesses. In our preliminary studies, we observed that a larger cell thickness requires a small number of undulations to induced the order reconstruction inside the cell. This reflexes on the electric current flowing across the cell. We observed that the cell thickness can be deduced from the number of induced biaxial undulations before the order reconstruction; by applying a known electric threshold and frequency. Further investigation are required to confirm our preliminary studies and to define a numerical model.

## References


[1] P.G. De Gennes, J. Prost: *The Physics of Liquid Crystals, 2nd Ed.* (Clarendon Press, Oxford) (1993)

[2] G. Lombardo, H. Ayeb, F. Ciuchi, M. P. De Santo, R. Barberi, R. Bartolino, E. G. Virga, and G. E. Durand, *Physical Review E* **77** (2) (2008).

[3] R. Barberi, F. Ciuchi, G. Durand, M. Iovane, D. Sikharulidze, A. Sonnet, and E. Virga, *Eur. Phys. J. E* **13**, 61 (2004).

[4] A. Amoddeo, R. Barberi, G. Lombardo, *Liquid Crystals*, **38:**1, 93-103 (2011).

[5] P. Biscari, P. Cesana. *Contin. Mech. Thermodyn.* **19** (2007) 285-298.

[6] G. Lombardo, H. Ayeb, and R. Barberi, *Physical Review E* **77** (5) (2008).

[7] Barberi, R.; Ciuchi, F.; Lombardo, G.; Bartolino, R.; Durand, G.E. *Phys. Rev. Lett.* (2004), **93**, 137801–4.

[8] P. G. de Gennes, *Phy. Lett. A* **30,** 454 (1969)

[9] Barberi, R.; Ciuchi, F.; Lombardo, G.; Bartolino, R.; Durand, G.E. *Phys. Rev. Lett.* (2006), **96**, 019802.

[10] C. Mauguin, *Comptes rendus de l'Académie des Sciences* **152,** 1680 (1911).

[11] H. Zöcher, *Transactions of the Faraday Society* **29**, 945 (1933).

[12] J Cognard, *Molecular Crystals and Liquid Crystals Supplement Series***, 1** (1983).

[13] T. J. Scheffer and J. Nehring, *Journal of Applied Physics* **48** (5), 1783 (1977).

[14] H. Mori, E. Gartland, J. Kelly, and P. Bos, *Jpn. J. Appl. Phys.*,Part 1 **38**, 135 (1999).

[15] K. Schiele and S. Trimper, *Phys. Status Solidi* B **118**, 267 (1983).

[16] D. W. Berreman and S. Meiboom, *Phys. Rev. A* **30**, 1955 (1984).

[17] E. Gramsbergen, L. Longa, and W. de Jeu, *Phys. Rep*. **135**, 195 (1986).

[18] E. Virga, *Variational Theories for Liquid Crystals* Chapman- Hall, London, (1994).

[19] A. Alexe-Ionescu, *Phys. Lett. A* **180**, 456 (1993).

[20] M. Nobili and G. Durand, *Phys. Rev. A* **46**, R6174 (1992).

[21] P.D. Brimicombe, E.P. Raynes, *Liq. Cryst*. **32** (2005) 1273.

[22] J. Anderson, P. Watson, and P. Bos, *LC3D: Liquid Crystal Display 3-D Directory Simulator, Software and Technology Guide* Artech House, Boston, (1999).

[23]J. Strutt, *Proc. London Math. Soc.* **s1-4**, 357 (1871).

[24] A. M. Sonnet and E. G. Virga, *Phys. Rev. E* **64**, 031705 (2001)

[25] A. Sonnet, P. Maffettone, and E. Virga, J. *Non-Newtonian Fluid Mech*. **119**, 51 (2004).

[26] G. Lombardo, A. Amoddeo, R. Hamdi, H. Ayeb, R. Barberi , *EPJB* **35**(5), 1-6 (2012)

[27] Y. W. Kwon and H. Bang: *The Finite Element Method Using MATLAB*(2000)

[28] G. Lombardo Ph.D. *Thesis University of Reggio Calabria* (2002)

[29] Costa, M.R.; Altafim, R.A.C.; Mammana, A.P. *IEEE Trans. Dielectr. Electr. Insulat.* **2006**, *13*, 204-210.

[30] N. Schopohl and T. J. Sluckin, *Phys. Rev. Lett.* **59**, 2582 (1987).

[31] N. Mottram, C J.P. Newton. *Cond Mat Soft* . Introduction to Q-tensor theory. (2014)

[32] R. Hamdi Ph.D Thesis University of Calabria (2011).

[33] H.J. Deuling, *Mol. Cryst. Liq. Cryst.* **19**, 123 (1972)

[34] Herbert De Smet, Jean Van den Steen & Dieter Cuypers (2004). Electrical model of a liquid crystal pixel with dynamic, voltage history-dependent capacitance value , Liquid Crystals, 31:5, 705-711.

[35] D. H. Chung, Y. Takanishi, K. Ishikawa, C. J. Yu, S. D. Lee, and H. Takezoe, *Japanese Journal of Applied Physics* **42** (4A), 1686 (2003).

[36] Denis Andrienko, Yuri Kurioz, Yuri Reznikov, Charles Rosenblatt, Rolfe Petschek, Oleg Lavrentovich, and Darius Subacius, *Journal of Applied Physics* **83** (1), 50 (1998).

[37] Fulvio Bisi, Epifanio G. Virga, et al, *Physical Review E* **70** (4), 042701 (2004).

[38] L.M. Blinov, V.G. Chigrinov, *Electrooptic Effects in Liquid Crystal Materials* (1996).

[39] I. Dozov, M. Nobili, and G. Durand, *Applied Physics Letters* **70** (9), 1179 (1997).

[40] P.J. Collings and M. Hird, Introduction to liquid crystals: Chemestry and Physics, Taylor and Francis, London (1997).

[41] F. Ciuchi, H. Ayeb, G. Lombardo, R. Barberi, Georges E. Durand, *Applied Physics Letters* **91** (24), 244104 (2007).

[42] A. Amoddeo, R. Barberi, G. Lombardo, *Computers & Mathematics with Applications* **60** (8), 2239-2252 (2010).

[43] A. Amoddeo, R. Barberi, G. Lombardo, *Liquid Crystals*, **40** (6), 799-809, Taylor&Francis (2013).

[44] F. Ciuchi, R. Barberi. *Molecular Crystals and Liquid Crystals*, **549** (1), 37-42. Taylor&Francis Group (2011).

[45] A. Amoddeo, R. Barberi, G. Lombardo. *Physical Review E* **86**, 6 061705 (2012).